

This discussion paper is/has been under review for the journal Biogeosciences (BG).
Please refer to the corresponding final paper in BG if available.

Identifying environmental controls on vegetation greenness phenology through model-data integration

M. Forkel¹, N. Carvalhais^{1,2}, S. Schaphoff³, W. v. Bloh³, M. Migliavacca¹,
M. Thurner¹, and K. Thonicke³

¹Max-Planck-Institute for Biogeochemistry, Department for Biogeochemical Integration,
Hans-Knöll-Str. 10, 07745 Jena, Germany

²Universidade Nova de Lisboa, Faculdade de Ciências e Tecnologia, 2829-516, Caparica,
Portugal

³Potsdam Institute for Climate Impact Research, Earth System Analysis, Telegraphenberg
A31, 14473 Potsdam, Germany

Received: 28 May 2014 – Accepted: 30 June 2014 – Published: 17 July 2014

Correspondence to: M. Forkel (mforkel@bgc-jena.mpg.de)

Published by Copernicus Publications on behalf of the European Geosciences Union.

BGD

11, 10917–11025, 2014

Phenology controls and model-data integration

M. Forkel et al.

Title Page

Abstract

Introduction

Conclusions

References

Tables

Figures



Back

Close

Full Screen / Esc

Printer-friendly Version

Interactive Discussion



Abstract

Existing dynamic global vegetation models (DGVMs) have a limited ability in reproducing phenology and decadal dynamics of vegetation greenness as observed by satellites. These limitations in reproducing observations reflect a poor understanding and description of the environmental controls on phenology, which strongly influence the ability to simulate longer term vegetation dynamics, e.g. carbon allocation. Combining DGVMs with observational data sets can potentially help to revise current modelling approaches and thus to enhance the understanding of processes that control seasonal to long-term vegetation greenness dynamics. Here we implemented a new phenology model within the LPJmL (Lund Potsdam Jena managed lands) DGVM and integrated several observational data sets to improve the ability of the model in reproducing satellite-derived time series of vegetation greenness. Specifically, we optimized LPJmL parameters against observational time series of the fraction of absorbed photosynthetic active radiation (FAPAR), albedo and gross primary production to identify the main environmental controls for seasonal vegetation greenness dynamics. We demonstrated that LPJmL with new phenology and optimized parameters better reproduces seasonality, inter-annual variability and trends of vegetation greenness. Our results indicate that soil water availability is an important control on vegetation phenology not only in water-limited biomes but also in boreal forests and the arctic tundra. Whereas water availability controls phenology in water-limited ecosystems during the entire growing season, water availability co-modulates jointly with temperature the beginning of the growing season in boreal and arctic regions. Additionally, water availability contributes to better explain decadal greening trends in the Sahel and browning trends in boreal forests. These results emphasize the importance of considering water availability in a new generation of phenology modules in DGVMs in order to correctly reproduce observed seasonal to decadal dynamics of vegetation greenness.

Phenology controls and model-data integration

M. Forkel et al.

[Title Page](#)

[Abstract](#)

[Introduction](#)

[Conclusions](#)

[References](#)

[Tables](#)

[Figures](#)



[Back](#)

[Close](#)

[Full Screen / Esc](#)

[Printer-friendly Version](#)

[Interactive Discussion](#)



1 Introduction

The greenness of the terrestrial vegetation is directly linked to plant productivity, surface roughness and albedo and thus affects the climate system (Richardson et al., 2013). Vegetation greenness can be quantified from satellite observations for example as Normalized Difference Vegetation Index (NDVI) (Tucker, 1979). NDVI is a remotely sensed proxy for structural plant properties like leaf area index (LAI) (Turner et al., 1999) and green leaf biomass (Gamon et al., 1995) but moreover for plant productivity. Especially, NDVI of green vegetation has a linear relationship with the fraction of absorbed photosynthetic active radiation (FAPAR) (Fensholt et al., 2004; Gamon et al., 1995; Myneni and Williams, 1994; Myneni et al., 1995, 1997b). Satellite-derived FAPAR estimates are often used to estimate terrestrial photosynthesis (Beer et al., 2010; Jung et al., 2008, 2011; Potter et al., 1999). Decadal satellite observations of NDVI demonstrate widespread positive trends (“greening”) especially in the high latitude regions (Lucht et al., 2002; Myneni et al., 1997a; Xu et al., 2013) but also in the Sahel, southern Africa and southern Australia (Fensholt and Proud, 2012; de Jong et al., 2011, 2013). Surprisingly, these trends are accompanied by negative trends (“browning”) which were observed regionally in parts of the boreal forests of North America and Eurasia, and in parts of eastern Africa and South America. Regionally different causes have been identified for the observed greening and browning trends. The greening of the high latitudes is supposed to be mainly induced by rising air temperatures (Lucht et al., 2002; Myneni et al., 1997a; Xu et al., 2013). On the other hand, the environmental controls on the browning of boreal forests have been intensively investigated but no concluding or general explanation has been found so far (Barichivich et al., 2014; Beck and Goetz, 2011; Beck et al., 2011; Bunn et al., 2007; Goetz et al., 2005; Piao et al., 2011; Wang et al., 2011). Trends in vegetation greenness are often related to changes in vegetation phenology like an earlier onset and an associated lengthening of the growing season in mid- and high-latitude regions (Atzberger et al., 2013; Høgda et al., 2001, 2013; Tucker et al., 2001; Zeng et al., 2011) Changes in vegetation greenness are linked to changes

Phenology controls and model-data integration

M. Forkel et al.

Title Page

Abstract

Introduction

Conclusions

References

Tables

Figures



Back

Close

Full Screen / Esc

Printer-friendly Version

Interactive Discussion



Phenology controls and model-data integration

M. Forkel et al.

[Title Page](#)

[Abstract](#)

[Introduction](#)

[Conclusions](#)

[References](#)

[Tables](#)

[Figures](#)



[Back](#)

[Close](#)

[Full Screen / Esc](#)

[Printer-friendly Version](#)

[Interactive Discussion](#)



in primary production and thus affect atmospheric CO₂ concentrations and the terrestrial carbon cycle (Barichivich et al., 2013; Keeling et al., 1996; Myneni et al., 1997a). Additionally, vegetation greenness affects the climate system by influencing surface albedo. For example, greening trends in high-latitudes are associated with decreasing surface albedo (Urban et al., 2013) which alters the surface radiation budget (Lorant

Dynamic global vegetation models (DGVM) or generally climate-carbon cycle models are used to analyze and project the response of the terrestrial vegetation to the past, recent and future climate variability (Prentice et al., 2007). DGVMs can be used to explain observed trends in vegetation greenness (Lucht et al., 2002) or to quantify the related terrestrial CO₂ uptake. While most global models simulate an increasing uptake of CO₂ by the terrestrial vegetation under future climate change scenarios, the magnitude of future changes in land carbon uptake largely differs among models (Friedlingstein et al., 2006; Sitch et al., 2008). The spread of land carbon uptake estimates among DGVMs might be partly related to insufficient representations of vegetation phenology and greenness (Richardson et al., 2012). Coupled climate-carbon cycle models and uncoupled DGVMs have been compared against 30 year satellite-derived time series of LAI (Anav et al., 2013; Murray-Tortarolo et al., 2013; Zhu et al., 2013). Models usually overestimate mean annual LAI in all biomes and have a too long growing season because of a delayed season end (Anav et al., 2013; Murray-Tortarolo et al., 2013; Zhu et al., 2013). Additionally, most DGVMs have more positive LAI trends than the satellite-derived LAI product, i.e. they underestimate browning trends in boreal forests while a few DGVMs do not reproduce the general greening of the high latitudes (Murray-Tortarolo et al., 2013). The limitations of DGVMs in reproducing observed LAI or FAPAR time series is mostly related to limited phenology routines that often miss environmental controls on seasonal leaf development (Kelley et al., 2013;

Murray-Tortarolo et al., 2013; Richardson et al., 2012). In conclusion, with improved modeling approaches for vegetation phenology and greenness, DGVMs can potentially more accurately reproduce the recent, and project the future response of the terrestrial vegetation to climate variability.

5 Past studies successfully demonstrated the use of vegetation greenness observations to improve stand-alone phenology models or to optimize phenology and productivity-related parameters in DGVMs. The growing season index (GSI) is an empirical phenology model that is used to estimate seasonal leaf developments (Jolly et al., 2005). Empirical parameters of GSI have been optimized against globally distributed 10 year FAPAR and LAI time series from MODIS to reanalyze climatic drivers for vegetation phenology (Stöckli et al., 2008, 2011). This optimization resulted in a good representation of temporal FAPAR and LAI dynamics in all major biomes except evergreen tropical forests (Stöckli et al., 2011). Model parameters of the Biome-BGC model were optimized against eddy covariance flux observations and NDVI time series from MODIS for poplar plantations in Northern Italy which resulted in a more accurate representation of carbon fluxes and NDVI (Migliavacca et al., 2009). The BETHY-CCDAS model was optimized against FAPAR time series from MERIS for seven eddy covariance sites (Knorr et al., 2010) and later for 170 land grid cells using coarse 8 by 10° spatial resolution (Kaminski et al., 2012). These studies demonstrated the improvements in simulated vegetation phenology by optimizing model parameters against observations of vegetation greenness.

Nevertheless, spatial patterns and temporal dynamics of vegetation greenness were not yet optimized in a DGVM globally at a higher spatial resolution (0.5°) and by using long-term (30 year) satellite-derived time series of vegetation greenness. Newly developed 30 year time series of LAI or FAPAR from the GIMMS3g dataset (Global Inventory Modeling and Mapping Studies, 3rd generation of datasets) (Zhu et al., 2013) allow improving DGVMs not only based on seasonal cycles of single years (i.e. phenology) but additionally against decadal time series properties including inter-variability and trends. By integrating the GIMMS3g FAPAR data set in a DGVM, we can potentially improve

BGD

11, 10917–11025, 2014

Phenology controls and model-data integration

M. Forkel et al.

Title Page

Abstract

Introduction

Conclusions

References

Tables

Figures



Back

Close

Full Screen / Esc

Printer-friendly Version

Interactive Discussion



Phenology controls and model-data integration

M. Forkel et al.

Title Page

Abstract

Introduction

Conclusions

References

Tables

Figures



Back

Close

Full Screen / Esc

Printer-friendly Version

Interactive Discussion



spatial patterns and seasonal to long-term temporal dynamics of vegetation greenness. We are using the LPJmL DGVM (Lund–Potsdam–Jena managed lands). Similar to other DGVMs, LPJmL does not accurately reproduce the growing season onset and seasonal amplitude of observed LAI and FAPAR time series presumably because of a limited phenology model (Kelley et al., 2013; Murray-Tortarolo et al., 2013). Thus integrating long-term observations of FAPAR in the LPJmL DGVM potentially requires the development of an improved phenology scheme.

We are aiming to improve environmental controls on vegetation phenology and greenness in LPJmL by (1) developing a new phenology module for LPJmL, by (2) optimizing FAPAR, productivity and phenology-related parameters of LPJmL against 30 year satellite-derived time series of FAPAR, against 10 year satellite-derived time series of vegetation albedo and against spatial patterns of mean annual gross primary production (GPP) from a data-oriented estimate and by (3) integrating further data streams in LPJmL to constrain land cover dynamics and disturbance effects on vegetation greenness in diagnostic model simulations. This model-data integration approach for LPJmL (LPJmL-MDI) will be applied to explain the role of phenological controls on seasonal to long-term dynamics of vegetation greenness.

2 Model, data sets and model-data integration

2.1 Overview

LPJmL is a dynamic global vegetation model that simulates ecosystem processes as carbon and water fluxes, carbon allocation in plants and soils, permafrost dynamics, fire spread and behaviour and vegetation establishment and mortality. We were using LPJmL version 3.5. This version is based on the original LPJ model (Sitch et al., 2003). The model has been extended for human land use (Bondeau et al., 2007), and agricultural water use (Rost et al., 2008). It includes a process-oriented fire model (Thonicke et al., 2010), an improved representation of surface albedo and snow cov-

erage (Strengers et al., 2010) and a newly implemented soil hydrology scheme and permafrost module (Schaphoff et al., 2013) This study focusses on the natural vegetation plant functional types (PFTs) (Sitch et al., 2003), i.e. our model developments and optimizations we were not applied for crop functional types (CFTs) (Bondeau et al., 2007) because crop phenology is highly driven by human practices.

We developed a model-data integration approach for the LPJmL DGVM (LPJmL-MDI, Fig. 1). LPJmL-MDI allows to (1) directly insert land cover, tree cover and burnt area data sets in LPJmL for diagnostic model applications (Sec. 2.4.1), (2) to optimize LPJmL model parameters against datasets (here FAPAR, GPP, albedo; Sec. 2.4.2); and (3) to evaluate and benchmark LPJmL simulations against observations or observation-based data sets (Sec. 2.4.3). Like in a prognostic mode, LPJmL was driven by climate forcing data. Additionally, observed burnt areas were directly inserted in LPJmL to consider observed fire dynamics in diagnostic model applications. For this, we directly replaced the simulated burnt area in the LPJmL-SPITFIRE fire module (Thonicke et al., 2010) by observed burnt areas using the approach of Lehsten et al. (2008). Thus, the timing and location of fire spread is constrained by observations whereas fire effects on vegetation are still simulated by LPJmL-SPITFIRE. We further prescribed observed land cover and tree cover fractions to control for vegetation dynamics in parameter optimization experiments. Observed FAPAR and albedo time series as well as observation-based mean annual spatial patterns of GPP were used in a joint cost function to optimize productivity, phenology, radiation, and albedo-related model parameters using a genetic optimization algorithm.

LPJmL was previously evaluated against site measurements of net carbon ecosystem exchange (Schaphoff et al., 2013; Sitch et al., 2003), atmospheric CO₂ fractions (Sitch et al., 2003), soil moisture (Wagner et al., 2003), evapotranspiration and runoff (Gerten et al., 2004; Schaphoff et al., 2013), fire regimes (Thonicke et al., 2010), and permafrost distribution (Schaphoff et al., 2013). We are evaluating LPJmL against additional and partly new available global data sets of FAPAR (Baret et al., 2013; Zhu et al.,

BGD

11, 10917–11025, 2014

Phenology controls and model-data integration

M. Forkel et al.

Title Page

Abstract

Introduction

Conclusions

References

Tables

Figures



Back

Close

Full Screen / Esc

Printer-friendly Version

Interactive Discussion



2013), GPP and evapotranspiration (ET) (Jung et al., 2011), tree cover (Townshend et al., 2011) and biomass (Saatchi et al., 2011; Thurner et al., 2014).

2.2 FAPAR and phenology in the LPJmL DGVM

2.2.1 FAPAR

5 FAPAR is defined as the ratio between the photosynthetic active radiation absorbed by the green canopy (APAR) and the total incident photosynthetic active radiation (PAR). Thus, the total FAPAR of a grid cell is the sum of FAPAR that is distributed among the individual PFTs:

$$\text{FAPAR}_{\text{PFT}} = \frac{\text{APAR}_{\text{PFT}}}{\text{PAR}} \quad (1)$$

$$10 \text{ FAPAR}_{\text{gridcell}} = \sum_{\text{PFT}=1}^{\text{PFT}=n} \text{FAPAR}_{\text{PFT}} \quad (2)$$

where n is the number of established PFTs in a grid cell. The FAPAR of a PFT depends on the annual maximum foliar projective cover (FPC), on the daily snow coverage in the green canopy ($F_{\text{snow, gv}}$), green-leaf albedo (β_{leaf}) and the daily phenology status (Phen):

$$15 \text{ FAPAR}_{\text{PFT}} = \text{FPC}_{\text{PFT}} \times (\text{Phen}_{\text{PFT}} - (\text{Phen}_{\text{PFT}} \times F_{\text{snow, gv, PFT}})) \times (1 - \beta_{\text{leaf, PFT}}) \quad (3)$$

Thus, the temporal dynamic of FAPAR in LPJmL is affected on an annual time step by changes in foliar projective cover (FPC_{PFT}) and on daily time steps by changes in phenology (Phen_{PFT}) and snow coverage in the green canopy ($F_{\text{snow, gv, PFT}}$) (Fig. A1). This approach extends the previous implementation of Sitch et al. (2003) where FAPAR depended only on FPC and phenology but leaf albedo and snow effects on FAPAR were missing.

Phenology controls and model-data integration

M. Forkel et al.

Title Page

Abstract

Introduction

Conclusions

References

Tables

Figures

⏪

⏩

◀

▶

Back

Close

Full Screen / Esc

Printer-friendly Version

Interactive Discussion



FPC_{PFT} expresses the land cover fraction of a PFT. It is the annual maximum fractional green canopy coverage of a PFT and is annually calculated from crown area (CA), population density (P) and LAI (Sitch et al., 2003):

$$FPC_{PFT} = CA_{PFT} \times P_{PFT} \times (1 - e^{-k_{PFT} \times LAI_{PFT}}) \quad (4)$$

The last term expresses the light extinction in the canopy which depends exponentially on LAI and the light extinction coefficient k of the Lambert–Beer law (Monsi and Saeki, 1953). The parameter k had a constant value of 0.5 for all PFTs in the original LPJmL formulation (Sitch et al., 2003). We changed k to a PFT-dependent parameter because it varies for different plant species as seen from field observations (Bolstad and Gower, 1990; Kira et al., 1969; Monsi and Saeki, 1953). Crown area and leaf area index are calculated based on allocation rules and are depending on the annual biomass increment (Sitch et al., 2003). Population density depends on establishment and mortality processes in LPJmL (Sitch et al., 2003).

2.2.2 Phenology

The daily phenology and green leaf status of a PFT ($Phen_{PFT}$) in LPJmL expresses the fractional cover of green leaves (from 0 = no leaves to 1 = full leave cover). Thus, it represents the temporal dynamic of the canopy greenness. We explored two phenology models in this study: first, we were trying to optimize model parameters of the original phenology model in LPJmL (LPJmL-OP, Sitch et al., 2003, Appendix A1). Secondly, we implemented a new phenology model based on the growing season index (GSI) concept (Jolly et al., 2005), hereinafter called LPJmL-GSI.

LPJmL-OP has three different routines for summergreen (i.e. temperature-driven deciduous), evergreen (no seasonal variation) and rain-green (i.e. water-driven deciduous) PFTs (details in Appendix A1). Obviously, LPJmL-OP misses important controls on phenology like effects of light in all PFTs or effects of water in summergreen and herbaceous PFTs. Additionally, in herbaceous PFTs the end of the growing season

Phenology controls and model-data integration

M. Forkel et al.

Title Page

Abstract

Introduction

Conclusions

References

Tables

Figures



Back

Close

Full Screen / Esc

Printer-friendly Version

Interactive Discussion



is not controlled by environmental conditions but is defined based on fixed calendar dates.

Because of the obvious limitations of LPJmL-OP, we developed the alternative LPJmL-GSI phenology module. The growing season index (GSI) is an empirical phenology model that multiplies limiting effects of temperature, day length and vapour pressure deficit (VPD) to a common phenology status (Jolly et al., 2005). We modified the GSI concept for the specific use in LPJmL (LPJmL-GSI). We defined the phenology status as a function of cold temperature, short-wave radiation and water availability. Additionally to the original GSI model, we added a heat stress limiting function because it has been suggested that vegetation greenness is limited by temperature-induced heat stress in several ecosystems (Bunn et al., 2007; Verstraeten et al., 2006) and has been demonstrated that heat stress reduces plant productivity also without additional water stress (Jiang and Huang, 2001; Van Peer et al., 2004; Poirier et al., 2012). Thus, the daily phenology status of a PFT is the product of the daily cold temperature ($f_{\text{cold, PFT}}$), light ($f_{\text{light, PFT}}$), water ($f_{\text{water, PFT}}$) and heat stress ($f_{\text{heat, PFT}}$) limiting functions:

$$\text{Phen}_{\text{PFT}} = f_{\text{cold, PFT}} \times f_{\text{light, PFT}} \times f_{\text{water, PFT}} \times f_{\text{heat, PFT}} \quad (5)$$

Examples for the four functions are shown in Fig. 2.

The cold temperature limiting function at a daily time step t is defined as:

$$f_{\text{cold, PFT}}^t = f_{\text{cold, PFT}}^{t-1} + \left(\frac{1}{1 + e^{-\text{sl}_{\text{cold, PFT}} \times (T - \text{base}_{\text{cold, PFT}})}} - f_{\text{cold, PFT}}^{t-1} \right) \times \tau_{\text{cold, PFT}} \quad (6)$$

where $\text{sl}_{\text{cold, PFT}}$ and $\text{base}_{\text{cold, PFT}}$ are PFT-dependent slope and inflection point parameters of a logistic function based on daily air temperature T ($^{\circ}\text{C}$). The parameter $\tau_{\text{cold, PFT}}$ is the change rate parameter based on the difference between the actual predicted limiting function value and the previous-day cold temperature limiting function value. This parameter introduces a temporal autocorrelation in the phenology status and avoids abrupt phenological changes because of changing weather conditions.

Phenology controls and model-data integration

M. Forkel et al.

Title Page

Abstract

Introduction

Conclusions

References

Tables

Figures



Back

Close

Full Screen / Esc

Printer-friendly Version

Interactive Discussion



The light-limiting function was implemented accordingly:

$$f_{\text{light, PFT}}^t = f_{\text{light, PFT}}^{t-1} + \left(\frac{1}{1 + e^{-s_{\text{light, PFT}} \times (SW - \text{base}_{\text{light, PFT}})}} - f_{\text{light, PFT}}^{t-1} \right) \times \tau_{\text{light, PFT}} \quad (7)$$

where $s_{\text{light, PFT}}$ and $\text{base}_{\text{light, PFT}}$ are the PFT-dependent slope and inflection point parameters of a logistic function based on daily shortwave downward radiation SW (W m^{-2}). The parameter $\tau_{\text{light, PFT}}$ is the temporal change rate for the light-limiting function.

The water-limiting function $f_{\text{water, PFT}}$ depends on the daily water availability W (%) in LPJmL:

$$f_{\text{water, PFT}}^t = f_{\text{water, PFT}}^{t-1} + \left(\frac{1}{1 + e^{-s_{\text{water, PFT}} \times (W - \text{base}_{\text{water, PFT}})}} - f_{\text{water, PFT}}^{t-1} \right) \times \tau_{\text{water, PFT}} \quad (8)$$

where $s_{\text{water, PFT}}$ and $\text{base}_{\text{water, PFT}}$ are the PFT-dependent slope and inflection point parameters of a logistic function based on daily water availability. W is a ratio between water supply from soil moisture and atmospheric water demand (Appendix A.2) (Gerten et al., 2004). The parameter $\tau_{\text{water, PFT}}$ is the temporal change rate for the water-limiting function.

The heat-stress limiting function is defined as the cold-temperature limiting function based on daily air temperature but with a negative slope parameter:

$$f_{\text{heat, PFT}}^t = f_{\text{heat, PFT}}^{t-1} + \left(\frac{1}{1 + e^{s_{\text{heat, PFT}} \times (T - \text{base}_{\text{heat, PFT}})}} - f_{\text{heat, PFT}}^{t-1} \right) \times \tau_{\text{heat, PFT}} \quad (9)$$

where $s_{\text{heat, PFT}}$ and $\text{base}_{\text{heat, PFT}}$ are the PFT-dependent slope and inflection point parameters of a logistic function based on T . The parameter $\tau_{\text{heat, PFT}}$ is the temporal change rate for the heat limiting function.

Besides the additional use of the heat stress limiting function, LPJmL-GSI has important differences to the original GSI phenology model (Jolly et al., 2005) We made

time scales. Two recently developed datasets provide 30 year time series of FAPAR. The Geoland2 BioPar (GEOV1) FAPAR dataset (Baret et al., 2013) (hereinafter called GL2 FAPAR) and the GIMMS3g FAPAR (Zhu et al., 2013) datasets were used in this study.

5 GL2 FAPAR is defined as the black-sky green canopy FAPAR at 10:15 solar time and has been produced based on SPOT VGT (1999–2012) and AVHRR (1981–2000) (Baret et al., 2013). The GL2 FAPAR dataset has a temporal resolution of 10 days and a spatial resolution of 0.05° for the AVHRR-period and of $1/112^\circ$ for the SPOT VGT period. GIMMS3g FAPAR corresponds to black-sky FAPAR at 10:35 solar time and has
10 been produced based on the GIMMS3g NDVI dataset (Zhu et al., 2013). GIMMS3g FAPAR has a 15 day temporal resolution and a $1/12^\circ$ spatial resolution and covers July 1981 to December 2011. We excluded in both FAPAR datasets observations that were flagged as contaminated by snow, aerosols or clouds. Additionally, we excluded FAPAR observations for months with temperatures $< 0^\circ\text{C}$ to exclude potential remain-
15 ing distortions of snow cover. Both datasets were aggregated to a 0.5° spatial and monthly temporal resolution to be comparable with LPJmL simulations. We found that the GL2 AVHRR and GL2 VGT FAPAR datasets have not been well harmonized (Appendix B1). Thus, we did not use the combined GL2 VGT and AVHRR FAPAR dataset for parameter optimization and for analyses of inter-annual variability and trends but
20 only for analyses and evaluations of mean seasonal cycles and spatial patterns of FAPAR. The GIMMS3g FAPAR dataset has no uncertainty estimates. Uncertainty estimates are necessary in multiple data stream parameter optimization to weight single data streams in the total cost function. As a workaround we estimated the uncertainty based on monthly-varying quantile regressions to the 0.95 quantile between FAPAR
25 and the FAPAR uncertainty in the GL2 VGT dataset. We applied the fitted regressions to the GIMMS3g dataset to estimate FAPAR uncertainties (Appendix B2). The fit to the upper quantile provides conservative uncertainty estimates for the GIMMS3g FAPAR dataset.

Phenology controls and model-data integration

M. Forkel et al.

[Title Page](#)[Abstract](#)[Introduction](#)[Conclusions](#)[References](#)[Tables](#)[Figures](#)[Back](#)[Close](#)[Full Screen / Esc](#)[Printer-friendly Version](#)[Interactive Discussion](#)

Phenology controls and model-data integration

M. Forkel et al.

Title Page

Abstract

Introduction

Conclusions

References

Tables

Figures



Back

Close

Full Screen / Esc

Printer-friendly Version

Interactive Discussion



We used monthly shortwave white-sky albedo time series ranging from 2000 to 2010 from the MODIS C5 dataset (Lucht et al., 2000; Schaaf et al., 2002) to constrain vegetation albedo parameters. Albedo observations in months with $< 5^{\circ}\text{C}$ air temperature and above an albedo of 0.3 were excluded from optimization because we are optimizing only vegetation-related albedo parameters. High albedo values at low temperatures are probably affected by changing snow regimes which is not within our focus of model development and optimization. Thus we are only optimizing growing season albedo.

We used mean annual total GPP patterns from the data-oriented MTE (model tree ensemble) GPP estimate (Jung et al., 2011). This GPP estimate uses FLUXNET eddy covariance observations together with satellite observations and climate data to up-scale GPP using a machine learning approach (Jung et al., 2011). This dataset is not an observation but a result of an empirical model. Nevertheless, evaluation and cross-validation analyses have shown that this dataset well represents the mean annual spatial patterns and mean seasonal cycles of GPP whereas it has a poor performance in representing temporal GPP anomalies (trends and extremes) (Jung et al., 2011). Thus, we are only using the mean annual total GPP from this dataset for parameter optimization to constrain LPJmL within small biases of mean annual GPP. We used the mean seasonal cycle from the MTE GPP product as an independent benchmark for model evaluation.

2.3.2 Data sets for the prescription of land cover, tree cover and burnt area

The FAPAR, albedo and GPP data sets do not presumably contain enough information to constrain all processes that control FAPAR dynamics. Especially, processes like establishment, mortality, competition between PFTs, allocation and disturbances control FPC and thus FAPAR. The optimization of parameters of these processes against appropriate data streams is not feasible within this study. Thus, we directly prescribed land and tree cover fractions as well as burnt areas from observed data to control for some of these processes.

Phenology controls and model-data integration

M. Forkel et al.

Title Page

Abstract

Introduction

Conclusions

References

Tables

Figures



Back

Close

Full Screen / Esc

Printer-friendly Version

Interactive Discussion



To prescribe land and tree cover in LPJmL, we combined several datasets to create observation-based maps of FPC (Appendix C2). Land cover maps from remote sensing products are not directly comparable with PFTs in global vegetation models due to differences in classification systems (Jung et al., 2006; Poulter et al., 2011a). PFTs in LPJmL are defined according to biome (tropical, temperate or boreal), leaf type (needle leaved, broadleaved) and phenology type (summergreen, evergreen, rain green). We extracted the biome information from the Köppen–Geiger climate classification (Kottek et al., 2006) whereas leaf type and phenology were extracted from the SYNMAP land cover map (Jung et al., 2006). FPC was derived from MODIS tree cover (Townshend et al., 2011). Because LPJmL so far classified herbaceous vegetation according to their photosynthetic pathway (i.e. C_3 , temperate herbaceous and C_4 , tropical herbaceous), we further sub-divided herbaceous PFTs according to biome and introduced a polar herbaceous PFT (PoH) based on the existing temperate herbaceous PFT (TeH) to differentiate tundra from temperate grasslands.

Burnt area data was prescribed directly in LPJmL by combining three data sets, the Global Fire Emissions Database (GFED) burnt area dataset (Giglio et al., 2010), the Alaska Large Fire Database (ALFDB) (Frames, 2012; Kasischke et al., 2002) and the Canadian National Fire Database (CNFDB) (CFS, 2010; Stocks et al., 2002). GFED provides monthly burnt area estimates in 0.5° resolution from 1996 to 2011. Burnt areas from the Alaska (ALFDB) and Canada (CNFDB) fire databases were used to extent burnt area time-series before 1996 for boreal North America. Fire perimeter observations from 1979 to 1996 from ALFDB and CNFDB were aggregated to 0.5° gridded monthly burnt area time series. Observations before 1979 were excluded because fires were not reported for all provinces in Canada. Although the CNFDB contains only fire perimeters > 200 ha, in both databases some fires are missing due to different mapping techniques, and fire perimeters do not agree with burned area, the integration of these datasets provides unique information about spatial-temporal patterns of disturbances especially in boreal ecosystems. It is necessary to simulate fire activity also during the model spin-up as fire influences the equilibrium between vegetation, soil and climate

as well. Otherwise biomass would be overestimated at the beginning of the transient model run. For this purpose, we created artificial burnt area time series for the periods 1901–1978 (North America) and 1901–1995 (rest of the world). Observed annual total burnt areas from the periods 1979–2011 (North America) and 1996–2011 (rest of the world) were resampled according to temperature and precipitation conditions and assigned to the pre-data period in order to include fire regimes that agree with observed fire regimes in the spin-up of LPJmL. This approach assumes that fire regimes in the pre-data period were not different than in the observation period.

2.3.3 Data sets for model evaluation

LPJmL was evaluated against data sets that are independent from the optimization and prescription data sets and against independent temporal or spatial scales of the optimization and prescription data sets. We compared LPJmL against mean annual patterns and mean seasonal cycles of ET from the MTE estimate (Jung et al., 2011). Further, we evaluated model results against spatial patterns of biomass. Ecosystem biomass estimates were taken from satellite-derived forest biomass maps for the tropics (Saatchi et al., 2011) and for the temperate and boreal forests (Thurner et al., 2014) including an estimation of herbaceous biomass. Additionally, we evaluated LPJmL against independent temporal and spatial scales of the integration data (mean seasonal cycle of GPP, tree cover, inter-annual variability and trends of FAPAR). We were using tree cover from MODIS to evaluate LPJmL model runs with dynamic vegetation.

2.3.4 Climate forcing data and model spin-up

LPJmL was driven by observed monthly temperature and precipitation data from the CRU TS3.1 dataset ranging from 1901 to 2011 (Harris et al., 2013) as well as by monthly shortwave downward radiation and long wave net radiation re-analysis data from ERA-Interim (Dee et al., 2011).

Phenology controls and model-data integration

M. Forkel et al.

[Title Page](#)

[Abstract](#)

[Introduction](#)

[Conclusions](#)

[References](#)

[Tables](#)

[Figures](#)



[Back](#)

[Close](#)

[Full Screen / Esc](#)

[Printer-friendly Version](#)

[Interactive Discussion](#)



Phenology controls and model-data integration

M. Forkel et al.

Title Page

Abstract

Introduction

Conclusions

References

Tables

Figures



Back

Close

Full Screen / Esc

Printer-friendly Version

Interactive Discussion



LPJmL needs a model spin-up to establish PFTs and to bring vegetation and soil carbon pools into equilibrium. The spin-up was performed according to the standard LPJmL modeling protocol (Schaphoff et al., 2013; Thonicke et al., 2010): LPJmL was run for 5000 years by repeating the climate data from 1900–1930. After the spin-up model run, the transient model run was restarted from the spin-up conditions in 1901 and LPJmL was run for the period 1901–2011. Model results were analyzed for the observation period (1982–2011).

For model optimization experiments we used a different spin-up scheme because the spin-up is computational time demanding and many model runs are needed during optimization experiments. As in the standard modeling protocol, we firstly spin-up the model for 5000 years by repeating the climate from 1901–1930. Secondly, a transient model run was restarted from the spin-up conditions in 1901 and was performed for the period 1901–1979. Thirdly, each optimization experiment was restarted from the conditions in 1979 and a second spin-up for 100 years by recycling the climate from 1979 to 1988 was performed. The transient model run was restarted from the conditions of the second spin-up and simulated for the period 1979–2011. This second spin-up is needed to bring the vegetation into a new equilibrium which can be caused by a new parameter combination during optimization. From visual analyses of model results, we found that a spin-up time of 100 years for the second spin-up was enough to eliminate trends in FAPAR and GPP that resulted from other equilibrium conditions.

2.4 Model-data integration

2.4.1 Prescription of land and tree cover

Land cover is expressed as FPC in LPJmL. We used the observation-based FPC dataset to prescribe land and tree cover in LPJmL (Sec. 2.3.2, Appendix C1). The presence of a PFT in a grid cell depends on establishment and mortality in LPJmL (Sitch et al., 2003). A PFT establishes in a grid cell if the climate is within the bioclimatic limits of the PFT for establishment and survival. On the other hand, a PFT dies

in a grid cell if the climate is no longer suitable for the PFT. Additionally, mortality occurs because of heat stress, low productivity, competition among PFTs for light, and because of fire disturbance (Sitch et al., 2003; Thonicke et al., 2010).

FPC is the major variable that contributes to inter-annual variability of FAPAR in LPJmL despite the daily phenological status. Thus fixing FPC to the observed value is not a desired solution to prescribe land cover in LPJmL. Fixing FPC would neglect mortality effects on land cover but would also permit the simulation of post-fire succession trajectories. Consequently, we prescribed land cover in LPJmL using a hybrid diagnostic-dynamic approach. In this approach we prescribed the annual maximum FPC in LPJmL similar to previous approaches (Poulter et al., 2011b). Firstly, we switched off the effects of bioclimatic limits on establishment and mortality. Only these PFTs were allowed to establish in a grid cell that occurred in the observed land-cover data set. Vegetation growth depends on the annual biomass increment and allocation rules in LPJmL. This leads to an extension of FPC of each PFT. We limited a further expansion of FPC if the simulated FPC values equals the observed FPC (prescribed maximum FPC). In this case, no new individuals are established and the population density P of a PFT is corrected in order to fit the observed FPC (FPC_{obs}):

$$P_{PFT,corr} = P_{PFT} \times FPC_{PFT} - (FPC_{PFT} - FPC_{obs, PFT}) \quad (10)$$

The biomass of the individuals that need to be killed in order to match the corrected population density $P_{PFT,corr}$ is transferred to the litter pools. The simulated FPC can be lower than the observed FPC because the PFT is still growing or because the FPC was reduced due to fire, heat stress or low productivity. For herbaceous PFTs we only reduced the FPC if the observed total fractional vegetation cover in a grid cell was exceeded. This allows herbaceous PFTs to replace tree PFTs if the FPC of trees is reduced due to fire or other mortality effects in the model. With this approach a prescription of land cover can be achieved in LPJmL which still allows for main processes of dynamic vegetation.

BGD

11, 10917–11025, 2014

Phenology controls and model-data integration

M. Forkel et al.

Title Page

Abstract

Introduction

Conclusions

References

Tables

Figures



Back

Close

Full Screen / Esc

Printer-friendly Version

Interactive Discussion



2.4.2 Parameter optimization

Photosynthesis, albedo, FAPAR and phenology-related model parameters of LPJmL were optimized against observed FAPAR and albedo satellite observations and data-oriented estimates of GPP. A description of all parameters including parameter values is given in Appendix D1. The parameter α_a is the most important parameter in LPJmL for photosynthesis (Zaehle et al., 2005). This parameter accounts for the amount of radiation that is absorbed at leaf level in comparison to the total canopy. Thus, this parameter is a replacement for a more enhanced model formulation for canopy structure and leaf clumping. We used this parameter to adjust biases in GPP. The PFT-dependent leaf, stem and litter albedo parameters (β_{leaf} , β_{stem} and β_{litter}) are mostly sensitive for model simulations of albedo. The parameter β_{leaf} affects additionally the maximum FAPAR of a PFT. The light extinction coefficient k controls the FPC of a PFT and thus affects mainly land cover, maximum FAPAR and the available radiation for photosynthesis. All other parameters that were considered in optimization experiments are the parameters of the LPJmL-OP and LPJmL-GSI phenology modules. These parameters contribute mainly to seasonal variations in FAPAR. Some parameters were excluded from optimization experiments that were identified as insensitive to GPP and FAPAR simulations in PFTs. The temporal change rate parameters τ_{tmin} , τ_{light} , τ_{heat} and τ_{water} are insensitive in most PFTs because of the monthly temporal resolution of the used climate forcing data.

The optimization of model parameters was performed by minimizing a cost function between model simulations and observations using a combined genetic and gradient-based optimization algorithm (GENOUD, genetic optimization using derivatives, Mebane and Sekhon, 2011, see Appendix D2 for details). The cost function J of LPJmL for a single model grid cell (gc) depends on the scaled model parameter vector \mathbf{d} (\mathbf{d} = parameter value/prior parameter value) and is the sum of square error (SSE) between model simulation and observation weighted by the number of observations

BGD

11, 10917–11025, 2014

Phenology controls and model-data integration

M. Forkel et al.

Title Page

Abstract

Introduction

Conclusions

References

Tables

Figures



Back

Close

Full Screen / Esc

Printer-friendly Version

Interactive Discussion



(nobs) for each data stream (DS):

$$J(\mathbf{d})_{\text{gc}} = \sum_{\text{DS}=1}^{\text{DS}=n} \frac{\text{SSE}_{\text{DS}}(\mathbf{d})}{\text{nobs}_{\text{DS}}} \quad (11)$$

The SSE for a single data stream is calculated from the LPJmL simulation of this data stream (x_{LPJmL}) and the corresponding observed values (x_{obs}) weighted by the uncertainty of the observations (x_{obsunc}) for each time step t :

$$\text{SSE}(\mathbf{d}) = \sum_{t=1}^{t=n} \frac{(x_{\text{LPJmL}, t}(\mathbf{d} \times p_0) - x_{\text{obs}, t})^2}{x_{\text{obsunc}, t}^2} \quad (12)$$

where p_0 are LPJmL prior parameters. That means the minimization of the cost function J is based on scalars of LPJmL parameters relative to the prior parameter values.

Different model optimization experiments were performed for individual grid cell and for multiple grid cells of the same PFT for LPJmL-OP as well as for LPJmL-GSI (Table 1). In the grid cell-based optimization experiments model parameters of the established target tree PFT and the established herbaceous PFT were optimized at the same time. The purpose of grid cell-level optimization experiments was to explore the variability of parameters within different regions and PFTs. In the PFT-level optimization experiments the cost of LPJmL was calculated as the sum of the cost for each grid cell weighted by the grid cell area A :

$$J(\mathbf{d})_{\text{PFT}} = \frac{\sum_{\text{gc}=1}^{\text{gc}=n} J(\mathbf{d})_{\text{gc}} \times A_{\text{gc}}}{\sum_{\text{gc}=1}^n A_{\text{gc}}} \quad (13)$$

For PFT-level optimizations parameters of herbaceous PFTs were first optimized for grid cells where only the herbaceous PFT is dominant. In a second step, the optimized parameters of the herbaceous PFTs were used in the optimization of the target tree

Phenology controls and model-data integration

M. Forkel et al.

Title Page

Abstract

Introduction

Conclusions

References

Tables

Figures



Back

Close

Full Screen / Esc

Printer-friendly Version

Interactive Discussion



PFT. The purpose of PFT-level optimization experiments is to derive optimized parameter sets that can be used for one PFT in global model runs.

For grid cell as well PFT-level optimization experiments, we only used grid cells that are vegetated, dominated by one PFT and that are only marginally affected from agricultural use or fire disturbances. These grid cells are called candidate grid cells in the following. We randomly selected grid cells from the set of candidate grid cells to perform grid cell- or PFT-level optimization experiments. Table 1 gives an overview of all optimization experiments for LPJmL-OP and LPJmL-GSI with the number of used grid cells. Grid cells that were selected for optimization experiments are also shown in Fig. 3. The PFT-level optimization of LPJmL-OP (OP.pft) did not result in plausible posterior parameter sets because of structural limitations of the LPJmL-OP phenology model for herbaceous PFTs (i.e. no water effects, calendar day as end of growing season), raingreen PFT (i.e. binary phenology) and evergreen PFTs (i.e. constant phenology) and was therefore excluded from further analysis.

Parameter sensitivities and uncertainties were explored by analyzing the maximum likelihood and the posterior range of each parameter as derived from all parameter sets from the genetic optimization algorithm (Appendix D3).

2.4.3 Model evaluation and time series analysis

Global model runs of LPJmL were performed in order to evaluate model results against the integration data, against independent metrics of the integration data and against independent data streams. We evaluated results from LPJmL-OP with standard parameters (LPJmL-OP-prior), from LPJmL-OP with optimized productivity, albedo and FAPAR parameters from grid-cell level optimization experiments (LPJmL-OP-gc) and from LPJmL-GSI with optimized parameters from PFT-level optimization experiments (Table 2). We did not use optimized phenology parameters in the LPJmL-OP-gc model run because we were not able to derive plausible phenology parameters in optimization experiments of LPJmL-OP. All model runs were performed with dynamic vegetation and prescribed burnt areas.

BGD

11, 10917–11025, 2014

Phenology controls and model-data integration

M. Forkel et al.

Title Page

Abstract

Introduction

Conclusions

References

Tables

Figures



Back

Close

Full Screen / Esc

Printer-friendly Version

Interactive Discussion



We aggregated monthly FAPAR time series to mean annual FAPAR to evaluate inter-annual variability and trends. Mean annual FAPAR time series were averaged from all monthly values with mean monthly air temperatures $> 0^{\circ}\text{C}$ to exclude potential remaining effects of snow in the observed FAPAR time series. Trends in mean annual FAPAR time series and trend breakpoints were computed using the “greenbrown” package for R software (Forkel et al., 2013). In this implementation, trends are computed by fitting piece-wise linear trends to the annual FAPAR time series using ordinary least squares regression. The significance of trends was computed using the Mann–Kendall trend test (Mann, 1945).

3 Results and discussions

3.1 Parameter optimization

3.1.1 Performance of phenology models

The newly developed LPJmL-GSI phenology model resulted in significantly higher correlations with monthly GIMMS3g FAPAR than LPJmL-OP in all PFTs except in the tropical broadleaved evergreen (TrBE) and boreal broadleaved summergreen (BoBS) PFTs (Fig. 4). LPJmL-OP with prior parameters had high correlations with monthly GIMMS3g FAPAR in broad-leaved summergreen PFTs (TeBS median $r = 0.87$, BoBS median $r = 0.92$) PFTs and medium correlations in boreal needle-leaved PFTs (BoNE median $r = 0.53$, BoNS median $r = 0.6$). In all other PFTs, LPJmL-OP had low correlations with monthly GIMMS3g FAPAR. The correlation against monthly GIMMS3g FAPAR did not significantly improve in all PFTs after grid cell-level optimization experiments of LPJmL-OP (Fig. 4). The use of the newly developed LPJmL-GSI phenology model already significantly improved the correlation with monthly GIMMS3g FAPAR in all PFTs except in the temperate herbaceous (TeH) and BoBS PFTs. LPJmL-GSI had significantly higher correlations with monthly GIMMS3g FAPAR after grid cell-level opti-

BGD

11, 10917–11025, 2014

Phenology controls and model-data integration

M. Forkel et al.

Title Page

Abstract

Introduction

Conclusions

References

Tables

Figures

◀

▶

◀

▶

Back

Close

Full Screen / Esc

Printer-friendly Version

Interactive Discussion



Phenology controls and model-data integration

M. Forkel et al.

Title Page

Abstract

Introduction

Conclusions

References

Tables

Figures



Back

Close

Full Screen / Esc

Printer-friendly Version

Interactive Discussion



mization experiments in the TrBR, TeNE, TeBS, TeH, BoBS and BoNS PFTs. After PFT-level optimization experiments, LPJmL-GSI had median correlation coefficients > 0.5 in all PFTs except in broadleaved evergreen PFTs (TrBE, TeBE). These results prove that the rain-green, evergreen and herbaceous phenology schemes of LPJmL-OP were not able to reproduce temporal FAPAR dynamics despite the attempt of parameter optimization and that LPJmL-GSI can reproduce seasonal FAPAR dynamics in most PFTs.

The low correlations coefficients between LPJmL-GSI and GIMMS3g FAPAR after optimization experiments in broadleaved evergreen PFTs (TrBE, TeBE) might be caused by the specific properties of the FAPAR dataset in these PFTs. GIMMS3g FAPAR does not have a clear seasonal cycle but a high short-term variability in tropical broadleaved evergreen forests. These regions are often covered by clouds that inhibit continuous optical satellite observations. The high short-term variability results ultimately in low correlation coefficients between both LPJmL versions (LPJmL-OP and LPJmL-GSI) and GIMMS3g FAPAR time series. Besides climatic factors, phenology in tropical forests is more driven by leaf age (Caldararu et al., 2012, 2014) and nutrient availability (Wright, 1996). These affects are neither considered in the original GSI phenology model (Jolly et al., 2005; Stöckli et al., 2011) nor in the LPJmL-GSI phenology model. In temperate broadleaved evergreen forests, the GIMMS3g FAPAR dataset might have a wrong seasonality. In these regions, the mean seasonal FAPAR cycles from the GIMMS3g and GL2 VGT FAPAR datasets are anti-correlated and FAPAR from LPJmL-GSI agrees better with the GL2 VGT dataset. Because of these reasons, we did not expect to improve seasonal FAPAR dynamics in broadleaved evergreen forests with the current model-data integration setup.

All optimization experiments of LPJmL-OP and LPJmL-GSI resulted in a significant reduction of the cost in comparison to the respective prior models (Appendix D4, Fig. D2). Nevertheless, the prior parameter set of LPJmL-GSI resulted already in a significant lower cost than the grid cell-level optimized parameter sets of LPJmL-OP in tropical and polar herbaceous PFTs, and in temperate broad-leaved summergreen and

Phenology controls and model-data integration

M. Forkel et al.

Title Page

Abstract

Introduction

Conclusions

References

Tables

Figures



Back

Close

Full Screen / Esc

Printer-friendly Version

Interactive Discussion



boreal needle-leaved summergreen PFTs. The reduction of the overall cost was in all model optimization experiments usually associated with a significant reduction of the annual GPP bias (Fig. D3). LPJmL-OP with prior parameters underestimated mean annual GPP in the tropical broad-leaved evergreen PFT and overestimated mean annual GPP in all other PFTs. Grid cell-level optimization experiments of LPJmL-OP resulted in a significant reduction of the GPP bias in all PFTs except in the polar herbaceous PFT (PoH). We were not able to remove the GPP bias and to reduce the cost of LPJmL-OP and of LPJmL-GSI in the PoH PFT (i.e. tundra) in optimization experiments because of inconsistencies between the FAPAR and GPP datasets or in the LPJmL formulation. LPJmL was not able to sustain the relatively high peak FAPAR in Tundra regions as seen in the GIMMS3g dataset given the low mean annual GPP of the MTE dataset (Appendix D4). These inconsistencies might be related to higher uncertainties of the GPP and FAPAR datasets in tundra regions where the MTE GPP dataset is not covered by many eddy covariance measurement sites, and where satellite-based FAPAR observations are affected from high sun zenith angles (Tao et al., 2009; Walter and Shea et al., 1998). On the other hand, dominant tundra plant communities like mosses and lichen are not represented in LPJmL (Appendix D4). All model optimizations experiments kept growing season albedo within reasonable ranges in comparison to MODIS albedo (Fig. D4). These results demonstrate an improved performance of optimized model parameter sets over prior model parameter sets and of LPJmL-GSI over LPJmL-OP regarding a cost that is defined based on 30 years of monthly FAPAR, mean annual GPP and 10 years of monthly vegetation albedo.

3.1.2 Parameter sensitivities and uncertainties

The uncertainty of productivity and albedo-related parameters was reduced after optimization of LPJmL-GSI in most PFTs while the reduction of the uncertainty of phenology-related parameters depended often on plant functional type (Fig. 5). Prior and posterior parameter values from each optimization experiment are listed in the Appendix (Tables D2 to D5).

Phenology controls and model-data integration

M. Forkel et al.

Title Page

Abstract

Introduction

Conclusions

References

Tables

Figures



Back

Close

Full Screen / Esc

Printer-friendly Version

Interactive Discussion



The parameter α_a (absorption of light at leaf level in relation to canopy level) was sensitive within a narrow parameter range for all PFTs. The posterior α_a parameter range was smaller than the uniform prior range in all PFTs. In all optimization experiments we found for the parameter α_a a gradient from high values in tropical to low values in boreal PFTs (Fig. D5). This pattern reflects the initial overestimation of mean annual GPP in temperate and boreal PFTs and underestimation of GPP in tropical regions with the prior parameter set of LPJmL-OP. Thus, the low α_a parameter values accounts for nitrogen limitation effects on productivity in boreal forests (Vitousek and Howarth, 1991) that are currently not considered in LPJmL. A future implementation of nitrogen limitation processes in LPJmL requires a re-optimization of the α_a parameter.

The leaf albedo parameter β_{leaf} was sensitive in all PFTs and the posterior β_{leaf} parameter range was smaller than the prior parameter range in evergreen PFTs. In these evergreen PFTs the β_{leaf} parameter was well constrained because albedo satellite observations are less affected by variations in background albedo (soil, snow) than in deciduous PFTs. In all other PFTs the β_{leaf} posterior parameter range was equal the prior parameter range or the optimized parameter value was close to a boundary of the prior parameter range. This result indicates that the albedo routines in LPJmL should consider variations in background albedo caused by changes in soil properties, soil moisture or snow conditions in order to accurately reproduce satellite-observed albedo time series (see supplementary discussion in Appendix D5). Nevertheless, the optimization of the leaf albedo parameter β_{leaf} resulted in values that differed especially between broadleaved and needle-leaved evergreen PFTs as well as herbaceous PFTs (Figs. 5 and D6). Low leaf albedo parameters in needle-leaved evergreen PFTs (TeNE and BoNE) and high leaf albedo parameters in broad-leaved summergreen and herbaceous PFTs agree well with the patterns reported by Cescatti et al. (2012).

The light extinction coefficient k was sensitive for all PFTs but the posterior parameter range was only in herbaceous PFTs and in the BoBS PFT smaller than the prior parameter range (Fig. 5). In all PFTs this parameter had a large spatial variability (Fig. D7). The parameter k affects mostly the FPC and thus the maximum FAPAR.

Phenology controls and model-data integration

M. Forkel et al.

Title Page

Abstract

Introduction

Conclusions

References

Tables

Figures



Back

Close

Full Screen / Esc

Printer-friendly Version

Interactive Discussion



Thus, this parameter cannot be well constrained for tree PFTs in the current optimization setup because the maximum FPC of trees was prescribed from the land and tree cover dataset. On the other hand, the maximum FPC of herbaceous PFTs was not prescribed from observations which resulted in narrow k posterior parameter ranges for herbaceous PFTs. The parameter k was optimized towards a very high value in the BoNS PFT ($k = 0.7$) due to high tree mortality rates after low-productivity years (Appendix D5). This parameter would result in a overestimated PFT coverage in model runs with dynamic vegetation. Thus, we performed a second optimization experiment for this PFT (blue in Fig. 5) where k_{BoNS} was limited to 0.65. This optimization experiment resulted in similar posterior values for the other parameters. Although the k parameter was well constrained for the TrH, TeH and PoH PFTs, these parameters cannot be used in the final parameter set of LPJmL-GSI. In dynamic vegetation model runs, the relatively low k parameter values for the TrH and TeH PFTs and relatively high values for the PoH PFT would result in an underestimation of herbaceous coverage in temperate and tropical climates and an overestimation of herbaceous coverage in boreal and polar climates, respectively. Therefore, we performed three more optimization experiments for herbaceous PFTs where we fixed k at 0.5 (blue in Fig. 5). These optimization experiments resulted in similar α_a parameters but different albedo parameters and phenology parameters in order to compensate for biases in FAPAR and albedo that were introduced by the fixed k parameter. Thus, the high spatial variability and the large uncertainty of the light extinction coefficient k require re-addressing this parameter in a model optimization setup with dynamic vegetation using tree and vegetation cover data or perhaps a replacement by a better representation of canopy architecture and radiative transfer.

The sensitivity and posterior uncertainty of phenology-related model parameters depended often on plant functional type. The parameter $\text{base}_{\text{tmin}}$ which controls the effect of cold temperature on phenology was sensitive in all PFTs except the TrBE and TrH PFTs. The posterior parameter range was smaller than the prior parameter range in temperate PFTs (TeNE, TeBS and TeH). The parameter $\text{base}_{\text{heat}}$ which controls the

effect of heat stress on phenology was sensitive in TrBR, TrH, TeH, BoNE and BoNS PFTs while in other PFTs this parameter was only sensitive towards the boundaries of the prior parameter range. Nevertheless, the posterior parameter range was only smaller than the prior parameter range in TrBR and TrH PFTs. The parameter $base_{light}$ was sensitive in temperate and boreal PFTs. In tropical PFTs this parameter is only sensitive above a certain threshold (i.e. 60 W m^{-2} for TrBE and 100 W m^{-2} for TrBR). The parameter $base_{water}$ was sensitive in all PFTs. The posterior parameter range of this parameter was smaller in all PFTs except in TeBS, BoNE, BoBS and BoNS PFTs. Although, the parameter $base_{water}$ had a large variability among PFTs, it was generally optimized towards higher values in PFTs that are presumably water-controlled (TrBR, TeBS, TrH, TeH) and optimized towards lower values in PFTs that are presumably less water controlled (TrBE, TeNE, BoNE, BoNS, PoH). This result indicates that FAPAR of water-controlled PFTs reacts already to small decreases in water availability whereas other PFTs react only to strong decreases in water availability. As the $base_{water}$ parameter was the only phenology parameter which was sensitive in all PFTs, indicates that water availability is the only phenological control that acts in all PFTs.

3.2 Global model evaluation

3.2.1 GPP, ET, biomass and tree cover

LPJmL-GSI and LPJmL-OP-gc with optimized parameters better represented global patterns of gross primary production, biomass and tree cover than LPJmL with original phenology and prior parameters (LPJmL-OP-prior) (Fig. 6). LPJmL-OP-prior overestimated mean annual GPP and biomass in most polar, boreal and temperate regions. LPJmL-OP-prior underestimated mean annual GPP but overestimated mean annual biomass in tropical regions around the Equator. These biases were reduced in LPJmL-OP-gc and LPJmL-GSI. LPJmL generally overestimated GPP also in arid regions but these biases were reduced after optimization in LPJmL-OP-gc and LPJmL-GSI (Fig. E1). We also found that the mean seasonal cycle of GPP from LPJmL-GSI

Phenology controls and model-data integration

M. Forkel et al.

Title Page

Abstract

Introduction

Conclusions

References

Tables

Figures



Back

Close

Full Screen / Esc

Printer-friendly Version

Interactive Discussion



Phenology controls and model-data integration

M. Forkel et al.

Title Page

Abstract

Introduction

Conclusions

References

Tables

Figures



Back

Close

Full Screen / Esc

Printer-friendly Version

Interactive Discussion



better agreed with the mean seasonal GPP cycle from the MTE estimate especially in temperate forests and in tropical, temperate and polar grasslands (Fig. E2) although no information about the seasonality of GPP was included in optimization experiments. LPJmL-GSI still overestimated biomass in some tropical regions (African Savannas, south-east Brazil, south and south-east Asia) (Fig. E3). These regions were mainly simulated as managed lands in LPJmL, i.e. as different crop functional types (CFTs). The LPJmL-GSI phenology module was not applied and no parameter optimization was performed for CFTs. Generally, LPJmL-GSI estimated global total carbon fluxes and stocks that were closer to data-oriented estimates than the estimates from LPJmL-OP-prior and LPJmL-OP-gc (Table E1, Appendix E1). These results demonstrate that besides the optimization of productivity parameters in LPJmL, the implementation of the new GSI-based phenology improved estimates of spatial patterns, seasonal dynamics, and global totals of gross primary production and biomass.

Evapotranspiration from LPJmL agreed well with the data-oriented MTE estimate. The implementation and optimization of the new GSI-based phenology did not affect much ET (Fig. 6b). Although LPJmL had lower mean annual ET than the data-oriented MTE estimate in tropical and boreal regions, it followed the global pattern of ET. We detected no major differences between the mean seasonal cycle of ET from LPJmL-OP and LPJmL-GSI (not shown). These results show that evapotranspiration was not sensitive to the implementation and optimization of the new GSI-based phenology model in LPJmL.

LPJmL-GSI with dynamic vegetation better represented spatial patterns of tree cover in high latitude regions than LPJmL-OP-prior and LPJmL-OP-gc (Fig. 6d). LPJmL-OP-prior highly overestimated tree cover in boreal and arctic regions and simulated a too northern arctic tree line in comparison with tree cover from MODIS observations. Although this overestimation was reduced after optimization, LPJmL-OP-gc still highly overestimated tree cover in boreal and temperate regions. The occurrence of trees was shifted southwards in LPJmL-GSI. Although LPJmL-GSI still overestimated tree cover in boreal regions, this overestimation was much lower than in LPJmL-OP-gc. LPJmL-

OP-prior and LPJmL-OP-gc slightly underestimated tree cover in temperate regions around 45° N but this was well reproduced by LPJmL-GSI. We found no differences in tree cover between LPJmL-OP and LPJmL-GSI in other parts of the world where tree cover is highly affected from agricultural land use and thus implicitly prescribed to LPJmL. These results demonstrate that additional to the optimization of productivity parameters in LPJmL-OP-gc, the newly developed GSI-based phenology model and the optimized model parameters contribute to a better representation of tree cover in high-latitude regions.

3.2.2 Improved spatial patterns of FAPAR

LPJmL with GSI-based phenology and optimized parameters better represents observed spatial patterns than LPJmL with original phenology module. LPJmL-OP-prior and LPJmL-OP-gc overestimated mean annual FAPAR in high-latitude regions of North America and Asia, in western North America, central Asia, the Mediterranean, China, the Sahel and in northern Australia (Fig. 7). These overestimations were removed in most regions in LPJmL-GSI. LPJmL-OP-gc and LPJmL-OP-prior overestimated FAPAR especially in wet boreal and arctic regions with mean annual temperatures < 0 °C in comparison to the GIMMS3g and GL2 VGT FAPAR datasets. Mean annual FAPAR from LPJmL-GSI was close to mean annual FAPAR from both datasets and within the uncertainty of the GL2 VGT FAPAR dataset under most climate conditions. Under wet temperate and tropical conditions all three model versions had mean annual FAPAR close to both datasets and within the uncertainty of the GL2 VGT FAPAR dataset. Mean annual FAPAR from the GIMMS3g and GL2 datasets clearly differed in dry regions. GIMMS3g had in dry regions higher FAPAR and outside the uncertainty estimate of the GL2 VGT dataset. Despite these differences of the datasets in dry regions, LPJmL-OP-prior and LPJmL-OP-gc clearly overestimated FAPAR in dry regions. Although LPJmL-GSI overestimated mean annual FAPAR in temperate dry regions, this overestimation was reduced in comparison to LPJmL-OP. In tropical dry regions mean annual FAPAR from LPJmL-GSI was within the range of the datasets. These results

Phenology controls and model-data integration

M. Forkel et al.

[Title Page](#)

[Abstract](#)

[Introduction](#)

[Conclusions](#)

[References](#)

[Tables](#)

[Figures](#)



[Back](#)

[Close](#)

[Full Screen / Esc](#)

[Printer-friendly Version](#)

[Interactive Discussion](#)



demonstrate that LPJmL required an improved phenology model to represent spatial patterns of mean annual FAPAR.

3.2.3 Improved seasonal to inter-annual FAPAR dynamics

LPJmL-GSI better reproduced seasonal cycles of FAPAR than LPJmL-OP in comparison to the GIMMS3g and GL2 VGT FAPAR datasets (Fig. 8). The mean seasonal cycle of FAPAR from LPJmL-GSI was higher correlated with both datasets than the mean seasonal cycle from LPJmL-OP in all PFTs. Only in the temperate broad-leaved evergreen PFT, LPJmL-OP had a higher correlation with the GIMMS3g dataset than LPJmL-GSI. Nevertheless, the mean seasonal cycle of both datasets was negatively correlated ($r = -0.48$) in this PFT, which suggests that the GIMMS3g FAPAR dataset has a wrong seasonality in this PFT because LPJmL-GSI agreed better with the GL2 FAPAR dataset ($r = 0.419$) than with the GIMMS3g dataset ($r = -0.131$). In boreal PFTs LPJmL-GSI was higher correlated with GIMMS3g FAPAR than with GL2 VGT FAPAR. In these boreal PFTs, LPJmL-OP simulated a too late end of the growing season. In temperate PFTs, LPJmL-OP simulated a too early spring onset. LPJmL-GSI better reproduced the spring onset and the end of the growing season in temperate and boreal PFTs than LPJmL-OP in comparison with the GIMMS3g FAPAR dataset. Nevertheless, GIMMS3g FAPAR has an earlier spring onset in temperate and boreal forest PFTs than the GL2 FAPAR dataset. As LPJmL-GSI was optimized against GIMMS3g FAPAR it reproduced the early spring onset of the GIMMS3g dataset. LPJmL-OP had a too long growing season in temperate and polar herbaceous PFTs because the end of the growing season is defined as fixed calendar date in LPJmL-OP. LPJmL-GSI does not depend on calendar dates but on environmental conditions and thus more appropriately reproduced the end of the growing season in herbaceous PFTs than LPJmL-OP.

LPJmL-GSI significantly better reproduced monthly FAPAR time series than LPJmL-OP in all PFTs in comparison with the GIMMS3g FAPAR dataset (Fig. 10). LPJmL-OP prior had low correlations with monthly GIMMS3g FAPAR in boreal forests of eastern Siberia, in the North American tundra, in temperate and tropical grasslands of central

Phenology controls and model-data integration

M. Forkel et al.

Title Page

Abstract

Introduction

Conclusions

References

Tables

Figures



Back

Close

Full Screen / Esc

Printer-friendly Version

Interactive Discussion



Phenology controls and model-data integration

M. Forkel et al.

Title Page

Abstract

Introduction

Conclusions

References

Tables

Figures



Back

Close

Full Screen / Esc

Printer-friendly Version

Interactive Discussion



Asia, North America, Australia and especially, in the Sahel (Fig. E4). LPJmL-GSI had higher correlation coefficients with GIMMS3g than LPJmL-OP in all these regions. Only in 11 % of the global land area LPJmL-OP-prior or LPJmL-OP-gc had a significantly higher correlation ($p < 0.05$, Fisher z -transformation) with monthly GIMMS3g FAPAR than LPJmL-GSI (Fig. 9a). These regions were located in agriculture-dominated grid cells in the central United States, eastern China and Argentina. In 10 % of the land area the correlation coefficient of all LPJmL versions was smaller than 0.2 compared to the GIMMS3g dataset. These grid cells were mostly located in the Amazon, the Kongo Basis and the Sunda Islands where FAPAR time series of tropical forests do not exhibit seasonal cycles and where optical satellite observations are often distorted from clouds. LPJmL-GSI better represents monthly FAPAR dynamics under all climate conditions than LPJmL-OP-prior or LPJmL-OP-gc (Fig. 9b). The correlation coefficient improved the most with LPJmL-GSI in boreal climates with mean annual air temperatures between -15°C and 0°C and in temperate and tropical dry regions with mean annual air temperatures $> 5^{\circ}\text{C}$. LPJmL-GSI had higher correlations with GIMMS3g FAPAR in boreal and cold temperate climates than the two datasets with each other. These results demonstrate that the implementation of a new phenology model in LPJmL was needed to appropriately simulate seasonal and long-term FAPAR dynamics globally.

LPJmL-GSI better reproduced annual time series of mean annual FAPAR (averaged for months $> 0^{\circ}\text{C}$ mean monthly temperature) than LPJmL-OP in many regions in comparison with the GIMMS3g FAPAR dataset (Fig. 10). Annual time series of mean annual FAPAR from LPJmL-GSI were in 20 % of all global land areas significant higher correlated with the GIMMS3g dataset than LPJmL-OP (Fig. 10a). In 40 % of the global land areas, LPJmL-GSI and LPJmL-OP-prior or LPJmL-OP-gc had equal correlations with mean annual GIMMS3g FAPAR. Only in 15 % of the global land area, LPJmL-OP had a higher correlation with mean annual GIMMS3g FAPAR than LPJmL-GSI. These regions were mostly located in agricultural regions in the eastern United States and in parts of South America and south-eastern Asia where an improvement because of the GSI-based phenology model was not expected. LPJmL-GSI better explained the

inter-annual variability of GIMMS3g FAPAR especially in grasslands (western United States, central Asia, the Sahel, southern Africa, and Australia) (Figure E5). Especially in these temperate and tropical dry regions, LPJmL-GSI had the highest improvements over LPJmL-OP regarding the inter-annual variability of FAPAR (Fig. 10b). Although the absolute correlation coefficients between mean annual FAPAR from LPJmL and GIMMS3g were relatively low under all climate conditions, LPJmL was in arctic, boreal and temperate climates usually higher correlated with the GIMMS3g dataset than the GIMMS3g dataset with the GL2 VGT dataset. Only in subtropical and tropical climates the two datasets were higher correlated with each other than LPJmL with the GIMMS3g FAPAR dataset. These results demonstrate that datasets have large difference in term of inter-annual variability of FAPAR but LPJmL-GSI can explain the inter-annual variability of the GIMMS3g FAPAR dataset especially in temperate and boreal forests and temperate and tropical grasslands.

3.2.4 Improved representation of FAPAR trends

LPJmL-GSI better represented observed trends and trend changes in mean annual FAPAR than LPJmL-OP-prior and LPJmL-OP-gc (Fig. 11). Spatial patterns of trend slopes from LPJmL-GSI were higher correlated with the GIMMS3g FAPAR dataset than from LPJmL-OP. LPJmL-OP and LPJmL-GSI both reproduced greening trends in tundra, boreal and temperate forests. Nevertheless, LPJmL-GSI had higher correlation coefficients with mean annual GIMMS3g FAPAR than LPJmL-OP in these regions. LPJmL-GSI reproduced observed browning trends in some parts of the boreal forests of North America that were not reproduced by LPJmL-OP. In the Sahel, LPJmL-OP simulated widespread browning trends while the GIMMS3g dataset shows greening trends. Although LPJmL-GSI still underestimated the area extent of greening in the Sahel, it reproduces the general greening in this region. These results demonstrate that the implementation of environmental controls like light, heat stress and water availability in the LPJmL-GSI phenology model contributed to better explain regional greening and browning trends.

Phenology controls and model-data integration

M. Forkel et al.

Title Page

Abstract

Introduction

Conclusions

References

Tables

Figures



Back

Close

Full Screen / Esc

Printer-friendly Version

Interactive Discussion



Phenology controls and model-data integration

M. Forkel et al.

[Title Page](#)

[Abstract](#)

[Introduction](#)

[Conclusions](#)

[References](#)

[Tables](#)

[Figures](#)



[Back](#)

[Close](#)

[Full Screen / Esc](#)

[Printer-friendly Version](#)

[Interactive Discussion](#)



identify phenological controls on seasonal FAPAR dynamics. The importance of phenological controls differed by climate regions, ecosystems and season (Fig. 12). We identified environmental controls on seasonal FAPAR dynamics by analyzing the mean seasonal cycles of FAPAR, of the cold temperature, light, water availability and heat stress limiting functions for phenology from the LPJmL-GSI model run. This analysis is comparable to previous investigations of limiting factors for vegetation phenology (e.g. Jolly et al., 2005; Caldararu et al., 2014). FAPAR seasonality in high-latitude regions (tundra, boreal forests) was mainly controlled by cold temperature (entire year) and light (October to February). We also found an important control by water availability in February to April in the tundra and in boreal forests of North America and eastern Siberia. This water limitation in early spring was due to the seasonal freezing of the upper permafrost layer in LPJmL. FAPAR seasonality in temperate grasslands in western North America and central Asia was controlled from a mixture of cold temperature (January to April), of water availability (May to November) and light (November to January). FAPAR seasonality in temperate forests in Europe was mainly limited by cold temperature in spring and by a combination of cold temperature and light in autumn. Additionally, heat stress and water availability contributed to a small reduction in summer FAPAR in temperate and boreal forests. The FAPAR seasonality in savannas (Sahel) was limited by water availability in the entire year and additionally by heat stress before the beginning of the rain season. The FAPAR seasonality of temperate regions in South America was limited by water availability in the entire year. Cold temperature was additionally limiting between May and September. Thus, water availability was the only environmental factor in LPJmL-GSI that controlled phenology globally from tropical to arctic biomes.

The implementation of the water limiting function on phenology in LPJmL-GSI resulted in unique patterns of phenological controls that were different from results reported in similar analyses (Jolly et al., 2005; Caldararu et al., 2014). LPJmL-GSI showed water limitation on phenology in many sub-tropical and dry temperate regions (especially Mediterranean, Pampas and Patagonia in South America, Mongolia, and

northern Great Plains). The original GSI model showed mainly temperature and light limitation in these regions. In contrast to the original GSI, we prescribe water limitations on phenological development as controlled by the plant available water and not on VPD (Jolly et al., 2005). As considered by Caldararu et al. (2014), soil water availability exerts a more direct control on phenology development, which has been demonstrated for Mediterranean ecosystems (Kramer et al., 2000; Richardson et al., 2013) and in dry temperate grasslands (Yuan et al., 2007; Liu et al., 2013).

Interestingly, Caldararu et al. (2014) identify leaf age as the dominant factor for phenology development in many permanent moist subtropical and tropical forests, but also in several water limited regions which were here identified as seasonally controlled by water availability. We cannot identify a dominant control on seasonal FAPAR dynamics in these regions, as leaf age is not explicitly simulated in LPJmL-GSI. We acknowledge that the consideration of leaf age effects on phenology would clearly further enhance the representation of ecosystem processes. However, the seasonal co-variation between LAI or FAPAR and environmental controls on phenology complicates the ability to disentangle the leaf aging signal from a temperature, light or water availability-driven signal, especially in seasonally deciduous vegetation types, where climate-driven models explain a significant fraction of seasonal variability and the realized age of leaves is shorter than a year. In addition, cloud cover contamination over the tropics pertain usually a weak seasonal signal and a high short-term variability, hinging on the reliability of the seasonal signal in moist tropical or subtropical forests. Especially, Morton et al. (2014) show that seasonal changes in MODIS LAI in the Amazon forests are linked to insufficient corrections of the sun-sensor geometry, which challenge the representation of vegetation phenology. However, in these tropical moist regions, where we find no environmental seasonal controls, and the realized age of oldest leaves are higher than a year, leaf age may be an important contributor for further consideration regarding the above-seasonal frequency of phenology. Hence, grasping the relevance of leaf longevity, especially in tropical perennial systems, would necessarily require ground observations of leaf development and litter fall to constrain leaf age parame-

BGD

11, 10917–11025, 2014

Phenology controls and model-data integration

M. Forkel et al.

[Title Page](#)

[Abstract](#)

[Introduction](#)

[Conclusions](#)

[References](#)

[Tables](#)

[Figures](#)



[Back](#)

[Close](#)

[Full Screen / Esc](#)

[Printer-friendly Version](#)

[Interactive Discussion](#)



ters, as well as measurements of soil water content to address the appropriateness of soil moisture effects.

5 Additionally, we identify water availability as an important limiting function for spring phenology in boreal and arctic regions in LPJmL-GSI because of the seasonal freezing of the upper active layer in permafrost soils. Although no relationships between active layer depth and vegetation greenness were found so far (Mcmichael et al., 1997), frozen grounds limit the seasonal tree growth in boreal forests because of limited water supply and nutrient uptake (Benninghoff, 1952; Jarvis and Linder, 2000). It also has been observed that the seasonal freezing in permafrost regions limits soil moisture and thus can contribute to drought conditions that regulate ecosystem evapotranspiration (Ohta et al., 2008) and that contribute to extreme fire events (Forkel et al., 2012). The seasonal regulation of soil moisture through freezing and thawing in permafrost regions contributes to spring leaf development in boreal summergreen forests. The heat stress limiting function was newly introduced in LPJmL-GSI. Heat stress had no importance for seasonal FAPAR dynamics in most regions except in temperate and tropical grasslands. The heat stress function was highly correlated with the water availability function in temperate grasslands. This suggests that summer FAPAR is both regulated by water-induced and temperature-induced drought conditions in temperate grasslands. In contrary, heat stress and water availability were driving seasonal FAPAR dynamics in temporal non-synchronized periods in tropical grasslands (Sahel). Whereas the FAPAR seasonality was driven by water availability in the entire year, heat stress regulated FAPAR seasonality only at the end of the dry season and before the beginning of the rain season. These results suggest that soil moisture needs to be considered in observational data analyses and in other ecosystem models as controlling factor for vegetation phenology in all biomes.

BGD

11, 10917–11025, 2014

Phenology controls and model-data integration

M. Forkel et al.

Title Page

Abstract

Introduction

Conclusions

References

Tables

Figures



Back

Close

Full Screen / Esc

Printer-friendly Version

Interactive Discussion



4 Conclusions

We have demonstrated a major improvement of the LPJmL dynamic global vegetation model by implementing a new set of phenological controls on vegetation greenness and by integrating multiple decadal satellite observations. We have proven that the original phenology model in LPJmL is unable to explain temporal dynamics of FAPAR. As an alternative we implemented a new phenology model (LPJmL-GSI) which considers effects of cold temperature, heat stress, light, and water availability on vegetation phenology. We developed a model-data integration approach for LPJmL (LPJmL-MDI) to (1) constrain model parameters against observations, (2) to directly integrate observed land cover fractions and burnt area time series and (3) to evaluate LPJmL against independent data streams. Specifically, phenology, productivity, and albedo-related model parameters of LPJmL-GSI were optimized jointly against 30 year time series of satellite observations of FAPAR, against 10 year time series of vegetation albedo and mean annual patterns of gross primary production using a genetic optimization algorithm.

The new phenology model and the parameter optimization clearly improved LPJmL model simulations. LPJmL-GSI better reproduces observed spatial patterns of gross primary production, tree cover, biomass and FAPAR than the original model. LPJmL-GSI simulates global total carbon stocks and fluxes that are closer to independent estimates than from the original model. LPJmL-GSI better represents observed seasonal, monthly, inter-annual and decadal FAPAR dynamics than the original model. Nevertheless, model optimization experiments and model evaluation demonstrated further weaknesses of LPJmL that might need to be improved in future studies. To more accurately simulate surface albedo in LPJmL it is necessary to implement time-varying effects of snow conditions and surface moisture on albedo. The optimization of the light extinction coefficient resulted in a large spatial variability and large parameter uncertainty. This model parameter needs to be addressed in future and perhaps needs to be replaced by a more enhanced representation of canopy architecture and canopy radiative transfer to improve simulations of tree coverage and peak FAPAR.

Phenology controls and model-data integration

M. Forkel et al.

[Title Page](#)

[Abstract](#)

[Introduction](#)

[Conclusions](#)

[References](#)

[Tables](#)

[Figures](#)



[Back](#)

[Close](#)

[Full Screen / Esc](#)

[Printer-friendly Version](#)

[Interactive Discussion](#)



Phenology controls and model-data integration

M. Forkel et al.

Title Page

Abstract

Introduction

Conclusions

References

Tables

Figures



Back

Close

Full Screen / Esc

Printer-friendly Version

Interactive Discussion



The improvements of LPJmL in representing observed patterns and temporal dynamics of vegetation greenness allows assessing environmental controls on vegetation phenology and greenness. Contrasting to previous studies (Jolly et al., 2005; Stöckli et al., 2011), our results indicate that soil water availability is a major control of seasonal FAPAR dynamics not only in water-limited biomes but also in boreal forests and the arctic tundra where water availability is regulated through seasonal thawing and freezing of the active permafrost layer. Until now phenology of these ecosystems was mostly considered as temperature-limited. The consideration of the effect of soil water availability on phenology in LPJmL improved model simulations of greening trends in the Sahel and of browning trends in boreal forests of North America. Our results demonstrate that improved phenology models that consider seasonal effects of water availability are needed in order to correctly explain seasonal to long-term dynamics in vegetation greenness.

Appendix A: LPJmL model details

A1 Original phenology model (LPJmL-OP)

The phenology model in the original LPJmL formulation has three different routines for summergreen (i.e. temperature-driven deciduous), evergreen (no seasonal variation) and rain-green (i.e. water-driven deciduous) PFTs (Sitch et al., 2003). Evergreen PFTs have a constant phenology status (Phen = 1). The daily phenology status of summergreen PFTs depends on growing degree-days (GDD):

$$\begin{aligned}\Delta T &= T - \text{GDD}_{\text{base}} \\ \text{GDD}_t &= \text{GDD}_{t-1} + \Delta T_t \quad \text{if } \Delta T > 0\end{aligned}\tag{A1}$$

Where T is the daily air temperature and GDD_{base} is the minimum temperature threshold to start counting GDDs. Daily GDD is scaled to the phenology status using a pa-

parameter ramp which is the amount of GDDs to get full leave cover:

$$\text{Phen}_{\text{PFT}|\text{summergreen}} = \begin{cases} \text{GDD}/\text{ramp} & \text{if } \text{aphen} < \text{aphen}_{\text{max}} \\ 0 & \text{if } \text{aphen} \geq \text{aphen}_{\text{max}} \\ 0 & \text{if } \text{aphen} > \text{aphen}_{\text{min}} \text{ and } \Delta T < 0 \end{cases} \quad (\text{A2})$$

The daily phenology status is set back to 0 if the accumulated phenology status (aphen) is larger than a parameter $\text{aphen}_{\text{max}}$ or if aphen is greater than $\text{aphen}_{\text{min}}$ and the daily temperature is below GDD_{base} . The daily accumulated phenology status is calculated as:

$$\text{aphen}_t = \text{aphen}_{t-1} + \text{Phen}_t \quad (\text{A3})$$

For rain-green PFTs the daily phenology status is calculated dependent on the daily water availability scaling factor Wscal in LPJmL (Appendix A2) (Gerten et al., 2004) and a threshold value ($\text{Wscal}_{\text{min}}$):

$$\text{Phen}_{\text{PFT}|\text{raingreen}} = \begin{cases} 1 & \text{if } \text{Wscal} \geq \text{Wscal}_{\text{min}} \\ 0 & \text{if } \text{Wscal} < \text{Wscal}_{\text{min}} \end{cases} \quad (\text{A4})$$

The phenology of rain-green PFTs has no smooth behaviour but is a binary switch between full leave cover and no leaves according to this formulation. For herbaceous PFTs the same phenology scheme like for summergreen PFTs is used but the phenology status is only set back to 0 at the end of the phenology year (i.e. on the 14th day of the year for the Northern Hemisphere and on the 195th day of the year for the Southern Hemisphere).

BGD

11, 10917–11025, 2014

Phenology controls and model-data integration

M. Forkel et al.

[Title Page](#)

[Abstract](#)

[Introduction](#)

[Conclusions](#)

[References](#)

[Tables](#)

[Figures](#)



[Back](#)

[Close](#)

[Full Screen / Esc](#)

[Printer-friendly Version](#)

[Interactive Discussion](#)



A2 Water availability scaling factor

The water availability scaling factor W_{scal} in LPJmL is a ratio between water supply S and atmospheric water demand D for a dry canopy (Gerten et al., 2004):

$$W_{scal} = \frac{S}{D} \quad (A5)$$

In the LPJmL-GSI phenology model the water availability scaling factor is expressed as a percentage value:

$$W = W_{scal} \times 100 \quad (A6)$$

Water supply is dependent on the maximum transpiration E_{max} under water saturation and relative soil moisture w_r (Gerten et al., 2004):

$$S = E_{max} \times w_r \quad (A7)$$

Atmospheric water demand D for a dry canopy is calculated from potential evapotranspiration PET, maximum Priestley–Taylor coefficient $\alpha_{max} = 1.391$, scaling canopy conductance $g_m = 3.26 \text{ mm s}^{-1}$ and potential canopy conductance g_{pot} (Gerten et al., 2004):

$$D = \frac{PET \times \alpha_{max}}{1 + (g_m/g_{pot})} \quad (A8)$$

A3 Albedo

Surface albedo and snow coverage routines have been implemented in LPJmL to use it as a land surface scheme in a coupled vegetation-climate model (Strengers et al., 2010). We used this implementation but made the albedo parameters PFT-dependent as albedo differs between ecosystems (Cescatti et al., 2012). The albedo of a grid cell

Alb_{gc} is the area-weighted sum of the vegetation albedo Alb_{veg} , bare-soil albedo Alb_{bare} and snow albedo:

$$Alb_{gc} = Alb_{veg} + F_{bare} \times (F_{snow} \times \beta_{snow} + (1 - F_{snow}) \times \beta_{soil}) \quad (A9)$$

5 where F_{bare} and F_{snow} are the coverage of bare soil and snow on top of bare soil in a grid cell and β_{soil} and β_{snow} are the soil and snow albedo parameters, respectively. The parameters $\beta_{soil} = 0.4$ and $\beta_{snow} = 0.7$ were used as constants (Strengers et al., 2010) and not further considered in this study. Although soil and snow albedo has clear spatial and temporal variations which are due to changing moisture contents, an improvement of these processes is not within the scope of our study. The vegetation
10 albedo is computed as the albedo of each PFT Alb_{PFT} and its corresponding FPC:

$$Alb_{veg} = \sum_{PFT=1}^{PFT=n} Alb_{PFT} \times FPC_{PFT} \quad (A10)$$

The albedo of a PFT depends on the fraction of the PFT that is completely covered
15 by snow $F_{snow, PFT}$ and the albedo of the PFT without snow coverage ($Alb_{PFT, nosnow}$) (Strengers et al., 2010):

$$Alb_{PFT} = F_{snow, PFT} \times \beta_{snow} + (1 - F_{snow, PFT}) \times Alb_{PFT, nosnow} \quad (A11)$$

The albedo of a PFT without snow coverage is the sum of leaf, stem/branches and litter
20 (background) albedo:

$$Alb_{PFT, nosnow} = Alb_{leaf, PFT} + Alb_{stem, PFT} + Alb_{litter, PFT} \quad (A12)$$

The albedo of green leaves depends on the foliar projective cover, the daily phenology status and the PFT-dependent leaf albedo parameter:

$$25 \quad Alb_{leaf, PFT} = FPC_{PFT} \times Phen_{PFT} \times \beta_{leaf, PFT} \quad (A13)$$

**Phenology controls
and model-data
integration**

M. Forkel et al.

Title Page	
Abstract	Introduction
Conclusions	References
Tables	Figures
◀	▶
◀	▶
Back	Close
Full Screen / Esc	
Printer-friendly Version	
Interactive Discussion	



The albedo of stems and branches depends on the fractional coverage of the ground by stems and branches (c_{stem}) and a PFT-dependent stem albedo parameter $\beta_{\text{stem, PFT}}$:

$$\text{Alb}_{\text{stem, PFT}} = \text{FPC}_{\text{PFT}} \times (1 - \text{Phen}_{\text{PFT}}) \times c_{\text{stem}} \times \beta_{\text{stem, PFT}} \quad (\text{A14})$$

- 5 The parameter $c_{\text{stem}} = 0.7$ (Strengers et al., 2010) was used as a constant and not further considered in this study. The background (i.e. litter) albedo of a PFT depends additionally on a PFT-dependent litter albedo parameter $\beta_{\text{litter, PFT}}$:

$$\text{Alb}_{\text{litter, PFT}} = \text{FPC}_{\text{PFT}} \times (1 - \text{Phen}_{\text{PFT}}) \times (1 - c_{\text{stem}}) \times \beta_{\text{litter, PFT}} \quad (\text{A15})$$

- 10 The parameters $\beta_{\text{leaf, PFT}}$, $\beta_{\text{stem, PFT}}$ and $\beta_{\text{litter, PFT}}$ were implemented as PFT-dependent albedo parameters which differs from the previous implementation (Strengers et al., 2010). The fraction of snow in the green part of the canopy that is used to compute FAPAR (Eq. 3) depends on the daily phenological status and the fraction of the PFT that is covered by snow:

$$15 F_{\text{snow, gv, PFT}} = \text{Phen}_{\text{PFT}} \times F_{\text{snow, PFT}} \quad (\text{A16})$$

The fraction of the PFT that is covered by snow depends on snow height and the daily calculated snow water equivalent (Strengers et al., 2010).

Appendix B: FAPAR datasets

20 B1 Comparison of the Geoland2 and GIMMS3g FAPAR datasets

We compared the Geoland2 and GIMMS3g FAPAR datasets to assess (1) the agreement of two newly developed FAPAR products and (2) to evaluate the suitability of these products for the optimization of FAPAR and phenology-related parameters in LPJmL. We found important differences between the Geoland2 and GIMMS3g FAPAR datasets

Phenology controls and model-data integration

M. Forkel et al.

Title Page

Abstract

Introduction

Conclusions

References

Tables

Figures



Back

Close

Full Screen / Esc

Printer-friendly Version

Interactive Discussion



during our analyses. The differences are mostly related to inter-annual variability and trends.

The GL2 FAPAR dataset had a higher inter-annual variability in most regions especially in northern Russia, central North America, Africa and eastern Australia (Fig. B1).

Despite the different amplitudes of inter-annual variability, the temporal dynamic of annual aggregated FAPAR values was well correlated in most regions (Fig. B2). Nevertheless, in some regions like in the North American Tundra, in parts of the Siberian boreal forest and in the tropical forests the inter-annual temporal FAPAR dynamic was weakly or even negatively correlated (Fig. B2).

The temporal dynamics of mean annual FAPAR agreed relatively well between GIMMS3g FAPAR and GL2 FAPAR in the AVHRR period. The temporal dynamic of mean annual FAPAR agreed poorly between GIMMS3g and GL2 FAPAR in the VGT period. Both datasets had higher biases in boreal needle-leaved evergreen forests (Fig. B3). An offset between the GL2 AVHRR and GL VGT FAPAR time series in the overlapping years 1999 and 2000 is evident in all biomes. Additionally, the GL2 VGT time series shows an abrupt jump from 2002 to 2003. Because of these reasons, the Geoland2 FAPAR dataset cannot be used for a long-term analysis of FAPAR trends and extremes.

B2 Estimation of uncertainty for the GIMMS3g FAPAR dataset

The GIMMS3g FAPAR dataset was used for parameter optimization. For parameter optimization it is necessary to consider data uncertainty in multiple data stream cost functions. Unfortunately, the GIMMS3g dataset has no uncertainty estimates. On the other hand the GL2 FAPAR dataset has uncertainty estimates but time series are not well harmonized. Thus we were using the GIMMS3g dataset for parameter optimization but estimated uncertainties by using regression to the uncertainty of the GL2 FAPAR dataset (Fig. B4). Therefore we fitted for each month polynomial quantile regressions to the quantile 0.95 between FAPAR and FAPAR uncertainty from the GL2 VGT FA-

BGD

11, 10917–11025, 2014

Phenology controls and model-data integration

M. Forkel et al.

Title Page

Abstract

Introduction

Conclusions

References

Tables

Figures



Back

Close

Full Screen / Esc

Printer-friendly Version

Interactive Discussion



PAR dataset. Then we were using these regressions to estimate uncertainties for the GIMMS3g FAPAR dataset.

Appendix C: Land cover

C1 Creation of an observation-based map of plant functional types

5 Land cover maps from remote sensing products are not directly comparable with plant functional types in global vegetation models because they are using different legends for the description of vegetation (Jung et al., 2006; Poulter et al., 2011a). Land cover classes have to be reclassified into the corresponding PFTs. We were using the SYNMAP land cover map (Jung et al., 2006), the Köppen–Geiger climate classification (Kottek et al., 2006) and tree coverage from MODIS (Townshend et al., 2011). We decided to use the SYNMAP land cover map because it offers fractional land coverage and synergizes already the GLCC, MODIS and GLC2000 land cover maps (Jung et al., 2006). PFTs in LPJmL are defined according to biome (tropical, temperate or boreal), leaf type (needle leaved, broadleaved) and phenology (summergreen, evergreen, rain green). We extracted the biome information from the Köppen–Geiger climate classification whereas leaf type and phenology were extracted from the SYNMAP land cover map. The FPC of a PFT was derived from MODIS tree cover.

15 In a first step, we reclassified the Köppen–Geiger climate classification in to bioclimatic zones (biomes) that correspond to the definition used in LPJmL (Fig. C1). This reclassification followed to a large extent the rules of Poulter et al. (2011a):

- The climate zone A was reclassified to the tropical biome.
- The climate regions BWh and BSh were reclassified to the tropical biome.
- The climate regions BWk and BSk were reclassified to the temperate biome.
- The climate region Cw was reclassified to the tropical biome.

Phenology controls and model-data integration

M. Forkel et al.

Title Page

Abstract

Introduction

Conclusions

References

Tables

Figures



Back

Close

Full Screen / Esc

Printer-friendly Version

Interactive Discussion



- The climate regions Cf and Cs were reclassified to the temperate biome.
- The climate regions *D* and *E* were reclassified to the boreal biome.

In a second step, we created a land cover map with PFT legend by crossing the land cover information from SYNMAP with the map of biomes following rules for each tree PFT:

- TrBE: EBF (evergreen broadleaved forest) AND tropical biome
- TrBR: DBF (deciduous broadleaved forest) AND tropical biome
- TeNE: ENF (evergreen needleleaved forest) AND temperate biome
- TeBE: EBF (evergreen broadleaved forest) AND temperate biome
- TeBS: DBF (deciduous broadleaved forest) AND temperate biome
- BoNE: ENF (evergreen needleleaved forest) AND boreal biome
- BoBS: DBF (deciduous broadleaved forest) AND boreal biome
- BoNS: DNF (deciduous needleleaved forest) AND boreal biome

Although we translated in this step the land cover classes into PFTs, the fractions represent still fraction of land cover and not FPC. For example, a grid cell can be covered by 100 % forest but this forest contains only 70 % trees while the rest is covered by herbaceous plants. This difference becomes evident by comparing the total coverage of forest land cover classes from SYNMAP with tree cover from MODIS (Fig. C2). MODIS tree cover is always lower than forest cover but shows more spatial variability.

In a third step, we need to correct the land cover fraction with tree cover to create a map of FPC. Thus, we calculated the FPC of each tree PFT by correcting the land

Phenology controls and model-data integration

M. Forkel et al.

[Title Page](#)

[Abstract](#)

[Introduction](#)

[Conclusions](#)

[References](#)

[Tables](#)

[Figures](#)



[Back](#)

[Close](#)

[Full Screen / Esc](#)

[Printer-friendly Version](#)

[Interactive Discussion](#)



cover fraction of a PFT (LC_{PFT}) with the ratio of fractional tree coverage from MODIS (F_{Tree}) and the total land coverage of all 8 forest PFTs:

$$FPC_{PFT} = LC_{PFT} \times \frac{F_{Tree}}{\sum_{PFT=1}^{PFT=8} LC_{PFT}} \quad (C1)$$

5 This calculation of FPC differs from the approach of Poulter et al. (2011a) who divided each land cover class in fixed fractions of tree and herbaceous PFTs.

In the last step we need to calculate the FPC of herbaceous PFTs:

$$FPC_{herb} = 1 - F_{Tree} - LC_{Barren} - LC_{Water} - LC_{Snow/Ice} \quad (C2)$$

10 which is the residual area by removing the fractional tree coverage from MODIS and the land cover fractions of bare soil and rocks, water and permanent snow and ice from the total grid cell. Thus, grasslands, croplands and shrub lands were assigned to herbaceous vegetation. Then we divided the herbaceous FPC into the TeH, PoH and TrH PFTs according to biomes:

- 15 – TrH: FPC_{herb} AND tropical biome
- Old TeH: FPC_{herb} AND temperate OR boreal biome

The TeH was further splitted in a new temperate herbaceous and a polar herbaceous PFT to separate between temperate grasslands and tundra:

- TeH (new): old TeH AND temperate OR boreal biome AND boreal trees < 0.3
- 20 – PoH: old TeH AND (boreal biome OR Koeppen–Geiger E climate) AND boreal trees > 0.3

These steps yielded in observation-based maps of foliar projective cover for each PFT (Fig. C3). As the input data (SYNMAP and MODIS VCF) is based on satellite data from the years 2000/2001 the retrieved maps reflect the distribution of PFTs of the year 2000.

25

Phenology controls and model-data integration

M. Forkel et al.

Title Page	
Abstract	Introduction
Conclusions	References
Tables	Figures
⏪	⏩
◀	▶
Back	Close
Full Screen / Esc	
Printer-friendly Version	
Interactive Discussion	



C2 Comparison of simulated and observed PFT distributions

We compared the observation-based PFT map with the simulated PFT distribution from LPJmL-OP for the year 2000. LPJmL with dynamic vegetation simulated usually too high tree and too low herbaceous cover in all regions (Fig. C4). In the central tropical forests (Amazon, Kongo basin) LPJmL simulated too low cover of TrBE but too high cover of TrBR. The coverage of BoNE was too low in some regions in North America and Eastern Siberia. The simulated distribution of BoNS did not agree much with the observed distribution which is almost limited to eastern Siberia. Tree cover was especially overestimated in regions with only sparse tree cover (Savannahs, Steppe/boreal forest transition, eastern Siberia). The extent of boreal forest PFTs (BoNE, BoBS, BoNS) is generally too large with far southward extensions into the Steppe and northward extensions into the Tundra.

As expected, the prescription of the observed PFT maps into LPJmL generally improved the representation of the observed PFT distributions (Fig. C4). The spatial patterns of PFT distributions were highly correlated and the bias in comparison to the observed distribution was clearly reduced in comparison with the model run with dynamic vegetation. The PFT distribution of the LPJmL model run with prescribed land cover does not perfectly agree with the observed PFT distribution which is due to the applied prescription approach. Tree PFTs can have a lower FPC in LPJmL than the prescribed FPC value because the trees are still growing or because mortality reduced the FPC. This effect especially happened in the BoNE PFT where fire reduced the FPC in large regions in Canada and eastern Siberia (Fig. C4). Herbaceous PFTs can have a higher FPC than the observed FPC value because these PFTs were allowed to establish the entire grid cell (except the fraction that is barren, water or permanent snow/ice in the observations). This happened for example when fires burnt tree PFTs and herbaceous PFTs succeeded afterwards in LPJmL. This is the reason for the overestimation of herbaceous coverage in large regions in Canada and eastern Siberia where the BoNE PFT was underestimated (Fig. C4). In summary, the prescription of

BGD

11, 10917–11025, 2014

Phenology controls and model-data integration

M. Forkel et al.

Title Page

Abstract

Introduction

Conclusions

References

Tables

Figures



Back

Close

Full Screen / Esc

Printer-friendly Version

Interactive Discussion



land cover improved the representation of observed spatial patterns of PFTs in LPJmL. Differences to the observed PFT distribution are due to the desired ability of LPJmL to represent important processes of vegetation dynamics like mortality processes.

Appendix D: Model parameter optimization

D1 Parameter definitions and values

This section documents the LPJmL parameters that were addressed in this study. The parameters and their use in the model are described in Table D1. The information sources from which prior parameter values were extracted for each optimization experiment are shown in Fig. D1. Tables D2–D5 list prior and posterior parameter values of each optimization experiment according to the logical flow of optimization experiments indicated in Fig. D1.

D2 Genetic optimization algorithm

We were using a genetic optimization algorithm to minimize the cost function $J(\mathbf{d})$ by optimizing the scaled parameter vector \mathbf{d} . The GENOUD algorithm (genetic optimization using derivatives) (Mebane and Sekhon, 2011) combines global genetic optimization search with local gradient-based search algorithms. In genetic optimization algorithms, each model parameter is called a gene and each parameter set is called an individual. The fitness of this individual is the cost of the model against the observations. At the beginning of the optimization, a first generation of individuals is initialized by random sampling of parameter sets within the prescribed parameter ranges. After the calculation of the cost of all individuals of the first generation, a next generation is generated by cloning the best individuals, by mutating the genes or by crossing different individuals (Mebane and Sekhon, 2011). This results after some generations in a set of individuals with highest fitness, i.e. parameter sets with minimized cost. Within

Phenology controls and model-data integration

M. Forkel et al.

Title Page

Abstract

Introduction

Conclusions

References

Tables

Figures



Back

Close

Full Screen / Esc

Printer-friendly Version

Interactive Discussion



the GENOUD algorithm we were using also the BFGS (Broyden–Fletcher–Goldfarb–Shanno) gradient search algorithm (Broyden, 1970; Fletcher, 1970; Goldfarb, 1970; Shanno, 1970) to find an optimum parameter set. An optimized parameter set of the BFGS algorithm is used as individual in the next generation. The BFGS gradient search algorithm was first applied on the best individual of the second last generation to avoid a too fast convergence of the optimization algorithm towards a local optimum. For grid cell-based optimization experiments we were applying the GENOUD algorithm with at least 20 generations and a population size of 1000 individuals per generation, i.e. at least 20 000 single model runs. For PFT-level optimization experiments we were applying the GENOUD algorithm with at least 15 generations and a population size of at least 700 individuals per generation, i.e. at least 10 500 single model runs.

D3 Parameter sensitivities and uncertainties

To explore the sensitivity and uncertainty of LPJmL-GSI parameters after PFT-level optimizations, we computed the likelihood L and Akaike's Information Criterion AIC from the cost J of each individual (i.e. parameter set d) of the genetic optimization:

$$L = e^{-J(d)} \quad (D1)$$

$$\text{AIC} = 2 \times n - 2 \times \log(L) \quad (D2)$$

Where n is the number of parameters. The optimum parameter set has the highest likelihood and the lowest AIC. Then, we selected only these individuals with an AIC difference dAIC of < 2 in comparison to the best parameter set:

$$\text{dAIC} = \text{AIC} - \text{AIC}_{\text{best}} \quad (D3)$$

Parameter sets or model formulations with an AIC difference < 2 are usually considered as equally plausible like the best parameter set (Burnham and Anderson, 2002, p. 70). The relationship between likelihood and the value of each parameter provides

Phenology controls and model-data integration

M. Forkel et al.

Title Page

Abstract

Introduction

Conclusions

References

Tables

Figures



Back

Close

Full Screen / Esc

Printer-friendly Version

Interactive Discussion



both a qualitative insight in the uncertainty of parameters as expressed by the parameter range and in the parameter sensitivity as expressed by the maximum likelihood at each parameter value.

D4 Supporting results and discussion on optimization performance

5 The optimization of LPJmL-OP and LPJmL-GSI resulted in a significant reduction of the cost in comparison to the respective prior models although there were differences between plant functional types (Fig. D2). LPJmL-OP with prior parameters had high costs especially in herbaceous PFTs (TrH and TeH) and in the boreal needle-leaved summer green PFT (BoNS). The optimization of single grid cells in LPJmL-OP resulted
10 in a significant reduction of the cost in all PFTs ($p \leq 0.01$, Wilcoxon rank-sum test) despite the polar herbaceous and tropical herbaceous PFTs. The global prior parameter set of LPJmL-GSI resulted in a significant lower cost than the grid cell-level optimized parameter sets of LPJmL-OP in TrH, TeBS, BoNS and PoH PFTs. The optimization of single grid cells in LPJmL-GSI resulted in a significant reduction of the cost in all
15 PFTs except BoNS and PoH. PFT-level optimizations of LPJmL-GSI resulted in a significant lower cost than the LPJmL-GSI prior parameter set in all PFTs except TeBE, BoNS and PoH. PFT-level optimizations of LPJmL-GSI resulted in a significant lower cost than the standard LPJmL-OP prior parameter set in all PFTs except TeNE. These results demonstrate an improved overall performance of optimized model parameter sets over prior model parameter sets and of LPJmL-GSI over LPJmL-OP regarding
20 a cost that is defined based on 30 years of monthly FAPAR, mean annual GPP and 10 years of monthly vegetation albedo.

Model optimization experiments resulted in a significant reduction of the annual GPP bias of LPJmL in comparison to the MTE data-oriented GPP product (Fig. D3). LPJmL-OP with prior parameters underestimated mean annual GPP in the TrBE PFT (median
25 Pbias -13%) and overestimated mean annual GPP in all other PFTs (up to 123% median Pbias in TeH). Grid cell-level optimization experiments of LPJmL-OP resulted in a significant reduction of the GPP bias in all PFTs except in the PoH PFT. Especially

Phenology controls and model-data integration

M. Forkel et al.

[Title Page](#)

[Abstract](#)

[Introduction](#)

[Conclusions](#)

[References](#)

[Tables](#)

[Figures](#)



[Back](#)

[Close](#)

[Full Screen / Esc](#)

[Printer-friendly Version](#)

[Interactive Discussion](#)



Phenology controls and model-data integration

M. Forkel et al.

[Title Page](#)

[Abstract](#)

[Introduction](#)

[Conclusions](#)

[References](#)

[Tables](#)

[Figures](#)



[Back](#)

[Close](#)

[Full Screen / Esc](#)

[Printer-friendly Version](#)

[Interactive Discussion](#)



in the TrBE, TrBR, TrH, TeNE, TeBE, TeBS and BoBS PFTs the bias of mean annual GPP of LPJmL was removed almost completely (i.e. Pbias within 5%). The LPJmL-GSI prior parameter set had significant lower biases of mean annual GPP than the prior parameter set of LPJmL-OP. This was because the median of each parameter from the OP.gc experiments was used as prior parameter for LPJmL-GSI. Grid cell-level optimization experiments of LPJmL-GSI resulted in significant reductions of the bias in mean annual GPP in most PFTs despite PFTs where the LPJmL-GSI prior parameter set resulted already in GPP biases close to 0 (i.e. TrH, TeBE and PoH). PFT-level optimization experiments of LPJmL-GSI resulted in significant lower biases of mean annual GPP than the prior parameter set of LPJmL-OP in all PFTs except PoH. These results demonstrate that through the applied model optimization biases in mean annual GPP were significantly reduced in all PFTs (except PoH) in LPJmL-OP as well as in LPJmL-GSI.

We were not able to remove the GPP bias and to reduce the cost of LPJmL-OP and of LPJmL-GSI in the PoH PFT (tundra) in optimization experiments because of inconsistencies between the FAPAR and GPP datasets or in the LPJmL formulation. Although a complete removal of the GPP bias is in principle possible by adjusting the α_a parameter, this would result in a too low FPC of the PoH PFT. Such a low FPC cannot explain the relatively high peak FAPAR values that are seen in the GIMMS3g FAPAR dataset in Tundra regions. It is not possible to explain the low mean annual MTE GPP and the relatively high GIMMS3g peak FAPAR with the current LPJmL model structure in tundra regions. The reasons for this mismatch can be caused by inconsistencies between the GPP and FAPAR datasets or by an insufficient model formulation. The MTE data-oriented GPP product has been upscaled from FLUXNET eddy covariance measurements (Jung et al., 2011). Nevertheless, not many eddy covariance measurement sites cover tundra regions with mean annual air temperatures $< 0^\circ\text{C}$. Thus, the MTE GPP estimates are not well supported by measurements in tundra regions. But also the FAPAR dataset might be more uncertain in tundra regions than in other parts of the globe. Optical remote sensing in high-latitude regions is usually performed under

Phenology controls and model-data integration

M. Forkel et al.

Title Page

Abstract

Introduction

Conclusions

References

Tables

Figures



Back

Close

Full Screen / Esc

Printer-friendly Version

Interactive Discussion



high-sun zenith angles. Radiation can penetrate deeper into vegetation under high-sun zenith angles which results in higher FAPAR (Tao et al., 2009; Walter-Shea et al., 1998). Thus, the high FAPAR values in the GIMMS3g FAPAR dataset might be caused by satellite observations under high-sun zenith angles. Finally, the inconsistencies between GPP and FAPAR might be also caused by an inappropriate representation of tundra plant communities in LPJmL. The PoH PFT in LPJmL was derived from a grass PFT but does not include shrubs or the large functional diversity of mosses and lichen that are the dominant plant communities in tundra ecosystems (Porada et al., 2013). We currently cannot decide if the inconsistency between FAPAR and GPP in our optimization of productivity and FAPAR parameters in tundra regions is more caused by the specific properties of the datasets or by an insufficient model structure.

All optimization experiments resulted in reasonable albedo biases of LPJmL-OP and LPJmL-GSI in comparison with monthly MODIS albedo time series (Fig. D4). LPJmL-OP with prior parameters overestimated growing season albedo in all PFTs. Grid cell-level optimization experiments of LPJmL-OP resulted in significant reductions of the bias in growing season albedo in TrBE, TeNE, TeBE, TeBS, BoNE, and BoNS PFTs but not in TrBR, TrH, TeH, BoBS and PoH PFTs. The bias in growing season albedo of the latter PFTs was significantly reduced with the LPJmL-GSI prior parameter set. The optimization of LPJmL-GSI for single grid cells significantly reduced the bias in growing season albedo in comparison to the LPJmL-GSI prior parameter set in all PFTs except in the TeH, BoNS and PoH PFTs. These results demonstrate that model optimizations experiments kept growing season albedo within reasonable ranges in comparison to MODIS albedo.

D5 Supporting results and discussion on parameter variability

The optimization of the leaf albedo parameter β_{leaf} resulted in values that differed especially between broadleaved and needle-leaved evergreen PFTs (Fig. D6). Needle-leaved evergreen PFTs (TeNE and BoNE) had in all optimization experiments the lowest β_{leaf} parameter values while the broad-leaved summergreen PFTs (TeBS and

Phenology controls and model-data integration

M. Forkel et al.

Title Page

Abstract

Introduction

Conclusions

References

Tables

Figures



Back

Close

Full Screen / Esc

Printer-friendly Version

Interactive Discussion



BoBS) had the highest β_{leaf} parameter values. After the PFT-level optimization of LPJmL-GSI herbaceous PFTs had high β_{leaf} parameters. The leaf albedo parameter β_{leaf} was sensitive in all PFTs (Fig. 5). The optimization resulted in many PFTs in leaf and litter albedo parameters that were close to the boundaries of the prior parameter ranges (Fig. 5). This indicates missing environmental controls on surface albedo. The albedo routines of LPJmL need to be further improved to account for moisture-driven changes in surface albedo. Such improved albedo routines would allow a more accurate and constrained estimation of albedo parameters. Because of these current limitations in the LPJmL albedo routines, albedo simulations in regions or time periods with low vegetation cover need to be assessed with care.

The light extinction coefficient k had a large spatial variability in all PFTs and in both grid cell-level optimization experiments of LPJmL-OP and LPJmL-GSI (Fig. D7). The spatial variability was lower after grid cell-level optimization experiments of LPJmL-GSI than after grid cell-level optimization experiments of LPJmL-OP. The largest variability was found in evergreen PFTs (TrBE, TeBE, TeNE and BoNE). This result demonstrates that unique or PFT-dependent light extinction coefficient parameter values are not meaningful. Moreover, the spatial variability of the light extinction coefficient needs to be analyzed more detailed and perhaps replaced by a more advanced representation of canopy architecture.

The highest values of the light extinction coefficient were found in the BoNS PFT. This was caused by an overestimation of tree mortality in years with simulated low productivity. Trees are killed in LPJmL as a result of negative net primary production which reduces FPC and results in a lower peak FAPAR in the following year. Having occurred more often in the simulated time period, it can explain why FAPAR is underestimated in some years. To remove these biases, the light extinction coefficient was optimized towards higher values in the BoNS PFT to reach FAPAR values that are closer to the observed FAPAR values after low-productivity years. However, such high values for the light extinction coefficient would overestimate tree cover and FAPAR under average conditions and when LPJmL is applied with dynamic vegetation. The approach to

certainty. All three version of LPJmL were within these uncertainties. LPJmL-GSI estimated global total biomass the closest to the data-oriented estimates. From Table E1 it is obvious that LPJmL with the model settings as in (Schaphoff et al., 2013) (i.e. without the BoNS and PoH PFTs and with simulated fire activity) resulted in global total GPP and ecosystem respiration that were even closer to the data-oriented estimates. This is mostly because LPJmL simulates larger burnt areas than seen in the observations and thus higher fire emissions but lower GPP and ecosystem respiration.

Acknowledgements. We thank Maarten Braakhekke and Enrico Tomelleri for testing model optimization algorithms. We thank Ulrich Weber for his assistance in data processing. We thank Ranga Myneni and Frédéric Baret for their comments on FAPAR datasets. We thank the IT departments at MPI-BGC Jena and PIK Potsdam for providing and maintaining the respective high performance computing infrastructures.

We gratefully thank the following researchers, groups and institutes for producing, providing and hosting their datasets:

- Compton Tucker, Jorge Pinzon, Ranga Myneni and the GIMMS group for the GIMMS FPAR3g dataset
- INRA, CNES and VITO for the Geoland2 FAPAR dataset
- Martin Jung for the MTE GPP and ET data, and the SYNMAP land cover map
- Sassan Saatchi for the tropical forest biomass map
- Markus Kottek, Franz Rubel and the University of Veterinary Medicine Vienna for providing the Koeppen–Geiger climate map
- Louis Giglio and Guido Van der Werf for providing the GFED database
- Jennifer L. Northway and Gary Schmunk for compiling the Alaska Large Fire Database
- Natural Resources Canada for providing the Canada National Fire Database
- Phil Jones, Ian Harris and the CRU research unit for providing the CRU climate dataset
- ECMWF for ERA-Interim climate reanalysis data.

Matthias Forkel received funding from the Max Planck Institute for Biogeochemistry and from the European Commission's 7th Framework Programme project CARBONES (grant agreement

Phenology controls and model-data integration

M. Forkel et al.

Title Page

Abstract

Introduction

Conclusions

References

Tables

Figures



Back

Close

Full Screen / Esc

Printer-friendly Version

Interactive Discussion



242316). Matthias Forkel conducted this work under the International Max Planck Research School for Global Biogeochemical Cycles.

The service charges for this open access publication have been covered by the Max Planck Society.

5 References

Anav, A., Murray-Tortarolo, G., Friedlingstein, P., Sitch, S., Piao, S., and Zhu, Z.: Evaluation of land surface models in reproducing satellite derived leaf area index over the high-latitude Northern Hemisphere, Part II: Earth system models, *Remote Sens.*, 5, 3637–3661, doi:10.3390/rs5083637, 2013.

Archibald, S. and Scholes, R. J.: Leaf green-up in a semi-arid African savanna – separating tree and grass responses to environmental cues, *J. Veg. Sci.*, 18, 583–594, 2007.

Atzberger, C., Klisch, A., Mattiuzzi, M., and Vuolo, F.: Phenological metrics derived over the European continent from NDVI3g data and MODIS time series, *Remote Sens.*, 6, 257–284, doi:10.3390/rs6010257, 2013.

Baret, F., Weiss, M., Lacaze, R., Camacho, F., Makhmara, H., Pacholczyk, P., and Smets, B.: GEOV1: LAI and FAPAR essential climate variables and FCOVER global time series capitalizing over existing products, Part 1: Principles of development and production, *Remote Sens. Environ.*, 137, 299–309, doi:10.1016/j.rse.2012.12.027, 2013.

Barichivich, J., Briffa, K. R., Myneni, R. B., Osborn, T. J., Melvin, T. M., Ciais, P., Piao, S., and Tucker, C.: Large-scale variations in the vegetation growing season and annual cycle of atmospheric CO₂ at high northern latitudes from 1950 to 2011, *Glob. Change Biol.*, 19, 3167–3183, doi:10.1111/gcb.12283, 2013.

Barichivich, J., Briffa, K. R., Myneni, R., van der Schrier, G., Dorigo, W., Tucker, C. J., Osborn, T. J., and Melvin, T. M.: Temperature and snow-mediated moisture controls of summer photosynthetic activity in northern terrestrial ecosystems between 1982 and 2011, *Remote Sens.*, 6, 1390–1431, doi:10.3390/rs6021390, 2014.

Beck, P. S. A. and Goetz, S. J.: Satellite observations of high northern latitude vegetation productivity changes between 1982 and 2008: ecological variability and regional differences, *Environ. Res. Lett.*, 6, 45501–45501, 2011.

BGD

11, 10917–11025, 2014

Phenology controls and model-data integration

M. Forkel et al.

Title Page

Abstract

Introduction

Conclusions

References

Tables

Figures

⏪

⏩

◀

▶

Back

Close

Full Screen / Esc

Printer-friendly Version

Interactive Discussion



Phenology controls and model-data integration

M. Forkel et al.

Title Page

Abstract

Introduction

Conclusions

References

Tables

Figures



Back

Close

Full Screen / Esc

Printer-friendly Version

Interactive Discussion



- Beck, P. S. A., Juday, G. P., Alix, C., Barber, V. A., Winslow, S. E., Sousa, E. E., Heiser, P., Herriges, J. D., and Goetz, S. J.: Changes in forest productivity across Alaska consistent with biome shift, *Ecol. Lett.*, 14, 373–379, doi:10.1111/j.1461-0248.2011.01598.x, 2011.
- Beer, C., Reichstein, M., Tomelleri, E., Ciais, P., Jung, M., Carvalhais, N., Rödenbeck, C., Arain, M. A., Baldocchi, D., Bonan, G. B., Bondeau, A., Cescatti, A., Lasslop, G., Lindroth, A., Lomas, M., Luysaert, S., Margolis, H., Oleson, K. W., Rouspard, O., Veenendaal, E., Viovy, N., Williams, C., Woodward, F. I., and Papale, D.: Terrestrial gross carbon dioxide uptake: global distribution and covariation with climate, *Science*, 329, 834–838, doi:10.1126/science.1184984, 2010.
- Benninghoff, W. S.: Interaction of vegetation and soil frost phenomena, *Arctic*, 5, 34–44, 1952.
- Berner, L. T., Beck, P. S. A., Bunn, A. G., Lloyd, A. H., and Goetz, S. J.: High-latitude tree growth and satellite vegetation indices: correlations and trends in Russia and Canada (1982–2008), *J. Geophys. Res.-Biogeo.*, 116, doi:10.1029/2010jg001475, 2011.
- Berner, L. T., Beck, P. S. A., Bunn, A. G., and Goetz, S. J.: Plant response to climate change along the forest-tundra ecotone in northeastern Siberia, *Glob. Change Biol.*, 19, 3449–3462, doi:10.1111/gcb.12304, 2013.
- Blok, D., Sass-Klaassen, U., Schaepman-Strub, G., Heijmans, M. M. P. D., Sauren, P., and Berendse, F.: What are the main climate drivers for shrub growth in Northeastern Siberian tundra?, *Biogeosciences*, 8, 1169–1179, doi:10.5194/bg-8-1169-2011, 2011.
- Bolstad, P. V. and Gower, S. T.: Estimation of leaf area index in fourteen southern Wisconsin forest stands using a portable radiometer, *Tree Physiol.*, 7, 115–124, 1990.
- Bondeau, A., Smith, P. C., Zaehle, S., Schaphoff, S., Lucht, W., Cramer, W., Gerten, D., Lotze-Campen, H., Müller, C., Reichstein, M., and Smith, B.: Modelling the role of agriculture for the 20th century global terrestrial carbon balance, *Glob. Change Biol.*, 13, 679–706, 2007.
- Broyden, C. G.: The convergence of a class of double-rank minimization algorithms, 1. General considerations, *IMA J. Appl. Math.*, 6, 76–90, doi:10.1093/imamat/6.1.76, 1970.
- Bunn, A. G. and Goetz, S. J.: Trends in satellite-observed circumpolar photosynthetic activity from 1982 to 2003: the influence of seasonality, cover type, and vegetation density, *Earth Interact.*, 10, 1–19, doi:10.1175/ei190.1, 2006.
- Bunn, A. G., Goetz, S. J., Kimball, J. S., and Zhang, K.: Northern High-Latitude Ecosystems Respond to Climate Change, *Eos Trans. Am. Geophys. Union*, 88, 333–333, doi:10.1029/2007eo340001, 2007.

Phenology controls and model-data integration

M. Forkel et al.

Title Page

Abstract

Introduction

Conclusions

References

Tables

Figures



Back

Close

Full Screen / Esc

Printer-friendly Version

Interactive Discussion



Burnham, K. P. and Anderson, D. R.: Model selection and multimodel inference a practical information-theoretic approach, Springer, New York, available at: <http://site.ebrary.com/id/10047705> (last Access: 17 December 2013), 2002.

Caldararu, S., Palmer, P. I., and Purves, D. W.: Inferring Amazon leaf demography from satellite observations of leaf area index, *Biogeosciences*, 9, 1389–1404, doi:10.5194/bg-9-1389-2012, 2012.

Caldararu, S., Purves, D. W., and Palmer, P. I.: Phenology as a strategy for carbon optimality: a global model, *Biogeosciences*, 11, 763–778, doi:10.5194/bg-11-763-2014, 2014.

Cescatti, A., Marcolla, B., Santhana Vannan, S. K., Pan, J. Y., Román, M. O., Yang, X., Ciais, P., Cook, R. B., Law, B. E., Matteucci, G., Migliavacca, M., Moors, E., Richardson, A. D., Seufert, G., and Schaaf, C. B.: Intercomparison of MODIS albedo retrievals and in situ measurements across the global FLUXNET network, *Remote Sens. Environ.*, 121, 323–334, doi:10.1016/j.rse.2012.02.019, 2012.

CFS (Canadian Forest Service): Canadian National Fire Database. Canadian Wildland Fire Information System, available at: <http://cwfis.cfs.nrcan.gc.ca/ha/nfdb>, 2012.

Chapin, F. S., Sturm, M., Serreze, M. C., McFadden, J. P., Key, J. R., Lloyd, A. H., McGuire, A. D., Rupp, T. S., Lynch, A. H., Schimel, J. P., Beringer, J., Chapman, W. L., Epstein, H. E., Euskirchen, E. S., Hinzman, L. D., Jia, G., Ping, C.-L., Tape, K. D., Thompson, C. D. C., Walker, D. A., and Welker, J. M.: Role of land-surface changes in arctic summer warming, *Science*, 310, 657–660, doi:10.1126/science.1117368, 2005.

De Jong, R., Verbesselt, J., Schaepman, M. E., and Bruin, S.: Trend changes in global greening and browning: contribution of short-term trends to longer-term change, *Glob. Change Biol.*, 18, 642–655, doi:10.1111/j.1365-2486.2011.02578.x, 2011.

De Jong, R., Verbesselt, J., Zeileis, A., and Schaepman, M.: Shifts in global vegetation activity trends, *Remote Sens.*, 5, 1117–1133, doi:10.3390/rs5031117, 2013.

Dee, D. P., Uppala, S. M., Simmons, A. J., Berrisford, P., Poli, P., Kobayashi, S., Andrae, U., Balmaseda, M. A., Balsamo, G., Bauer, P., Bechtold, P., Beljaars, A. C. M., van de Berg, L., Bidlot, J., Bormann, N., Delsol, C., Dragani, R., Fuentes, M., Geer, A. J., Haimberger, L., Healy, S. B., Hersbach, H., Hólm, E. V., Isaksen, L., Kòallberg, P., Köhler, M., Matricardi, M., McNally, A. P., Monge-Sanz, B. M., Morcrette, J. J., Park, B. K., Peubey, C., de Rosnay, P., Tavolato, C., Thépaut, J. N., and Vitart, F.: The ERA-interim reanalysis: configuration and performance of the data assimilation system, *Q. J. Roy. Meteor. Soc.*, 137, 553–597, doi:10.1002/qj.828, 2011.

Phenology controls and model-data integration

M. Forkel et al.

Title Page

Abstract

Introduction

Conclusions

References

Tables

Figures



Back

Close

Full Screen / Esc

Printer-friendly Version

Interactive Discussion



Fensholt, R. and Proud, S. R.: Evaluation of Earth Observation based global long term vegetation trends – comparing GIMMS and MODIS global NDVI time series, *Remote Sens. Environ.*, 119, 131–147, doi:10.1016/j.rse.2011.12.015, 2012.

Fensholt, R., Sandholt, I., and Rasmussen, M. S.: Evaluation of MODIS LAI, fAPAR and the relation between fAPAR and NDVI in a semi-arid environment using in situ measurements, *Remote Sens. Environ.*, 91, 490–507, doi:10.1016/j.rse.2004.04.009, 2004.

Fensholt, R., Rasmussen, K., Kaspersen, P., Huber, S., Horion, S., and Swinnen, E.: Assessing land degradation/recovery in the African Sahel from long-term earth observation based primary productivity and precipitation relationships, *Remote Sens.*, 5, 664–686, doi:10.3390/rs5020664, 2013.

Fletcher, R.: A new approach to variable metric algorithms, *Comput. J.*, 13, 317–322, doi:10.1093/comjnl/13.3.317, 1970.

Forbes, B. C., Macias Fauria, M., and Zetterberg, P.: Russian Arctic warming and “greening” are closely tracked by tundra shrub willows, *Glob. Change Biol.*, 16, 1542–1554, 2010.

Forkel, M., Thonicke, K., Beer, C., Cramer, W., Bartalev, S., and Schimmlius, C.: Extreme fire events are related to previous-year surface moisture conditions in permafrost-underlain larch forests of Siberia, *Environ. Res. Lett.*, 7, 044021, doi:10.1088/1748-9326/7/4/044021, 2012.

Forkel, M., Carvalhais, N., Verbesselt, J., Mahecha, M., Neigh, C., and Reichstein, M.: Trend change detection in NDVI time series: effects of inter-annual variability and methodology, *Remote Sens.*, 5, 2113–2144, doi:10.3390/rs5052113, 2013.

Frames: Alaska Large Fire Database, available at: <http://www.frames.gov/rcs/10000/10465.html>, 2012.

Friedlingstein, P., Cox, P., Betts, R., Bopp, L., von Bloh, W., Brovkin, V., Cadule, P., Doney, S., Eby, M., Fung, I., Bala, G., John, J., Jones, C., Joos, F., Kato, T., Kawamiya, M., Knorr, W., Lindsay, K., Matthews, H. D., Raddatz, T., Rayner, P., Reick, C., Roeckner, E., Schnitzler, K.-G., Schnur, R., Strassmann, K., Weaver, A. J., Yoshikawa, C., and Zeng, N.: Climate–carbon cycle feedback analysis: results from the C⁴ MIP model intercomparison, *J. Climate*, 19, 3337–3353, doi:10.1175/JCLI3800.1, 2006.

Galvez, D. A., Landhäusser, S. M., and Tyree, M. T.: Root carbon reserve dynamics in aspen seedlings: does simulated drought induce reserve limitation?, *Tree Physiol.*, 31, 250–257, 2011.

Phenology controls and model-data integration

M. Forkel et al.

Title Page

Abstract

Introduction

Conclusions

References

Tables

Figures



Back

Close

Full Screen / Esc

Printer-friendly Version

Interactive Discussion



Gamon, J. A., Field, C. B., Goulden, M. L., Griffin, K. L., Hartley, E., Joel, G., Peñuelas, J., and Valentini, R.: Relationships between NDVI, canopy structure, and photosynthesis in three Californian vegetation types, *Ecol. Appl.*, 5, 28–41, 1995.

Gerten, D., Schaphoff, S., Haberlandt, U., Lucht, W., and Sitch, S.: Terrestrial vegetation and water balance – hydrological evaluation of a dynamic global vegetation model, *J. Hydrol.*, 286, 249–270, 2004.

Giglio, L., Randerson, J. T., van der Werf, G. R., Kasibhatla, P. S., Collatz, G. J., Morton, D. C., and DeFries, R. S.: Assessing variability and long-term trends in burned area by merging multiple satellite fire products, *Biogeosciences*, 7, 1171–1186, doi:10.5194/bg-7-1171-2010, 2010.

Goetz, S. J., Bunn, A. G., Fiske, G. J., and Houghton, R. A.: Satellite-observed photosynthetic trends across boreal North America associated with climate and fire disturbance, *P. Natl. Acad. Sci. USA.*, 102, 13521–13525, 2005.

Goldfarb, D.: A family of variable-metric methods derived by variational means, *Math. Comput.*, 24, 23–26, doi:10.1090/S0025-5718-1970-0258249-6, 1970.

Harris, I., Jones, P. D., Osborn, T. J., and Lister, D. H.: Updated high-resolution grids of monthly climatic observations – the CRU TS3.10 dataset, *Int. J. Climatol.*, doi:10.1002/joc.3711, 2013.

Høgda, K. A., Karlsen, S. R., and Solheim, I.: Climatic change impact on growing season in Fennoscandia studied by a time series of NOAA AVHRR NDVI data, in: *Geoscience and Remote Sensing Symposium, 2001, IGARSS '01, IEEE 2001 International*, vol. 3, 1338–1340 vol. 3, 2001.

Høgda, K. A., Tømmervik, H., and Karlsen, S. R.: Trends in the start of the growing season in Fennoscandia 1982–2011, *Remote Sens.*, 5, 4304–4318, doi:10.3390/rs5094304, 2013.

Jarvis, P. and Linder, S.: Botany: constraints to growth of boreal forests, *Nature*, 405, 904–905, doi:10.1038/35016154, 2000.

Jiang, Y. and Huang, B.: Physiological responses to heat stress alone or in combination with drought: a comparison between tall fescue and perennial ryegrass, *Hortscience*, 36, 682–686, 2001.

Jolly, W. M., Nemani, R., and Running, S. W.: A generalized, bioclimatic index to predict foliar phenology in response to climate, *Glob. Change Biol.*, 11, 619–632, doi:10.1111/j.1365-2486.2005.00930.x, 2005.

Phenology controls and model-data integration

M. Forkel et al.

Title Page

Abstract

Introduction

Conclusions

References

Tables

Figures



Back

Close

Full Screen / Esc

Printer-friendly Version

Interactive Discussion



Jung, M., Henkel, K., Herold, M., and Churkina, G.: Exploiting synergies of global land cover products for carbon cycle modeling, *Remote Sens. Environ.*, 101, 534–553, doi:10.1016/j.rse.2006.01.020, 2006.

Jung, M., Verstraete, M., Gobron, N., Reichstein, M., Papale, D., Bondeau, A., Robustelli, M., and Pinty, B.: Diagnostic assessment of European gross primary production, *Glob. Change Biol.*, 14, 2349–2364, doi:10.1111/j.1365-2486.2008.01647.x, 2008.

Jung, M., Reichstein, M., Margolis, H. A., Cescatti, A., Richardson, A. D., Arain, M. A., Arneeth, A., Bernhofer, C., Bonal, D., Chen, J., Gianelle, D., Gobron, N., Kiely, G., Kutsch, W., Lasslop, G., Law, B. E., Lindroth, A., Merbold, L., Montagnani, L., Moors, E. J., Papale, D., Sottocornola, M., Vaccari, F., and Williams, C.: Global patterns of land-atmosphere fluxes of carbon dioxide, latent heat, and sensible heat derived from eddy covariance, satellite, and meteorological observations, *J. Geophys. Res.*, 116, G00J07–G00J07, doi:10.1029/2010jg001566, 2011.

Kaminski, T., Knorr, W., Scholze, M., Gobron, N., Pinty, B., Giering, R., and Mathieu, P.-P.: Consistent assimilation of MERIS FAPAR and atmospheric CO₂ into a terrestrial vegetation model and interactive mission benefit analysis, *Biogeosciences*, 9, 3173–3184, doi:10.5194/bg-9-3173-2012, 2012.

Kasischke, E. S., Williams, D., and Barry, D.: Analysis of the patterns of large fires in the boreal forest region of Alaska, *Int. J. Wildland Fire*, 11, 131–144, 2002.

Keeling, C. D., Chin, J. F. S., and Whorf, T. P.: Increased activity of northern vegetation inferred from atmospheric CO₂ measurements, *Nature*, 382, 146–149, doi:10.1038/382146a0, 1996.

Kelley, D. I., Prentice, I. C., Harrison, S. P., Wang, H., Simard, M., Fisher, J. B., and Willis, K. O.: A comprehensive benchmarking system for evaluating global vegetation models, *Biogeosciences*, 10, 3313–3340, doi:10.5194/bg-10-3313-2013, 2013.

Kira, T., Shinokazi, K., and Hozumi, K.: Structure of forest canopies as related to their primary productivity, *Plant Cell Physiol.*, 10, 129–142, 1969.

Knorr, W., Kaminski, T., Scholze, M., Gobron, N., Pinty, B., Giering, R., and Mathieu, P. P.: Carbon cycle data assimilation with a generic phenology model, *J. Geophys. Res.*, 115, G04017, doi:10.1029/2009jg001119, 2010.

Kottek, M., Grieser, J., Beck, C., Rudolf, B., and Rubel, F.: World map of the Köppen–Geiger climate classification updated, *Meteorol. Z.*, 15, 259–263, doi:10.1127/0941-2948/2006/0130, 2006.

Phenology controls and model-data integration

M. Forkel et al.

Title Page

Abstract

Introduction

Conclusions

References

Tables

Figures



Back

Close

Full Screen / Esc

Printer-friendly Version

Interactive Discussion



Kramer, K., Leinonen, I., and Loustau, D.: The importance of phenology for the evaluation of impact of climate change on growth of boreal, temperate and Mediterranean forests ecosystems: an overview, *Int. J. Biometeorol.*, 44, 67–75, 2000.

Lehsten, V., Tansey, K., Balzter, H., Thonicke, K., Spessa, A., Weber, U., Smith, B., and Ar-
neth, A.: Estimating carbon emissions from African wildfires, *Biogeosciences*, 6, 349–360,
doi:10.5194/bg-6-349-2009, 2009.

Liu, H., Tian, F., Hu, H. C., Hu, H. P., and Sivapalan, M.: Soil moisture controls on patterns of
grass green-up in Inner Mongolia: an index based approach, *Hydrol. Earth Syst. Sci.*, 17,
805–815, doi:10.5194/hess-17-805-2013, 2013.

Loranty, M. M., Goetz, S. J., and Beck, P. S. A.: Tundra vegetation effects on pan-Arctic albedo,
Environ. Res. Lett., 6, 024014, doi:10.1088/1748-9326/6/2/024014, 2011.

Lucht, W., Schaaf, C. B., and Strahler, A. H.: An algorithm for the retrieval of albedo
from space using semiempirical BRDF models, *IEEE T. Geosci. Remote*, 38, 977–998,
doi:10.1109/36.841980, 2000.

Lucht, W., Prentice, I. C., Myneni, R. B., Sitch, S., Friedlingstein, P., Cramer, W., Bousquet, P.,
Buermann, W., and Smith, B.: Climatic control of the high-latitude vegetation greening trend
and pinatubo effect, *Science*, 296, 1687–1689, doi:10.1126/science.1071828, 2002.

Mann, H. B.: Nonparametric tests against trend, *Econometrica*, 13, 245–259, 1945.

Mcmichael, C. E., Hope, A. S., Stow, D. A., and Fleming, J. B.: The relation between active
layer depth and a spectral vegetation index in arctic tundra landscapes of the North Slope of
Alaska, *Int. J. Remote Sens.*, 18, 2371–2382, doi:10.1080/014311697217666, 1997.

Mebane, W. R. and Sekhon, J. S.: Genetic optimization using derivatives?: the rgenoud Pack-
age for R, *J. Stat. Softw.*, 42, 2011.

Migliavacca, M., Meroni, M., Busetto, L., Colombo, R., Zenone, T., Matteucci, G., Manca, G.,
and Seufert, G.: Modeling gross primary production of agro-forestry ecosystems by assim-
ilation of satellite-derived information in a process-based model, *Sensors*, 9, 922–942, 2009.

Migliavacca, M., Galvagno, M., Cremonese, E., Rossini, M., Meroni, M., Sonnentag, O.,
Cogliati, S., Manca, G., Diotri, F., Busetto, L., Cescatti, A., Colombo, R., Fava, F., Morra
di Cella, U., Pari, E., Siniscalco, C., and Richardson, A. D.: Using digital repeat photography
and eddy covariance data to model grassland phenology and photosynthetic CO₂ uptake,
Agr. Forest Meteorol., 151, 1325–1337, doi:10.1016/j.agrformet.2011.05.012, 2011.

Monsi, M. and Saeki, T.: Über den Lichtfaktor in den Pflanzengesellschaften und seine Bedeu-
tung für die Stoffproduktion, *Jpn. J. Bot.*, 14, 22–52, 1953.

Phenology controls and model-data integration

M. Forkel et al.

Title Page

Abstract

Introduction

Conclusions

References

Tables

Figures



Back

Close

Full Screen / Esc

Printer-friendly Version

Interactive Discussion



Morton, D. C., Nagol, J., Carabajal, C. C., Rosette, J., Palace, M., Cook, B. D., Vermote, E. F., Harding, D. J., and North, P. R. J.: Amazon forests maintain consistent canopy structure and greenness during the dry season, *Nature*, advance online publication, doi:10.1038/nature13006, 2014.

5 Murray-Tortarolo, G., Anav, A., Friedlingstein, P., Sitch, S., Piao, S., Zhu, Z., Poulter, B., Zaehle, S., Ahlström, A., Lomas, M., Levis, S., Viovy, N., and Zeng, N.: Evaluation of land surface models in reproducing satellite-derived LAI over the high-latitude Northern Hemisphere. Part I: Uncoupled DGVMs, *Remote Sens.*, 5, 4819–4838, doi:10.3390/rs5104819, 2013.

10 Myers-Smith, I. H., Forbes, B. C., Wilmsking, M., Hallinger, M., Lantz, T., Blok, D., Tape, K. D., Macias-Fauria, M., Sass-Klaassen, U., Lévesque, E., Boudreau, S., Ropars, P., Hermanutz, L., Trant, A., Collier, L. S., Weijers, S., Rozema, J., Rayback, S. A., Schmidt, N. M., Schaeppman-Strub, G., Wipf, S., Rixen, C., Ménard, C. B., Venn, S., Goetz, S., Andreu-Hayles, L., Elmendorf, S., Ravolainen, V., Welker, J., Grogan, P., Epstein, H. E., and Hik, D. S.: Shrub expansion in tundra ecosystems: dynamics, impacts and research priorities, *Environ. Res. Lett.*, 6, 045509–045509, doi:10.1088/1748-9326/6/4/045509, 2011.

15 Myneni, R. B. and Williams, D. L.: On the relationship between FAPAR and NDVI, *Remote Sens. Environ.*, 49, 200–211, doi:10.1016/0034-4257(94)90016-7, 1994.

Myneni, R. B., Hall, F. G., Sellers, P. J., and Marshak, A. L.: The interpretation of spectral vegetation indexes, *IEEE T. Geosci. Remote*, 33, 481–486, doi:10.1109/36.377948, 1995.

20 Myneni, R. B., Keeling, C. D., Tucker, C. J., Asrar, G., and Nemani, R. R.: Increased plant growth in the northern high latitudes from 1981 to 1991, *Nature*, 386, 698–702, doi:10.1038/386698a0, 1997a.

Myneni, R. B., Ramakrishna, R., Nemani, R., and Running, S. W.: Estimation of global leaf area index and absorbed par using radiative transfer models, *IEEE T. Geosci. Remote*, 35, 1380–1393, doi:10.1109/36.649788, 1997b.

25 Ohta, T., Maximov, T. C., Dolman, A. J., Nakai, T., van der Molen, M. K., Kononov, A. V., Maximov, A. P., Hiyama, T., Iijima, Y., Moors, E. J., Tanaka, H., Toba, T., and Yabuki, H.: Interannual variation of water balance and summer evapotranspiration in an eastern Siberian larch forest over a 7-year period (1998–2006), *Agr. Forest Meteorol.*, 148, 1941–1953, 2008.

30 Piao, S., Wang, X., Ciais, P., Zhu, B., Wang, T., and Liu, J.: Changes in satellite-derived vegetation growth trend in temperate and boreal Eurasia from 1982 to 2006, *Glob. Change Biol.*, 17, 3228–3239, doi:10.1111/j.1365-2486.2011.02419.x, 2011.

Phenology controls and model-data integration

M. Forkel et al.

Title Page

Abstract

Introduction

Conclusions

References

Tables

Figures



Back

Close

Full Screen / Esc

Printer-friendly Version

Interactive Discussion



- Poirier, M., Durand, J.-L., and Volaire, F.: Persistence and production of perennial grasses under water deficits and extreme temperatures: importance of intraspecific vs. interspecific variability, *Glob. Change Biol.*, 18, 3632–3646, doi:10.1111/j.1365-2486.2012.02800.x, 2012.
- Porada, P., Weber, B., Elbert, W., Pöschl, U., and Kleidon, A.: Estimating global carbon uptake by lichens and bryophytes with a process-based model, *Biogeosciences*, 10, 6989–7033, doi:10.5194/bg-10-6989-2013, 2013.
- Potter, C. S., Klooster, S., and Brooks, V.: Interannual variability in terrestrial net primary production: exploration of trends and controls on regional to global scales, *Ecosystems*, 2, 36–48, doi:10.1007/s100219900056, 1999.
- Poulter, B., Ciais, P., Hodson, E., Lischke, H., Maignan, F., Plummer, S., and Zimmermann, N. E.: Plant functional type mapping for earth system models, *Geosci. Model Dev.*, 4, 993–1010, doi:10.5194/gmd-4-993-2011, 2011a.
- Poulter, B., Frank, D. C., Hodson, E. L., and Zimmermann, N. E.: Impacts of land cover and climate data selection on understanding terrestrial carbon dynamics and the CO₂ airborne fraction, *Biogeosciences*, 8, 2027–2036, doi:10.5194/bg-8-2027-2011, 2011b.
- Prentice, I. C., Bondeau, A., Cramer, W., Harrison, S. P., Hickler, T., Lucht, W., Sitch, S., Smith, B., and Sykes, M. T.: Dynamic global vegetation modeling: quantifying terrestrial ecosystem responses to large-scale environmental change, in: *Terrestrial Ecosystems in a Changing World*, edited by: Canadell, J. G., Pataki, D. E., and Pitelka, L. F., Springer, Berlin, Heidelberg, 175–192, available at: http://link.springer.com/chapter/10.1007/978-3-540-32730-1_15 (last access: 6 January 2014), 2007.
- Raynolds, M. K., Walker, D. A., Verbyla, D., and Munger, C. A.: Patterns of change within a tundra landscape: 22-year landsat NDVI trends in an area of the northern foothills of the Brooks Range, Alaska, *Arct. Antarct. Alp. Res.*, 45, 249–260, doi:10.1657/1938-4246-45.2.249, 2013.
- Richardson, A. D., Anderson, R. S., Arain, M. A., Barr, A. G., Bohrer, G., Chen, G., Chen, J. M., Ciais, P., Davis, K. J., Desai, A. R., Dietze, M. C., Dragoni, D., Garrity, S. R., Gough, C. M., Grant, R., Hollinger, D. Y., Margolis, H. A., McCaughey, H., Migliavacca, M., Monson, R. K., Munger, J. W., Poulter, B., Raczka, B. M., Ricciuto, D. M., Sahoo, A. K., Schaefer, K., Tian, H., Vargas, R., Verbeeck, H., Xiao, J., and Xue, Y.: Terrestrial biosphere models need better representation of vegetation phenology: results from the North American Carbon Program Site Synthesis, *Glob. Change Biol.*, 18, 566–584, doi:10.1111/j.1365-2486.2011.02562.x, 2012.

Phenology controls and model-data integration

M. Forkel et al.

Title Page

Abstract

Introduction

Conclusions

References

Tables

Figures



Back

Close

Full Screen / Esc

Printer-friendly Version

Interactive Discussion



- Richardson, A. D., Keenan, T. F., Migliavacca, M., Ryu, Y., Sonnentag, O., and Toomey, M.: Climate change, phenology, and phenological control of vegetation feedbacks to the climate system, *Agr. Forest Meteorol.*, 169, 156–173, doi:10.1016/j.agrformet.2012.09.012, 2013.
- Rost, S., Gerten, D., Bondeau, A., Lucht, W., Rohwer, J., and Schaphoff, S.: Agricultural green and blue water consumption and its influence on the global water system, *Water Resour. Res.*, 44, W09405, doi:10.1029/2007wr006331, 2008.
- Saatchi, S. S., Harris, N. L., Brown, S., Lefsky, M., Mitchard, E. T. A., Salas, W., Zutta, B. R., Buermann, W., Lewis, S. L., Hagen, S., Petrova, S., White, L., Silman, M., and Morel, A.: Benchmark map of forest carbon stocks in tropical regions across three continents, *P. Natl. Acad. Sci. USA*, 108, 9899–9904, doi:10.1073/pnas.1019576108, 2011.
- Schaaf, C. B., Gao, F., Strahler, A. H., Lucht, W., Li, X., Tsang, T., Strugnell, N. C., Zhang, X., Jin, Y., Muller, J.-P., Lewis, P., Barnsley, M., Hobson, P., Disney, M., Roberts, G., Dunderdale, M., Doll, C., d'Entremont, R. P., Hu, B., Liang, S., Privette, J. L., and Roy, D.: First operational BRDF, albedo nadir reflectance products from MODIS, *Remote Sens. Environ.*, 83, 135–148, doi:10.1016/S0034-4257(02)00091-3, 2002.
- Schaphoff, S., Heyder, U., Ostberg, S., Gerten, D., Heinke, J., and Lucht, W.: Contribution of permafrost soils to the global carbon budget, *Environ. Res. Lett.*, 8, 014026, 2013.
- Shanno, D. F.: Conditioning of quasi-Newton methods for function minimization, *Math. Comput.*, 24, 647–656, doi:10.1090/S0025-5718-1970-0274029-X, 1970.
- Sitch, S., Smith, B., Prentice, I. C., Arneth, A., Bondeau, A., Cramer, W., Kaplan, J. O., Levis, S., Lucht, W., Sykes, M. T., Thonicke, K., and Venevsky, S.: Evaluation of ecosystem dynamics, plant geography and terrestrial carbon cycling in the LPJ dynamic global vegetation model, *Glob. Change Biol.*, 9, 161–185, 2003.
- Sitch, S., Huntingford, C., Gedney, N., Levy, P. E., Lomas, M., Piao, S. L., Betts, R., Ciais, P., Cox, P., Friedlingstein, P., Jones, C. D., Prentice, I. C., and Woodward, F. I.: Evaluation of the terrestrial carbon cycle, future plant geography and climate-carbon cycle feedbacks using five Dynamic Global Vegetation Models (DGVMs), *Glob. Change Biol.*, 14, 2015–2039, doi:10.1111/j.1365-2486.2008.01626.x, 2008.
- Stöckli, R., Rutishauser, T., Dragoni, D., O'Keefe, J., Thornton, P. E., Jolly, M., Lu, L., and Denning, A. S.: Remote sensing data assimilation for a prognostic phenology model, *J. Geophys. Res.*, 113, G04021–G04021, 2008.

Phenology controls and model-data integration

M. Forkel et al.

Title Page

Abstract

Introduction

Conclusions

References

Tables

Figures



Back

Close

Full Screen / Esc

Printer-friendly Version

Interactive Discussion



- Stöckli, R., Rutishauser, T., Baker, I., Liniger, M. A., and Denning, A. S.: A global reanalysis of vegetation phenology, *J. Geophys. Res.*, 116, G03020–G03020, doi:10.1029/2010jg001545, 2011.
- Stocks, B. J., Mason, J. A., Todd, J. B., Bosch, E. M., Wotton, M., Amiro, B. D., Flannigan, M. D., Hirsch, K. G., Logan, K. A., Martell, D. L., and Skinner, W. R.: Large forest fires in Canada, 1959–1997, *J. Geophys. Res.*, 107, 8149–8149, doi:10.1029/2001jd000484, 2002.
- Strengers, B. J., Müller, C., Schaeffer, M., Haarsma, R. J., Severijns, C., Gerten, D., Schaphoff, S., van den Houdt, R., and Oostenrijk, R.: Assessing 20th century climate–vegetation feedbacks of land-use change and natural vegetation dynamics in a fully coupled vegetation–climate model, *Int. J. Climatol.*, 30, 2055–2065, doi:10.1002/joc.2132, 2010.
- Sturm, M., Racine, C. H., and Tape, K.: Climate change: increasing shrub abundance in the Arctic, *Nature*, 411, 546–547, doi:10.1038/35079180, 2001.
- Tao, X., Wang, D., Wu, D., Yan, B., Fan, W., Xu, X., and Yao, Y.: A model for instantaneous FAPAR retrieval: theory and validation, in: *Geoscience and Remote Sensing Symposium, 2009 IEEE International, IGARSS 2009*, vol. 1, pp. 1–144–1–147, 2009.
- Thonicke, K., Spessa, A., Prentice, I. C., Harrison, S. P., Dong, L., and Carmona-Moreno, C.: The influence of vegetation, fire spread and fire behaviour on biomass burning and trace gas emissions: results from a process-based model, *Biogeosciences*, 7, 1991–2011, doi:10.5194/bg-7-1991-2010, 2010.
- Thurner, M., Beer, C., Santoro, M., Carvalhais, N., Wutzler, T., Schepaschenko, D., Shvidenko, A., Kompter, E., Ahrens, B., Levick, S. R., and Schmillius, C.: Carbon stock and density of northern boreal and temperate forests, *Glob. Ecol. Biogeogr.*, 23, 297–310, doi:10.1111/geb.12125, 2014.
- Townshend, J., Carroll, M., Dimiceli, C., Sohlberg, R. A., Hansen, M. C., and DeFries, R. S.: Vegetation continuous fields MOD44B, 2000 percent tree cover, collection 5, available at: <http://glcf.umd.edu/data/vcf/> (last access: 15 January 2013), 2011.
- Tucker, C. J.: Red and photographic infrared linear combinations for monitoring vegetation, *Remote Sens. Environ.*, 150, 127–150, 1979.
- Tucker, C. J., Slayback, D. A., Pinzon, J. E., Los, S. O., Myneni, R. B., and Taylor, M. G.: Higher northern latitude normalized difference vegetation index and growing season trends from 1982 to 1999, *Int. J. Biometeorol.*, 45, 184–190, doi:10.1007/s00484-001-0109-8, 2001.

Phenology controls and model-data integration

M. Forkel et al.

Title Page

Abstract

Introduction

Conclusions

References

Tables

Figures



Back

Close

Full Screen / Esc

Printer-friendly Version

Interactive Discussion



Turner, D. P., Cohen, W. B., Kennedy, R. E., Fassnacht, K. S., and Briggs, J. M.: Relationships between leaf area index and landsat TM spectral vegetation indices across three temperate zone sites, *Remote Sens. Environ.*, 70, 52–68, 1999.

Urban, M., Forkel, M., Schmullius, C., Hese, S., Hüttich, C., and Herold, M.: Identification of land surface temperature and albedo trends in AVHRR pathfinder data from 1982 to 2005 for northern Siberia, *Int. J. Remote Sens.*, 34, 4491–4507, doi:10.1080/01431161.2013.779760, 2013.

Van Peer, L., Nijs, I., Reheul, D., and De Cauwer, B.: Species richness and susceptibility to heat and drought extremes in synthesized grassland ecosystems: compositional vs physiological effects, *Funct. Ecol.*, 18, 769–778, doi:10.1111/j.0269-8463.2004.00901.x, 2004.

van der Werf, G. R., Randerson, J. T., Giglio, L., Collatz, G. J., Mu, M., Kasibhatla, P. S., Morton, D. C., DeFries, R. S., Jin, Y., and van Leeuwen, T. T.: Global fire emissions and the contribution of deforestation, savanna, forest, agricultural, and peat fires (1997–2009), *Atmos. Chem. Phys.*, 10, 11707–11735, doi:10.5194/acp-10-11707-2010, 2010.

Verstraeten, W. W., Veroustraete, F., and Feyen, J.: On temperature and water limitation of net ecosystem productivity: implementation in the C-Fix model, *Ecol. Model.*, 199, 4–22, doi:10.1016/j.ecolmodel.2006.06.008, 2006.

Vitousek, P. M. and Howarth, R. W.: Nitrogen limitation on land and in the sea: how can it occur?, *Biogeochemistry*, 13, 87–115, doi:10.1007/BF00002772, 1991.

Wagner, W., Scipal, K., Pathe, C., Gerten, D., Lucht, W., and Rudolf, B.: Evaluation of the agreement between the first global remotely sensed soil moisture data with model and precipitation data, *J. Geophys. Res.-Atmos.*, 108, 4611, doi:10.1029/2003JD003663, 2003.

Walter-Shea, E. A., Blad, B. L., Mesarch, M. A., Hays, C. J., Deering, D. W., and Eck, T. F.: Absorbed photosynthetically active radiation and sun and view geometry effects on remote sensing relationships, *Remote Sens. Rev.*, 17, 89–102, doi:10.1080/02757259809532365, 1998.

Wang, X., Piao, S., Ciais, P., Li, J., Friedlingstein, P., Koven, C., and Chen, A.: Spring temperature change and its implication in the change of vegetation growth in North America from 1982 to 2006, *P. Natl. Acad. Sci. USA*, 108, 1240–1245, doi:10.1073/pnas.1014425108, 2011.

Wright, S. J.: Phenological responses to seasonality in tropical forest plants, in: *Tropical Forest Plant Ecophysiology*, edited by: Mulkey, S. S., Chazdon, R. L., and Smith, A. P., Springer US,

440–460, available at: http://link.springer.com/chapter/10.1007/978-1-4613-1163-8_15 (last access: 26 February 2014), 1996.

Xu, L., Myneni, R. B., Chapin III, F. S., Callaghan, T. V., Pinzon, J. E., Tucker, C. J., Zhu, Z., Bi, J., Ciais, P., Tømmervik, H., Euskirchen, E. S., Forbes, B. C., Piao, S. L., Anderson, B. T., Ganguly, S., Nemani, R. R., Goetz, S. J., Beck, P. S. A., Bunn, A. G., Cao, C., and Stroeve, J. C.: Temperature and vegetation seasonality diminishment over northern lands, *Nat. Clim. Change*, 3, 581–586, doi:10.1038/nclimate1836, 2013.

Yuan, W., Zhou, G., Wang, Y., Han, X., and Wang, Y.: Simulating phenological characteristics of two dominant grass species in a semi-arid steppe ecosystem, *Ecol. Res.*, 22, 784–791, doi:10.1007/s11284-006-0318-z, 2007.

Zaehle, S., Sitch, S., Smith, B., and Hatterman, F.: Effects of parameter uncertainties on the modeling of terrestrial biosphere dynamics, *Global Biogeochem. Cy.*, 19, doi:10.1029/2004gb002395, 2005.

Zeng, H., Jia, G., and Epstein, H.: Recent changes in phenology over the northern high latitudes detected from multi-satellite data, *Environ. Res. Lett.*, 6, 045508–045508, doi:10.1088/1748-9326/6/4/045508, 2011.

Zhu, Z., Bi, J., Pan, Y., Ganguly, S., Anav, A., Xu, L., Samanta, A., Piao, S., Nemani, R., and Myneni, R.: Global data sets of vegetation Leaf Area Index (LAI)3g and Fraction of Photosynthetically Active Radiation (FPAR)3g derived from Global Inventory Modeling and Mapping Studies (GIMMS) Normalized Difference Vegetation Index (NDVI3g) for the period 1981 to 2011, *Remote Sens.*, 5, 927–948, doi:10.3390/rs5020927, 2013.

BGD

11, 10917–11025, 2014

Phenology controls and model-data integration

M. Forkel et al.

Title Page

Abstract

Introduction

Conclusions

References

Tables

Figures



Back

Close

Full Screen / Esc

Printer-friendly Version

Interactive Discussion



Phenology controls and model-data integration

M. Forkel et al.

[Title Page](#)

[Abstract](#) [Introduction](#)

[Conclusions](#) [References](#)

[Tables](#) [Figures](#)

[◀](#) [▶](#)

[◀](#) [▶](#)

[Back](#) [Close](#)

[Full Screen / Esc](#)

[Printer-friendly Version](#)

[Interactive Discussion](#)

Table 1. Overview of optimization experiments with information sources for prior and posterior parameter sets. Parameter values and prior parameter ranges for each parameter set are listed in Appendix D.

Experiment	Description	Number of randomly selected grid cells	Prior parameter set and sources	Posterior parameter set
OP.prior	Parameters or model results of LPJmL-OP with standard parameters	–	Table D2 Sitch et al. (2003): α_{g1} , k , ramp, aphen_{\min} , aphen_{\max} , $W_{\text{scal}_{\min}}$ Strengers et al. (2010): sfc and albedo parameters (partly estimated from MODIS albedo)	–
OP.gc	Optimization of single grid cells of LPJmL-OP.	530 in total TrBE 66, TrBR 51, TeNE 46, TeBE 32, TeBS 32, BoNE 68, BoBS 40, BoNS 49, TeH 66, TrH 80	Table D2 Parameters as in OP.prior	One optimized parameter set per grid cell. Median-averaged values for PFTs (Table D3)
OP.pft (results not shown)	Optimization of multiple grid of LPJmL-OP. Multiple grid cells of the same dominant PFT were optimized at the same time.	673 in total TrBE 50, TrBR 80, TeNE 50, TeBE 50, TeBS 80, BoNE 50, BoBS 80, BoNS 158, TeH 50, TrH 25	Median-averaged values for PFTs from posterior values of OP.gc (Table D3)	– (No useful posterior parameter sets were found)
GSI.prior	Parameters or model results of LPJmL-GSI with standard parameters.	–	Table D4 OP.gc: α_{g1} , k , sfc , β_{leaf} , β_{litter} , and β_{stem} Stöckli et al. (2011): parameters for cold and light limiting functions derived from fitting logistic functions to stepwise functions as reported in Stöckli et al. (2011)	–
GSI.gc	Optimization of single grid cells of LPJmL-GSI.	348 in total TrBE 33, TrBR 33, TeNE 32, TeBE 22, TeBS 43, BoNE 30, BoBS 41, BoNS 30, TeH 46, TrH 38	Parameters as in GSI.prior (Table D4)	One optimized parameter set per grid cell.
GSI.pft	Optimization of multiple grid of LPJmL-GSI. Multiple grid cells of the same dominant PFT were optimized at the same time.	500 in total TrBE 30, TrBR 30, TeNE 30, TeBE 30, TeBS 30, BoNE 50, BoBS 30, BoNS 60, TeH 70, TrH 70, PoH 70	Parameters as in GSI.prior (Table D4)	Table D5 (one optimized parameter set per PFT)



Phenology controls and model-data integration

M. Forkel et al.

[Title Page](#)

[Abstract](#)

[Introduction](#)

[Conclusions](#)

[References](#)

[Tables](#)

[Figures](#)

[◀](#)

[▶](#)

[◀](#)

[▶](#)

[Back](#)

[Close](#)

[Full Screen / Esc](#)

[Printer-friendly Version](#)

[Interactive Discussion](#)



Table 2. Overview of global model runs that were used in this study for model evaluation.

Model run	Phenology model	Parameter set	Further settings
LPJmL-OP-prior	original phenology	LPJmL standard parameters as in the OP.prior experiment (Table D2)	dynamic vegetation/no prescribed land cover, prescribed agricultural land use, prescribed observed burnt area
LPJmL-OP-gc	original phenology	Optimized productivity, FA-PAR and albedo parameters from the OP.gc optimization experiment, but original phenology parameters as in the OP.prior experiment (Table D3)	dynamic vegetation/no prescribed land cover, prescribed agricultural land use, prescribed observed burnt area
LPJmL-GSI	GSI-based phenology	Parameters from the GSI.pft optimization experiment (Table D5)	dynamic vegetation/no prescribed land cover, prescribed agricultural land use, prescribed observed burnt area

Table D1. Description of LPJmL model parameters that were addressed in this study.

Parameter	Alternative name	Use	Description	Unit
α_a	ALPHAA	Photo-synthesis	Leaf-to-canopy scaling parameter (amount of radiation absorbed at leaf-level in comparison to total canopy)	–
β_{leaf}	ALBEDO_LEAF	Albedo, FAPAR	Albedo of green leaves	–
β_{stem}	ALBEDO_STEM	Albedo	Albedo of stems and branches	–
β_{litter}	ALBEDO_LITTER	Albedo	Albedo of litter	–
k	LIGHTTEXTCOEFF	FPC, FAPAR	Light extinction coefficient in Lambert–Beer relationship	–
sfc	SNOWCANOPYFRAC	Albedo, FAPAR	Maximum fraction of snow in the green canopy	–
W_{scal_min}	MINWSCAL	Original phenology	Minimum value of the water availability scaling factor for leaf onset in rain green PFTs	–
GDD_{base}	GDDBASE	Original phenology	Minimum daily temperature to start counting growing degree days	°C
ramp	RAMP	Original phenology	Number of growing degree days to reach full leave cover in summergreen PFTs	°C
$aphen_{min}$	APHEN_MIN	Original phenology	Minimum accumulated phenology state to allow senescence if temperature < GDDBASE	–
$aphen_{max}$	APHEN_MAX	Original phenology	Maximum accumulated phenology state. Phenology is set back to 0 if this value is passed.	–
sl_{min}	TMIN_SL	GSI phenology	Slope of cold temperature limiting logistic function for phenology	1/°C
$base_{min}$	TMIN_BASE	GSI phenology	Inflection point of cold temperature limiting logistic function for phenology	°C
τ_{min}	TMIN_TAU	GSI phenology	Change rate of actual to previous day cold temperature limiting function value for phenology	–
sl_{light}	LIGHT_SL	GSI phenology	Slope of light limiting logistic function for phenology	1/(W/m ²)
$base_{light}$	LIGHT_BASE	GSI phenology	Inflection point of light limiting logistic function for phenology	W/m ²
τ_{light}	LIGHT_TAU	GSI phenology	Change rate of actual to previous day light limiting function value for phenology	–
sl_{water}	WATER_SL	GSI phenology	Slope of water limiting logistic function for phenology	1/%
$base_{water}$	WATER_BASE	GSI phenology	Inflection point of water limiting logistic function for phenology	%
τ_{water}	WATER_TAU	GSI phenology	Change rate of actual to previous day water limiting function value for phenology	–
sl_{heat}	TMAX_SL	GSI phenology	Slope of heat limiting logistic function for phenology	1/°C
$base_{heat}$	TMAX_BASE	GSI phenology	Inflection point of heat limiting logistic function for phenology	°C
τ_{heat}	TMAX_TAU	GSI phenology	Change rate of actual to previous day heat limiting function value for phenology	–

Phenology controls
and model-data
integration

M. Forkel et al.

Table D2. Prior parameter values of LPJmL-OP (OP.prior). The values in brackets are ranges of uniform parameter distributions that were used during optimization. Note: * The parameter GDD_{base} was changed to 0 °C. This value gave better agreements between simulated and observed seasonal FAPAR dynamics than the original value of 5 °C. Nevertheless, GDD_{base} was not included in optimization experiments because this parameter is highly correlated with the parameter ramp.

	TrBE	TrBR	TeNE	TeBE	TeBS	BoNE	BoBS	BoNS	TeH	TrH
α_a	0.5 (0.1–0.9)	0.5 (0.1–0.9)								
β_{leaf}	0.15 (0.1–0.2)	0.15 (0.1–0.2)	0.15 (0.06–0.23)	0.15 (0.09–0.23)	0.16 (0.086–0.23)	0.14 (0.05–0.23)	0.15 (0.09–0.21)	0.12 (0.1–0.15)	0.14 (0.072–0.22)	0.15 (0.09–0.21)
β_{stem}	0.15 (0.018–0.29)	0.15 (0.073–0.23)	0.13 (0–0.31)	0.15 (0.029–0.28)	0.13 (0.038–0.23)	0.14 (0–0.31)	0.14 (0.059–0.23)	0.13 (0.052–0.32)	–	–
β_{litter}	0.15 (0.018–0.29)	0.14 (0.058–0.27)	0.13 (0.047–0.21)	0.15 (0.044–0.29)	0.14 (0.085–0.26)	0.13 (0.035–0.22)	0.14 (0.078–0.23)	0.12 (0.088–0.38)	0.14 (0.027–0.38)	0.13 (0.02–0.28)
sfc	0.4 (0.1–0.9)	0.4 (0.1–0.9)								
k	0.5 (0.1–0.9)	0.5 (0.1–0.9)								
GDD _{base}	–	–	–	–	0*	–	0*	0*	0*	0*
Wscal _{min}	–	0.3 (0–1)	–	–	–	–	–	–	–	–
Ramp	–	–	–	–	300 (0–1000)	–	200 (0–1000)	200 (0–1000)	100 (0–1000)	100 (0–1000)
aphen _{min}	–	–	–	–	10 (1–600)	–	10 (1–600)	10 (1–600)	–	–
aphen _{max}	–	–	–	–	210 (1–600)	–	210 (1–600)	210 (1–600)	–	–

Title Page

Abstract

Introduction

Conclusions

References

Tables

Figures

◀

▶

◀

▶

Back

Close

Full Screen / Esc

Printer-friendly Version

Interactive Discussion



Phenology controls and model-data integration

M. Forkel et al.

Table D3. Posterior parameter values for LPJmL-OP based on grid cell-level optimization experiments (OP.gc). Parameters written *in italics* were derived as the median value of the single grid cell optimization experiments whereas all other parameters were derived from prior parameter sources. For the parameter ramp no plausible parameter was found. The parameter GDDbase was changed to 0 but not included in the optimization.

	TrBE	TrBR	TeNE	TeBE	TeBS	BoNE	BoBS	BoNS	TeH	TrH
α_a	<i>0.6</i>	<i>0.56</i>	<i>0.38</i>	<i>0.41</i>	<i>0.38</i>	<i>0.28</i>	<i>0.34</i>	<i>0.27</i>	<i>0.32</i>	<i>0.39</i>
β_{leaf}	<i>0.13</i>	<i>0.1</i>	<i>0.06</i>	<i>0.1</i>	<i>0.16</i>	<i>0.05</i>	<i>0.18</i>	<i>0.11</i>	<i>0.08</i>	<i>0.15</i>
β_{stem}	0.15	<i>0.07</i>	0.13	0.15	<i>0.04</i>	0.14	<i>0.06</i>	<i>0.05</i>	–	–
β_{jitter}	0.15	<i>0.06</i>	0.13	0.15	<i>0.09</i>	0.13	<i>0.08</i>	<i>0.09</i>	<i>0.1</i>	<i>0.14</i>
sfc	0.4	0.4	<i>0.1</i>	0.4	0.4	0.1	<i>0.15</i>	<i>0.18</i>	0.4	0.4
k	<i>0.36</i>	<i>0.73</i>	<i>0.41</i>	<i>0.44</i>	<i>0.74</i>	<i>0.71</i>	<i>0.51</i>	<i>0.88</i>	<i>0.39</i>	<i>0.46</i>
GDD _{base}	–	–	–	–	0	–	0	0	0	0
Wscal _{min}	–	<i>0.85</i>	–	–	–	–	–	–	–	–
Ramp	–	–	–	–	300	–	200	200	100	100
aphen _{min}	–	–	–	–	10	–	10	10	–	–
aphen _{max}	–	–	–	–	<i>201.97</i>	–	<i>181.62</i>	<i>105.78</i>	–	–

Title Page

Abstract

Introduction

Conclusions

References

Tables

Figures



Back

Close

Full Screen / Esc

Printer-friendly Version

Interactive Discussion



Phenology controls
and model-data
integration

M. Forkel et al.

Table D4. Prior parameter values for LPJmL-GSI (GSI.prior). Parameters marked with * were identified as insensitive and were not included in the optimization. The values in brackets are ranges of uniform parameter distributions that were used during optimization. The values for the first 6 parameters were derived from the single grid-cell optimization experiments of LPJmL-OP (Table 3).

	TrBE	TrBR	TeNE	TeBE	TeBS	BoNE	BoBS	BoNS	TrH	TeH PoH
α_a	0.6 (0.2–0.8)	0.56 (0.1–0.9)	0.38 (0.23–0.49)	0.41 (0.1–0.9)	0.38 (0.15–0.6)	0.28 (0.16–0.57)	0.34 (0.15–0.61)	0.27 (0.16–0.55)	0.39 (0.21–0.83)	0.32 (0.1–0.83)
β_{leaf}	0.13 (0.1–0.2)	0.1 (0.05–0.2)	0.06 (0.01–0.23)	0.1 (0.09–0.23)	0.16 (0.13–0.19)	0.05 (0.01–0.23)	0.18 (0.09–0.21)	0.11 (0.1–0.14)	0.15 (0.09–0.21)	0.08 (0.072–0.22)
β_{stem}	0.15 (0.018–0.29)	0.07 (0.06–0.23)	0.13 (0–0.31)	0.15 (0.029–0.28)	0.04 (0.038–0.23)	0.14 (0–0.31)	0.06 (0.059–0.23)	0.05 (0.04–0.32)	–	–
β_{litter}	0.15 (0.054–0.29)	0.06 (0.058–0.27)	0.13 (0.047–0.21)	0.15 (0.044–0.29)	0.09 (0.085–0.2)	0.13 (0.035–0.26)	0.08 (0.078–0.22)	0.09 (0.088–0.23)	0.14 (0.02–0.28)	0.1 (0.027–0.38)
sfc	0.4*	0.4*	0.1 (0.01–0.9)	0.4*	0.4 (0.1–0.9)	0.1 (0.01–0.9)	0.15 (0.1–0.9)	0.18*	0.4*	0.4 (0.1–0.9)
k	0.36 (0.2–0.9)	0.73 (0.1–0.9)	0.41 (0.1–0.9)	0.44 (0.1–0.9)	0.74 (0.1–0.9)	0.71 (0.1–0.9)	0.51 (0.1–0.9)	0.88 (0.1–0.9)	0.46 (0.1–0.9)	0.39 (0.1–0.9)
sl _{min}	0.24 (0.1–2)	0.24*	0.24 (0.1–2)	0.24 (0.1–2)	0.24 (0.1–2)	0.24 (0.1–2)	0.24 (0.1–2)	0.24 (0.1–2)	0.24 (0.1–2)	0.24 (0.1–2)
base _{min}	8.8 (0–16)	8.8 (0–16)	–3.3 (–6–6)	–0.6 (–3–1)	7.4 (5–9)	3.7 (–6–6)	2.2 (0–5)	–4 (–6–6)	8.8 (0–16)	0.7 (–3–5)
τ_{min}	0.2*	0.2*	0.2*	0.2*	0.2*	0.2*	0.2*	0.2*	0.2*	0.2*
sh _{heat}	0.24 (0.01–3)	0.24 (0.01–3)	0.24 (0.01–3)	0.24 (0.01–3)	0.24 (0.01–3)	0.24*	0.24*	0.24*	0.24 (0.01–3)	0.24*
base _{heat}	35 (25–45)	35 (25–45)	35 (25–45)							
τ_{heat}	0.2 (0.01–0.9)	0.2*	0.2 (0.01–0.9)	0.2*	0.2*	0.2*	0.2 (0.01–0.9)	0.2*	0.2 (0.01–0.9)	0.2*
sl _{light}	57 (0.05–157)	23*	20*	0.2 (0.05–40)	58*	14*	101 (0.05–220)	95*	41 (0.05–130)	23*
base _{light}	125 (1–200)	62 (1–200)	73 (1–200)	23 (1–50)	123 (50–200)	57 (1–100)	166 (50–200)	156 (130–180)	104 (1–150)	67 (1–180)
τ_{light}	0.2 (0.01–0.9)	0.2*	0.2*	0.2*	0.2*	0.2*	0.2*	0.2*	0.2 (0.01–0.9)	0.2 (0.01–0.9)
sl _{water}	5 (0.1–10)	5 (0.1–10)	5*	5*	5 (0.1–10)	5*	5 (0.1–10)	5*	5 (0.1–10)	5 (0.1–10)
base _{water}	20 (1–99)	20 (1–99)	20 (1–99)							
τ_{water}	0.8 (0.01–0.99)	0.8 (0.01–0.99)	0.8*	0.8*	0.8*	0.8*	0.8*	0.8*	0.8 (0.01–0.99)	0.8 (0.01–0.99)

Title Page

Abstract Introduction

Conclusions References

Tables Figures

◀ ▶

◀ ▶

Back Close

Full Screen / Esc

Printer-friendly Version

Interactive Discussion



Phenology controls
and model-data
integration

M. Forkel et al.

Table D5. Final parameters for LPJmL-GSI. Parameters written *in italics* were derived from PFT-level optimization experiments (GSI.pft) whereas all other parameters were derived from prior parameter sources as described in Fig. D1.

	TrBE	TrBR	TeNE	TeBE	TeBS	BoNE	BoBS	BoNS	TrH	TeH	PoH
α_a	<i>0.63</i>	<i>0.52</i>	<i>0.44</i>	<i>0.45</i>	<i>0.61</i>	<i>0.22</i>	<i>0.41</i>	<i>0.34</i>	<i>0.40</i>	<i>0.32</i>	<i>0.43</i>
β_{leaf}	0.13	<i>0.12</i>	<i>0.12</i>	<i>0.12</i>	<i>0.18</i>	<i>0.10</i>	0.16	<i>0.12</i>	<i>0.24</i>	<i>0.18</i>	0.07
β_{stem}	0.10	0.10	0.04	0.04	0.04	0.06	0.06	0.04	0.15	0.15	0.15
β_{litter}	0.10	0.10	<i>0.05</i>	0.10	<i>0.14</i>	<i>0.01</i>	<i>0.00</i>	<i>0.01</i>	<i>0.12</i>	<i>0.07</i>	0.03
k	<i>0.52</i>	<i>0.74</i>	<i>0.47</i>	<i>0.70</i>	<i>0.60</i>	<i>0.44</i>	0.41	<i>0.66</i>	0.50	0.50	0.50
sl_{tmin}	1.01	0.24	<i>0.22</i>	0.55	<i>0.26</i>	<i>0.10</i>	0.22	0.15	0.91	0.31	0.13
$base_{\text{tmin}}$	8.30	7.66	<i>-7.81</i>	<i>-0.63</i>	<i>13.69</i>	<i>-7.52</i>	2.05	<i>-4.17</i>	6.42	<i>4.98</i>	<i>2.79</i>
τ_{tmin}	0.20	0.20	0.20	0.20	0.20	0.20	0.20	0.20	0.20	<i>0.01</i>	0.20
sl_{heat}	1.86	<i>1.63</i>	1.83	0.98	1.74	0.24	1.74	0.24	1.47	0.24	0.24
$base_{\text{heat}}$	<i>38.64</i>	<i>38.64</i>	<i>35.26</i>	<i>41.12</i>	<i>41.51</i>	<i>27.32</i>	<i>41.51</i>	<i>44.60</i>	<i>29.16</i>	<i>32.04</i>	<i>26.12</i>
τ_{heat}	0.20	0.20	0.20	0.20	0.20	0.20	0.20	0.20	0.20	0.20	0.20
sl_{light}	77.17	23.00	20.00	18.83	58.00	14.00	58.00	95.00	64.23	23.00	23.00
$base_{\text{light}}$	<i>55.53</i>	<i>13.01</i>	<i>4.87</i>	<i>39.32</i>	<i>59.78</i>	<i>3.04</i>	<i>59.78</i>	<i>130.1</i>	69.90	<i>75.94</i>	<i>50.00</i>
τ_{light}	0.52	0.20	0.20	0.20	0.20	0.20	0.20	0.20	0.40	0.22	0.38
sl_{water}	5.14	<i>7.97</i>	5.00	5.00	<i>5.24</i>	5.00	5.24	5.00	0.10	0.52	0.88
$base_{\text{water}}$	<i>5.00</i>	<i>22.21</i>	<i>8.61</i>	<i>8.82</i>	<i>20.96</i>	<i>0.01</i>	<i>20.96</i>	<i>2.34</i>	<i>41.72</i>	<i>53.07</i>	<i>1.00</i>
τ_{water}	0.44	<i>0.13</i>	0.80	0.80	0.80	0.80	0.80	0.80	0.17	0.01	0.94

Title Page

Abstract

Introduction

Conclusions

References

Tables

Figures

◀

▶

◀

▶

Back

Close

Full Screen / Esc

Printer-friendly Version

Interactive Discussion



Phenology controls and model-data integration

M. Forkel et al.

Title Page

Abstract

Introduction

Conclusions

References

Tables

Figures



Back

Close

Full Screen / Esc

Printer-friendly Version

Interactive Discussion



Table E1. Global total carbon fluxes and stocks from data-oriented estimates and from LPJmL simulations. LPJmL-OP-Standard and LPJmL-GSI-Standard are LPJmL model runs with settings as in (Schaphoff et al., 2013), i.e. without the use of the BoNS and PoH PFTs and with using simulated fires instead of prescribed observed burnt areas. Data sources: ¹ (Beer et al., 2010; Jung et al., 2011), ² (van der Werf et al., 2010), ³ (Saatchi et al., 2011; Thurner et al., 2014).

	Gross primary production (Pg C a ⁻¹)	Ecosystem respiration (Pg C a ⁻¹)	Fire carbon emissions (Pg C a ⁻¹)	Biomass (Pg C)	Soil organic carbon (Pg C)
Data estimate	124.7 ¹	100–110 ³	2.0 ²	451.2 ³	
Data lower uncertainty	110.7 ¹			208.8 ³	
Data upper uncertainty	138.3 ¹			695.9 ³	
LPJmL settings as in this study:					
LPJmL-OP-prior	161.3	150.7	1.93	674.1	2723
LPJmL-OP-gc	153.8	143.9	2.45	581.1	2503
LPJmL-GSI	145.8	141.4	1.65	546.4	2508
LPJmL settings as in Schaphoff et al. (2013):					
LPJmL-OP-Standard	138.9	125.8	3.48	597.8	2101
LPJmL-GSI-Standard	120.4	115.1	3.23	582.1	1392

Phenology controls and model-data integration

M. Forkel et al.

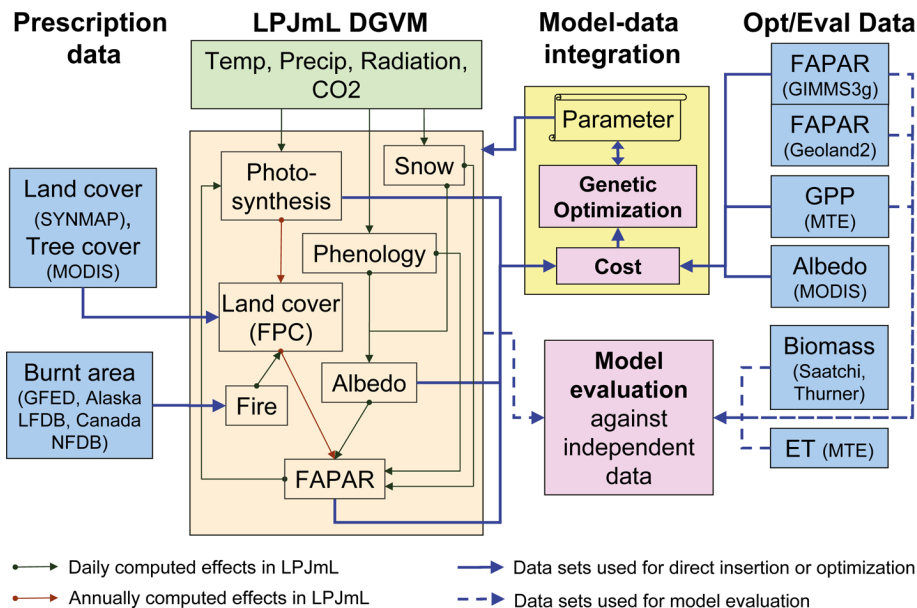


Figure 1. Structure of the model-data integration approach for LPJmL (LPJmL-MDI). The LPJmL model structure is highly simplified.

[Title Page](#)

[Abstract](#) [Introduction](#)

[Conclusions](#) [References](#)

[Tables](#) [Figures](#)

[◀](#) [▶](#)

[◀](#) [▶](#)

[Back](#) [Close](#)

[Full Screen / Esc](#)

[Printer-friendly Version](#)

[Interactive Discussion](#)



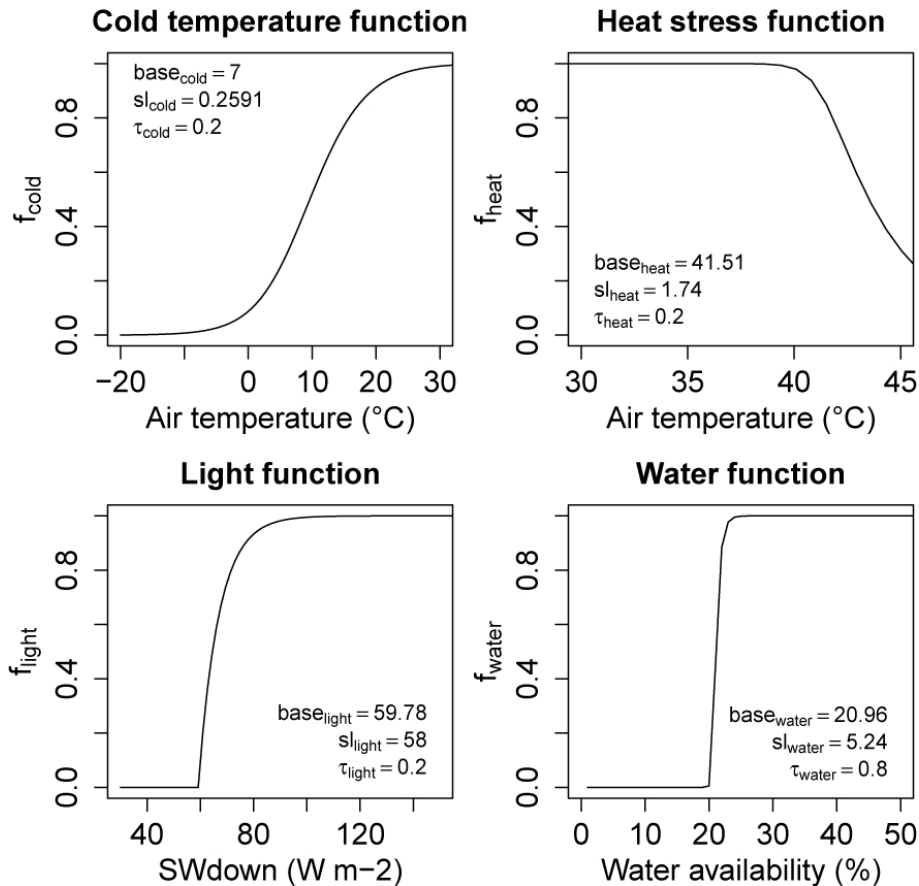


Figure 2. Examples of the cold temperature, heat stress, light and water limiting functions for phenology in LPJmL-GSI. Depending on the chosen parameters the functions have different shapes for each PFT.

Phenology controls and model-data integration

M. Forkel et al.

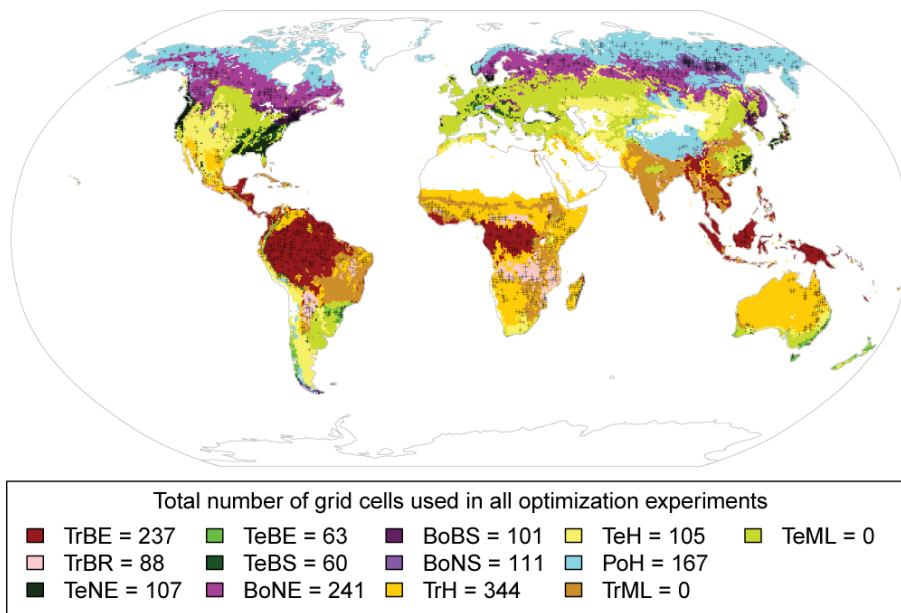


Figure 3. Map of the dominant PFT in each grid cell as derived from SYNMAP, Köppen–Geiger climate zones and MODIS VCF. Grid cells that were used in any of the optimization experiments are shown as black crosses. Some grid cells were used in multiple optimization experiments. Grid cells that are dominated by agriculture were not used for optimization (TrML, tropical managed lands and TeML, temperate managed lands).

Title Page

Abstract

Introduction

Conclusions

References

Tables

Figures



Back

Close

Full Screen / Esc

Printer-friendly Version

Interactive Discussion



Phenology controls and model-data integration

M. Forkel et al.

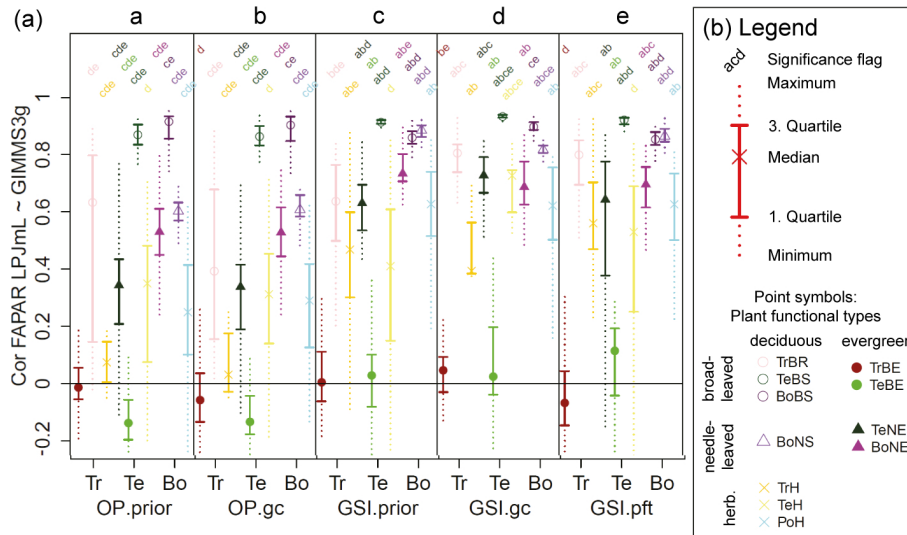


Figure 4. Distribution of the correlation coefficient between monthly LPJmL and GIMMS3g FAPAR (1982–2011) for several grid cells in prior model runs and optimization experiments grouped by plant functional types and biomes. **(a)** Correlation coefficient for LPJmL-OP with default parameters **(a, OP.prior)**, after grid cell-level optimizations **(b, OP.gc)**, cost for LPJmL-GSI with prior parameters **(c, GSI.prior)**, after grid cell-level optimizations **(d, GSI.gc)** and after PFT-level optimizations **(e, GSI.pft)**. Biomes are Tr (tropical), Te (temperate) and Bo (boreal/polar). **(b)** Legend for the plot. Each distribution is plotted according to usual boxplot statistics. The point symbols indicate the plant functional type. The significance flag on top of each distribution shows if a distribution is significant different ($p \leq 0.01$) to the corresponding distribution of the same PFT in another optimization experiment. The significance is based on the Wilcoxon rank-sum test. For example “acd” indicates a significant difference to the main categories **(a)** (OP.prior), **(c)** (GSI.prior) and **(d)** (GSI.gc) but no significant difference to **(b)** (OP.gc) and **(e)** (GSI.pft).

Title Page

Abstract Introduction

Conclusions References

Tables Figures

◀ ▶

◀ ▶

Back Close

Full Screen / Esc

Printer-friendly Version

Interactive Discussion



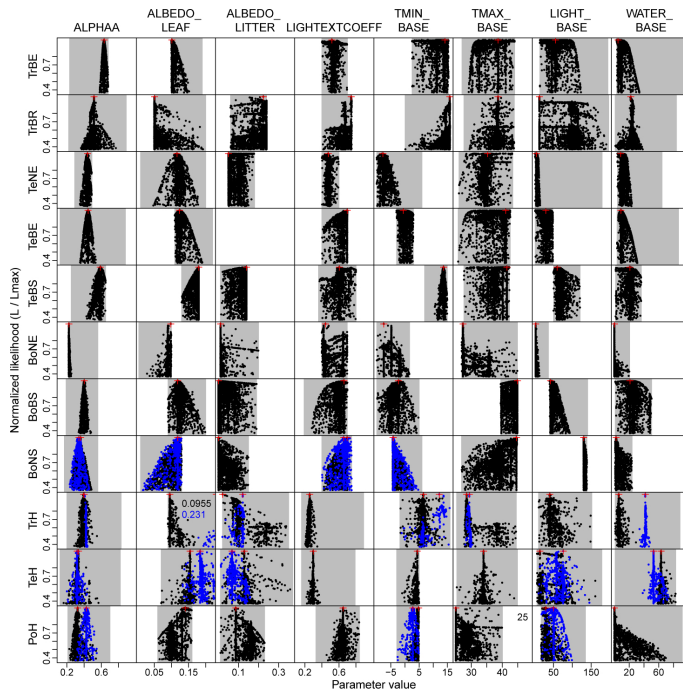


Figure 5. Uncertainty and sensitivity of LPJmL-GSI parameters derived from all individuals of genetic optimizations at PFT level. Shown is the relationship between parameter values and the likelihood of the corresponding parameter vector. The likelihood is normalized with the likelihood of the optimum parameter set. Only individuals with $dAIC < 2$ are shown. Grey areas indicate the uniform prior parameter range. Red crosses indicate the optimum parameter value. The optimum parameter value is indicated as text in a plot if it is outside of the plotting range. Results from two independent optimization experiments are shown for the BoNS, TrH, TeH and PoH PFTs (black and blue colours, respectively) but not all parameters were included in both experiments. The parameter ALBEDO_LITTER in the TrBE and TeBE PFTs was not considered in optimization experiments.

Phenology controls and model-data integration

M. Forkel et al.

Title Page

Abstract Introduction

Conclusions References

Tables Figures

◀ ▶

◀ ▶

Back Close

Full Screen / Esc

Printer-friendly Version

Interactive Discussion



Phenology controls
and model-data
integration

M. Forkel et al.

Title Page

Abstract

Introduction

Conclusions

References

Tables

Figures



Back

Close

Full Screen / Esc

Printer-friendly Version

Interactive Discussion

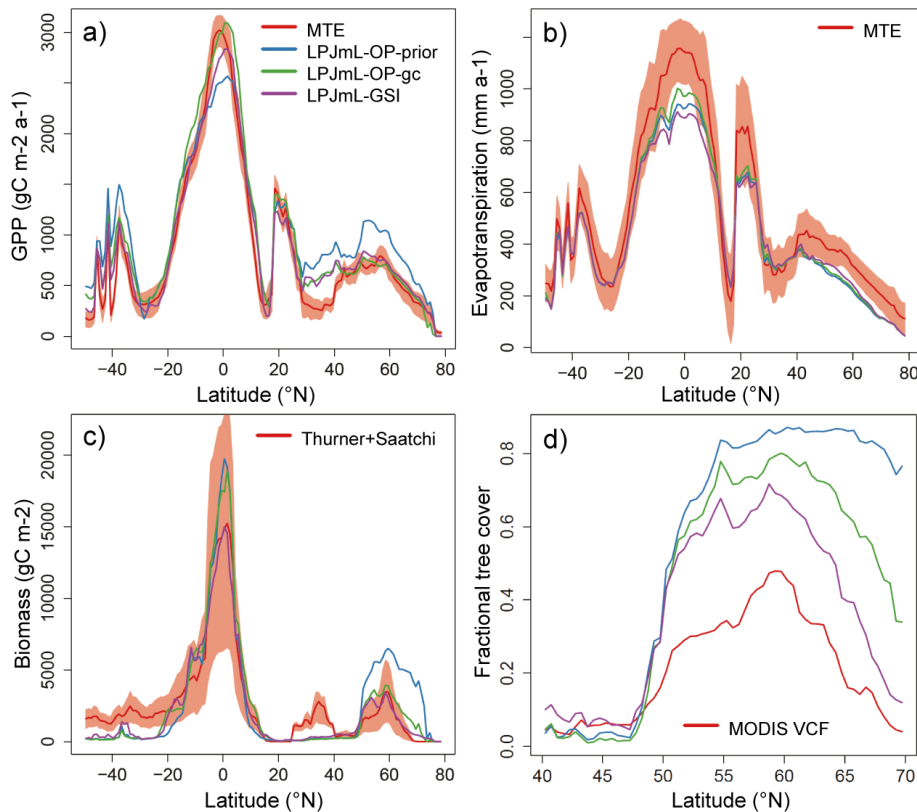


Figure 6. Latitudinal gradients of **(a)** gross primary production (GPP), **(b)** evapotranspiration, **(c)** biomass and **(d)** tree cover from data-oriented estimates and from LPJmL model simulations. Gradients were spatially averaged (median) from all 0.5° grid cells for latitudinal bands of 1° width. **(a)** The red areas represent uncertainty estimates for the data-oriented estimates.

Phenology controls
and model-data
integration

M. Forkel et al.

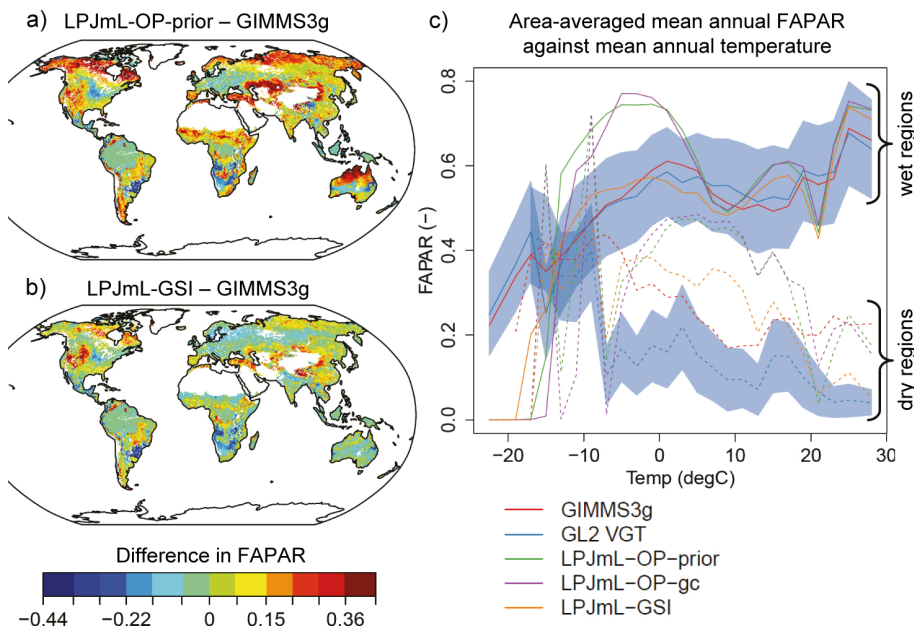


Figure 7. Comparison of mean annual FAPAR from LPJmL and remote sensing datasets. **(a)** Difference in mean annual FAPAR between LPJmL-OP-prior and GIMMS3g. **(b)** Difference in mean annual FAPAR between LPJmL-GSI and GIMMS3g. **(c)** Global spatial-averaged gradients of mean annual FAPAR from LPJmL and data sets. The uncertainty of the GL2 VGT FAPAR dataset is shown as blue area. Dashed lines are dry regions with mean annual $P/PET < 15$ and solid lines are wet regions with mean annual $P/PET \geq 15$.

Phenology controls and model-data integration

M. Forkel et al.

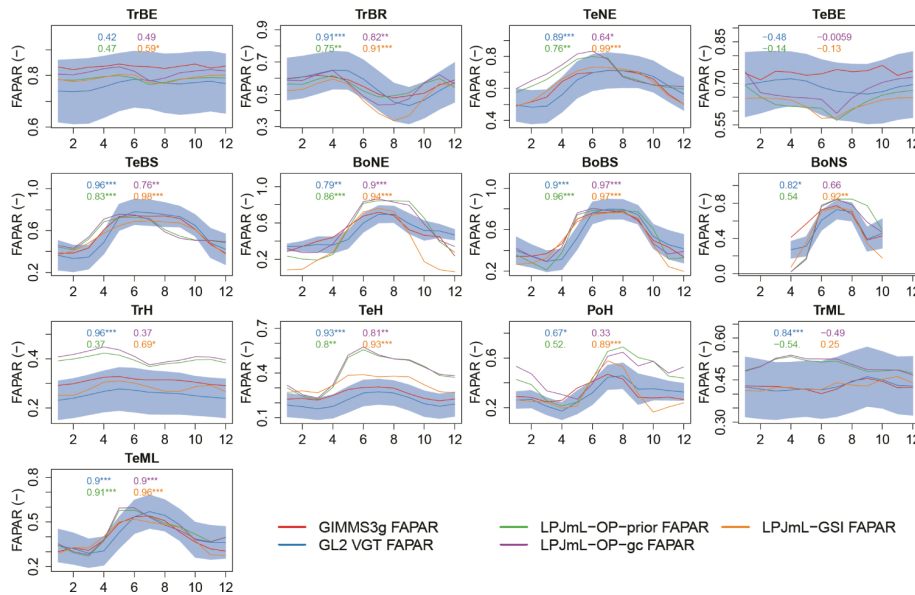


Figure 8. Comparison of the mean seasonal FAPAR cycle from GIMMS3g, GL2 VGT and LPJmL spatially averaged for regions with the same dominant PFT. The PFTs for which time series were averaged are shown in Fig. 3. Numbers in the figures are correlation coefficients between GIMMS3g and the corresponding time series from GL2 VGT or from LPJmL simulations. The significance of the correlation is indicated as point symbol: *** ($p \leq 0.001$), ** ($p \leq 0.01$), * ($p \leq 0.05$), . ($p \leq 0.1$).

Title Page

Abstract Introduction

Conclusions References

Tables Figures

◀ ▶

◀ ▶

Back Close

Full Screen / Esc

Printer-friendly Version

Interactive Discussion



Phenology controls
and model-data
integration

M. Forkel et al.

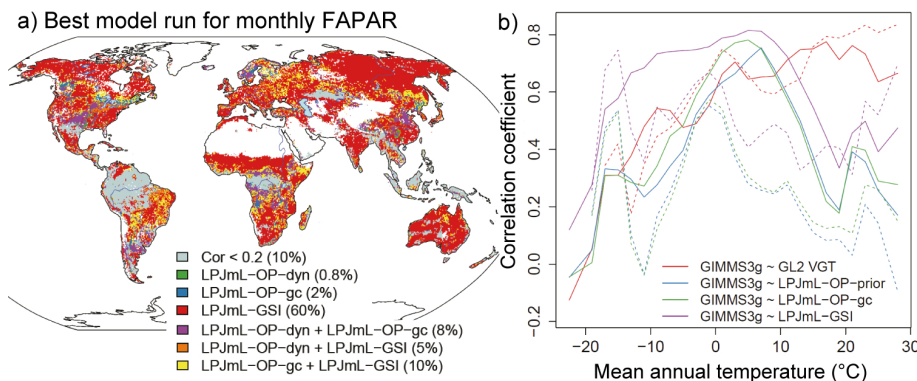


Figure 9. Evaluation of monthly FAPAR dynamics (1982–2011). **(a)** Best LPJmL model run regarding the correlation coefficient between monthly LPJmL FAPAR and GIMMS3g FAPAR. If one model run is shown the correlation coefficient of this best model is significant higher than of the second best model run. If two model runs are shown the correlation coefficients of the first and second best model runs are not significantly different from each other ($p > 0.05$). **(b)** Global spatial-averaged gradients of the correlation coefficient between monthly FAPAR time series. Dashed lines are dry areas with mean annual $P/PET < 15$ and solid lines are wet areas with mean annual $P/PET \geq 15$.

Title Page

Abstract

Introduction

Conclusions

References

Tables

Figures

◀

▶

◀

▶

Back

Close

Full Screen / Esc

Printer-friendly Version

Interactive Discussion



Phenology controls
and model-data
integration

M. Forkel et al.

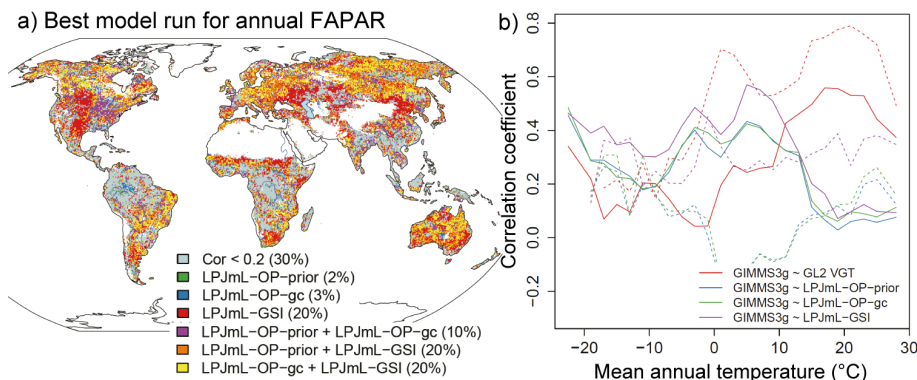


Figure 10. Evaluation of mean annual FAPAR dynamics (1982–2011). **(a)** Best LPJmL model run regarding the correlation coefficient between mean annual LPJmL FAPAR and GIMMS3g FAPAR. If one model run is shown the correlation coefficient of this best model is significant higher than of the second best model run. If two model runs are shown the correlation coefficients of the first and second best model runs are not significantly different from each other ($p > 0.05$). **(b)** Global spatial-averaged gradients of the correlation coefficient between annual FAPAR time series. Dashed lines are dry areas with mean annual $P/PET < 15$ and solid lines are wet areas with mean annual $P/PET \geq 15$.

Title Page

Abstract

Introduction

Conclusions

References

Tables

Figures



Back

Close

Full Screen / Esc

Printer-friendly Version

Interactive Discussion



Phenology controls
and model-data
integration

M. Forkel et al.

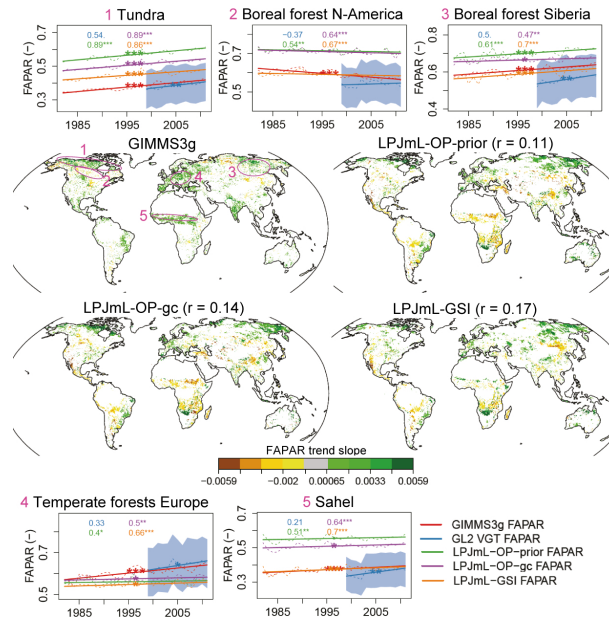


Figure 11. Comparison of trends in mean annual FAPAR from LPJmL and from satellite datasets. Trends were computed between 1982 and 2011 as linear trends. The significance of a trend was determined using the Mann–Kendall trend test. Only significant trends slopes ($p \leq 0.05$) are displayed in each map. Spatial correlations of trend slopes (Spearman coefficient) between LPJmL and the GIMMS3g dataset are given in the map titles. Time series are showing mean annual FAPAR time series and trends spatially averaged for the regions as indicated in the first map. The blue area in time series represents the uncertainty of the GL2 VGT FAPAR dataset. Numbers in the time series plot are correlation coefficients between mean annual FAPAR time series from GIMMS3g and from GL2 or LPJmL model runs, respectively. The significance of a trend and of the correlation is indicated as point symbol: *** ($p \leq 0.001$), ** ($p \leq 0.01$), * ($p \leq 0.05$), . ($p \leq 0.1$).

Phenology controls and model-data integration

M. Forkel et al.

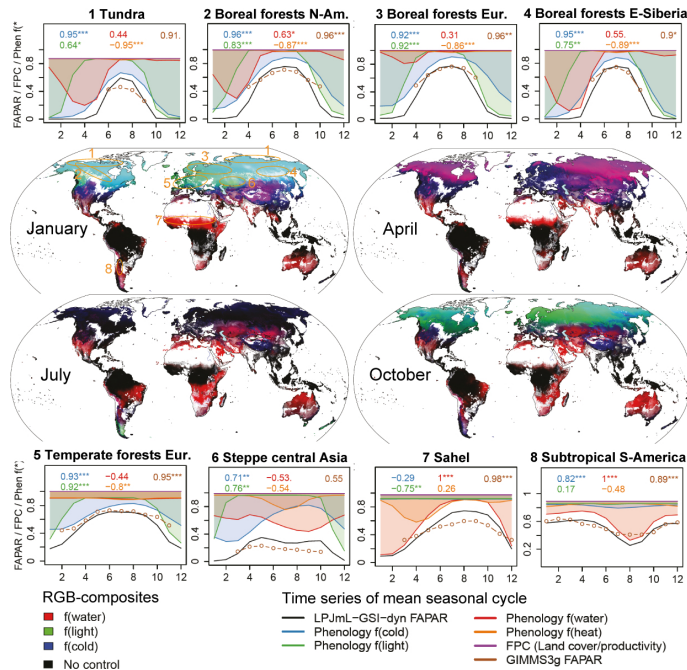


Figure 12. Phenological controls on seasonal FAPAR dynamics. The maps are red-green-blue composites of the mean monthly values for the water (red), light (green) and cold temperature (blue) phenology limiting function values from the LPJmL-GSI-dyn model run. White regions in the maps are without vegetation or dominated by croplands for which the LPJmL-GSI phenology model was not applied. Time series represent the mean seasonal cycles (January to December) (averaged over 1982–2011) of simulated and observed FAPAR and phenology limiting function values averaged for different regions as indicated in the first map. Phenology limiting function values close to 0 indicate a strong control by phenology limiting functions whereas values close to 1 indicate no phenological control. The correlation coefficients of each time series with the simulated FAPAR time series are shown in each time series plot. The significance of the correlation is indicated as point symbol: *** ($p \leq 0.001$), ** ($p \leq 0.01$), * ($p \leq 0.05$), . ($p \leq 0.1$).



Phenology controls and model-data integration

M. Forkel et al.

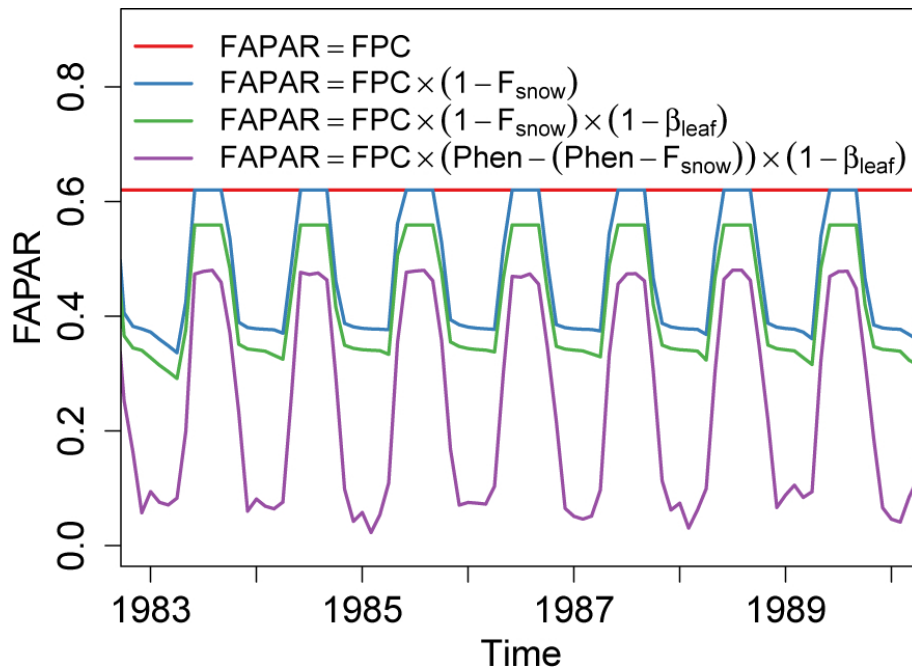


Figure A1. Effects on FAPAR in LPJmL for an example grid cell in Siberia. FAPAR in LPJmL is computed from foliar projective cover (FPC), from snow coverage in the green canopy (F_{snow}), leaf albedo (β_{leaf}) and phenology status (Phen).

Title Page

Abstract

Introduction

Conclusions

References

Tables

Figures



Back

Close

Full Screen / Esc

Printer-friendly Version

Interactive Discussion



Phenology controls and model-data integration

M. Forkel et al.

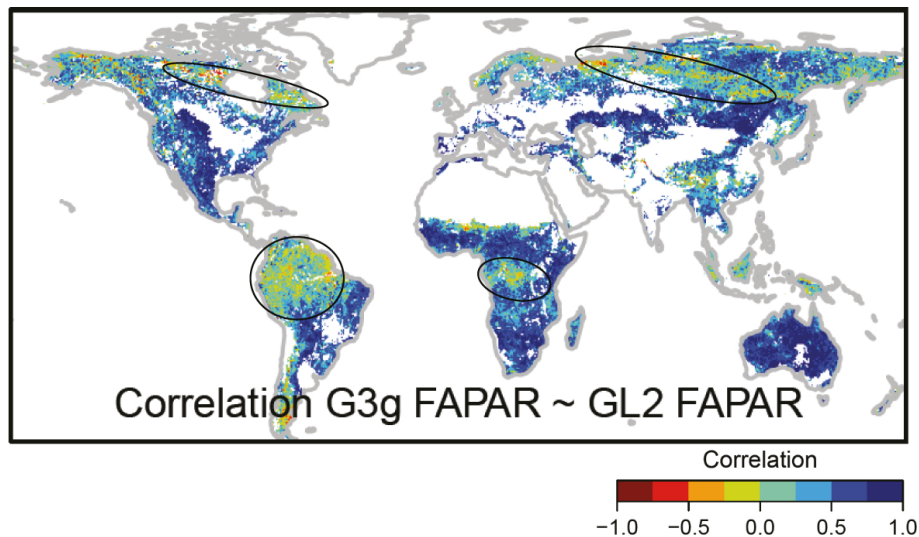


Figure B2. Correlation between mean annual FAPAR time series from the GIMMS3g and GL2 (AVHRR+VGT) FAPAR datasets in 1982–2011. The map shows the Pearson correlation coefficient between both datasets. Areas with large differences are highlighted with circles.

[Title Page](#)[Abstract](#)[Introduction](#)[Conclusions](#)[References](#)[Tables](#)[Figures](#)[Back](#)[Close](#)[Full Screen / Esc](#)[Printer-friendly Version](#)[Interactive Discussion](#)

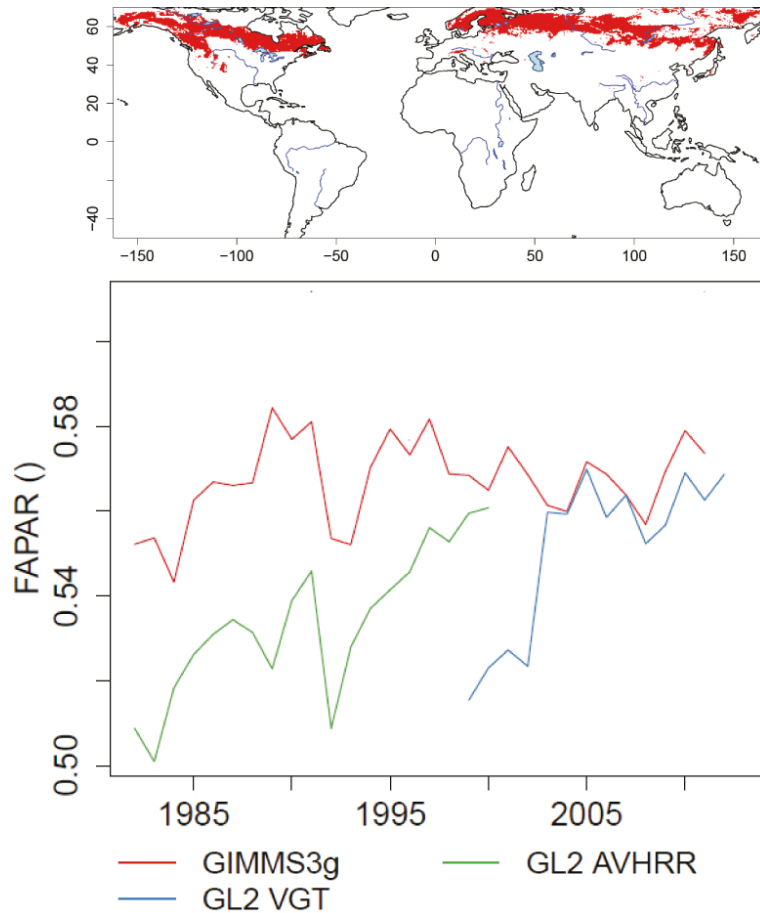


Figure B3. Comparison of mean annual FAPAR from different datasets averaged for the extent of boreal needle-leaved evergreen forests.

Phenology controls and model-data integration

M. Forkel et al.

Title Page

Abstract

Introduction

Conclusions

References

Tables

Figures

◀

▶

◀

▶

Back

Close

Full Screen / Esc

Printer-friendly Version

Interactive Discussion



Phenology controls and model-data integration

M. Forkel et al.

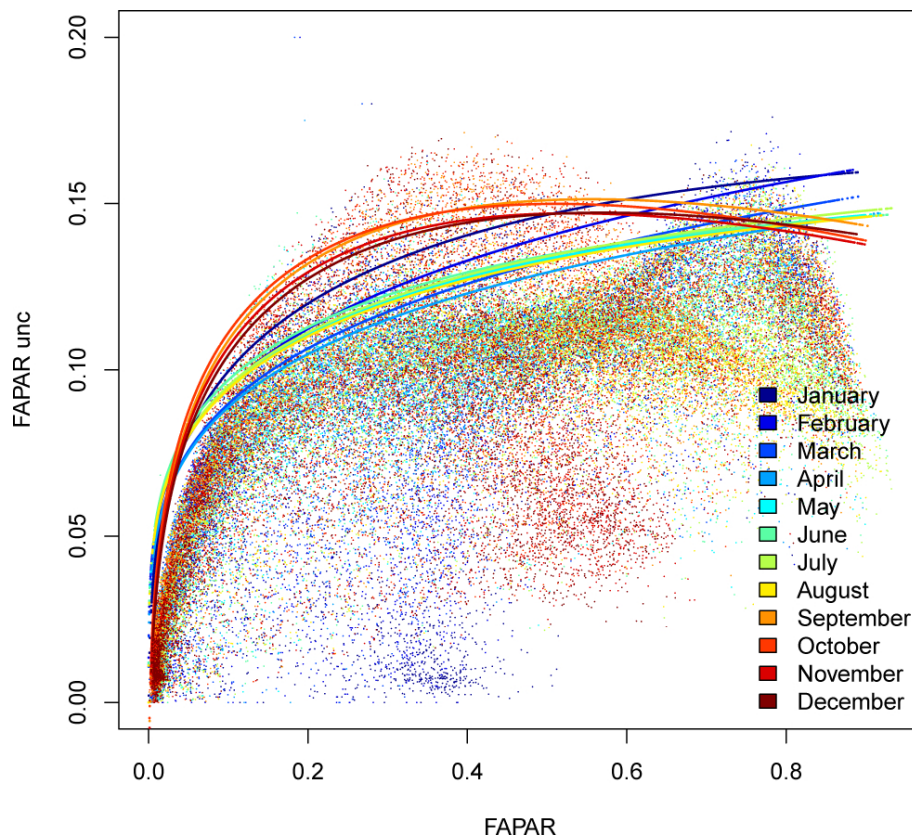


Figure B4. Monthly quantile regressions between GL2 VGT FAPAR and the GL2 VGT FAPAR fitted to the quantile 0.95. Each monthly quantile regression was applied to the GIMMS3g FAPAR dataset to estimate uncertainties for this dataset. Using 0.95 quantile regressions provides conservative uncertainty estimates for the GIMMS3g FAPAR dataset.

Title Page

Abstract

Introduction

Conclusions

References

Tables

Figures



Back

Close

Full Screen / Esc

Printer-friendly Version

Interactive Discussion



Phenology controls and model-data integration

M. Forkel et al.

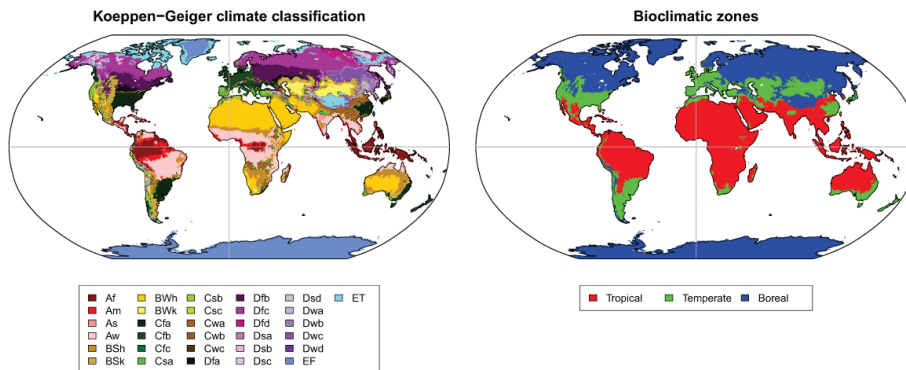


Figure C1. Reclassification of the Koeppen–Geiger climate classification in bioclimatic zones.

Title Page

Abstract

Introduction

Conclusions

References

Tables

Figures

⏪

⏩

◀

▶

Back

Close

Full Screen / Esc

Printer-friendly Version

Interactive Discussion



BGD

11, 10917–11025, 2014

Phenology controls and model-data integration

M. Forkel et al.

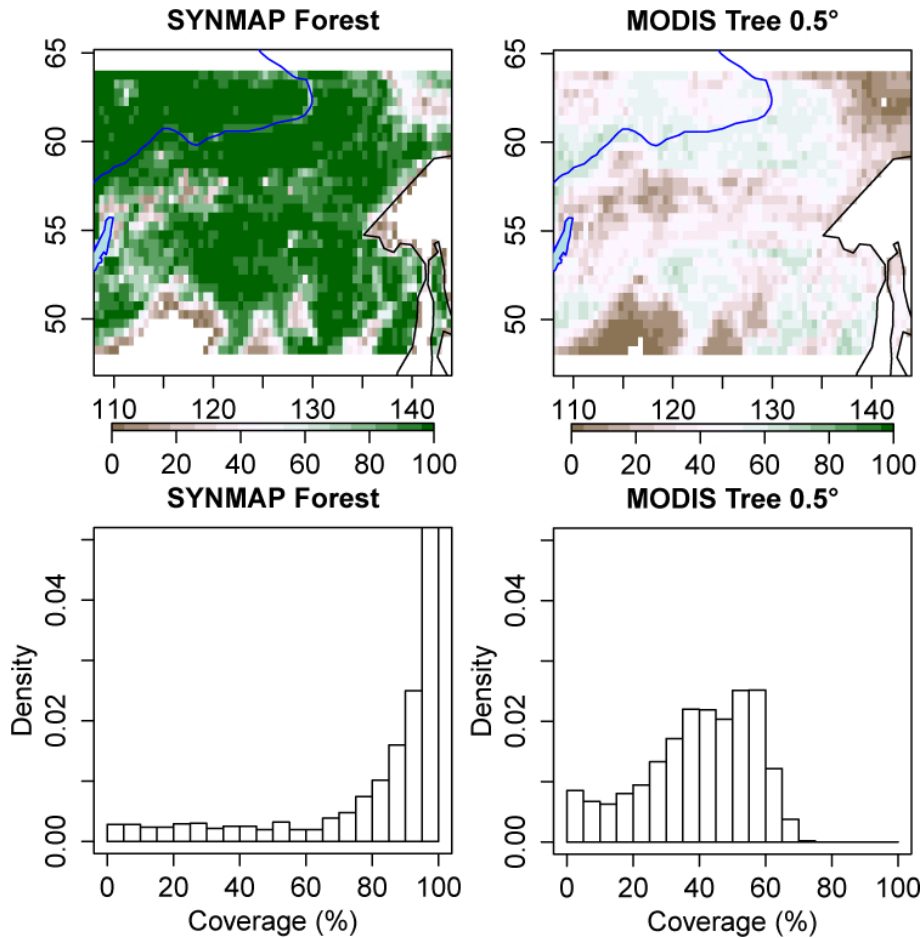


Figure C2. Comparison of total forest coverage from SYNMAP and MODIS tree coverage for a region in eastern Siberia.

[Title Page](#)

[Abstract](#) | [Introduction](#)

[Conclusions](#) | [References](#)

[Tables](#) | [Figures](#)

[◀](#) | [▶](#)

[◀](#) | [▶](#)

[Back](#) | [Close](#)

[Full Screen / Esc](#)

[Printer-friendly Version](#)

[Interactive Discussion](#)



Phenology controls and model-data integration

M. Forkel et al.

Title Page

Abstract

Introduction

Conclusions

References

Tables

Figures



Back

Close

Full Screen / Esc

Printer-friendly Version

Interactive Discussion

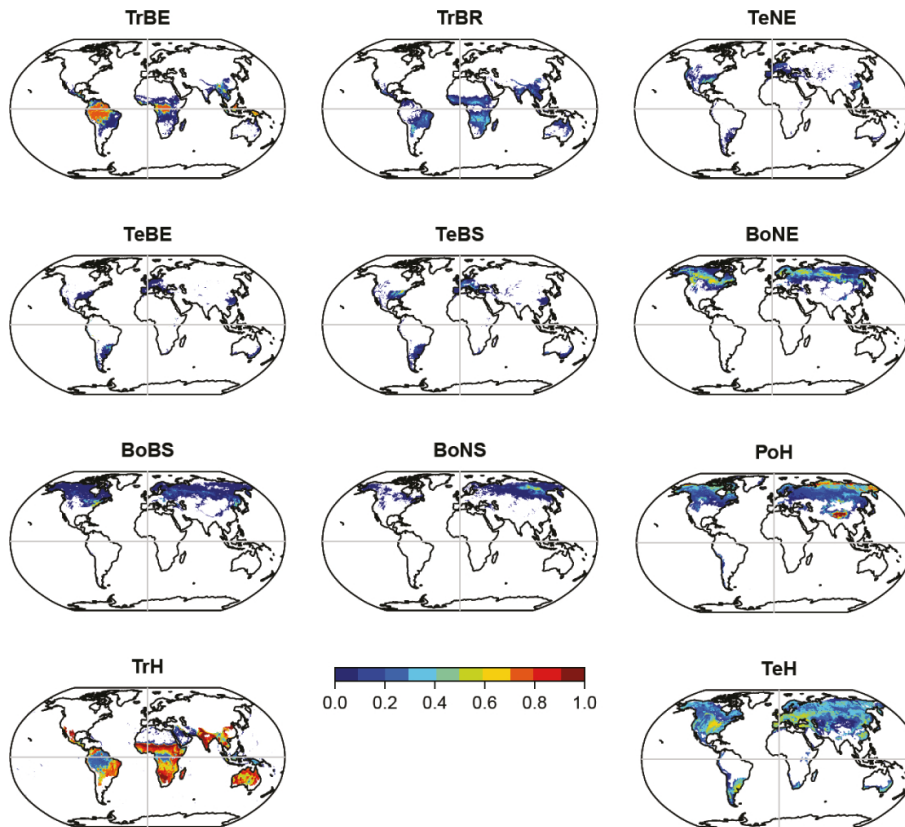


Figure C3. Observation-based maps of the foliar projective cover of plant functional types (agricultural areas are included in the TrH and TeH PFTs).

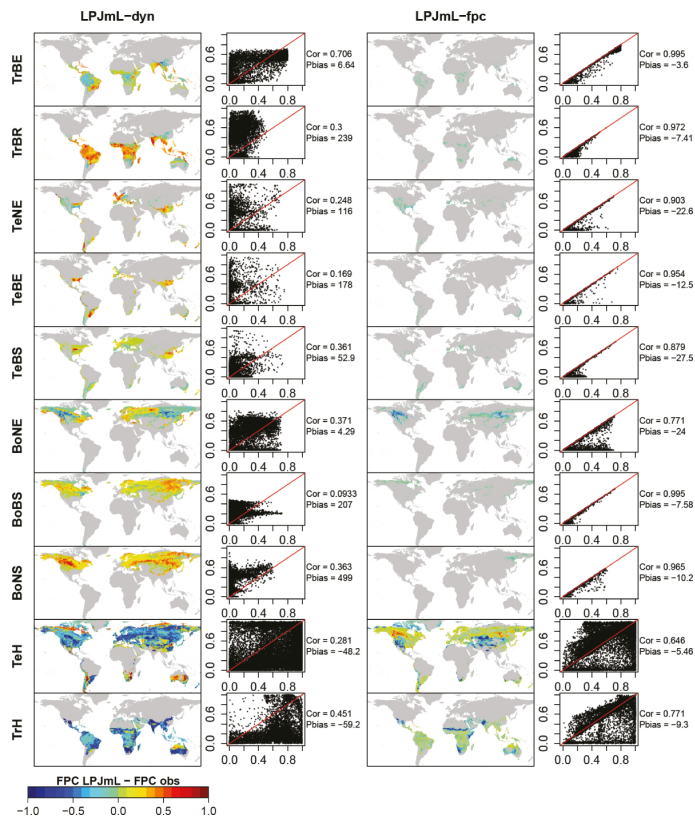


Figure C4. Comparison between simulated and observed PFT distributions for the year 2000. The maps are difference maps between simulated FPC values from LPJmL-OP and observed FPC values. The scatter plots show observed FPC values on the x-axis and simulated FPC values on the y-axis. Left: LPJmL-OP with dynamic vegetation and prescribed burnt areas. Right: LPJmL-OP with prescribed land cover and prescribed burnt areas.

Phenology controls and model-data integration

M. Forkel et al.

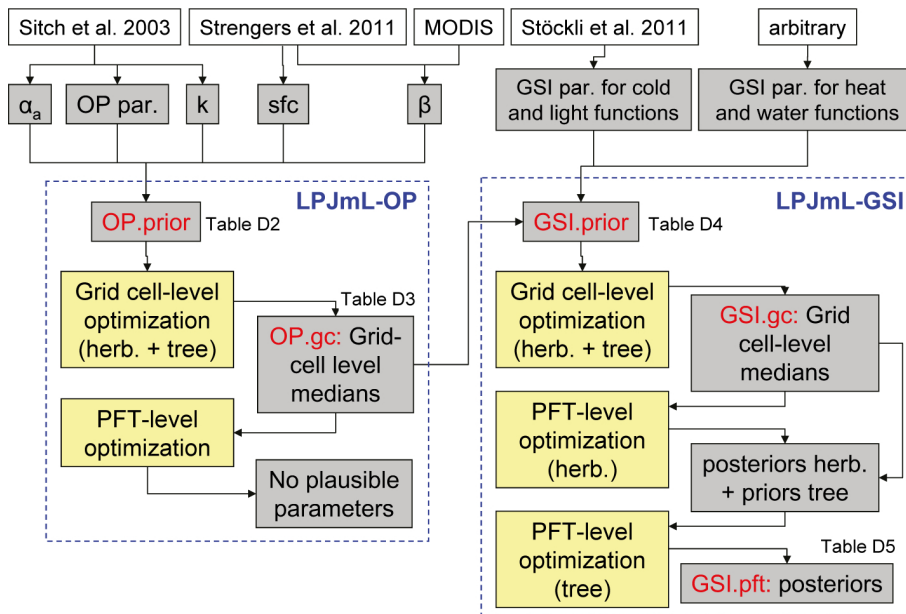


Figure D1. Information sources for prior and posterior parameter sets and overview of model optimization experiments. Grey boxes indicate model parameters or parameter sets. White boxes are information sources for parameters. Yellow boxes are optimization experiments.

Title Page	
Abstract	Introduction
Conclusions	References
Tables	Figures
⏪	⏩
⏴	⏵
Back	Close
Full Screen / Esc	
Printer-friendly Version	
Interactive Discussion	



Phenology controls
and model-data
integration

M. Forkel et al.

Title Page

Abstract

Introduction

Conclusions

References

Tables

Figures



Back

Close

Full Screen / Esc

Printer-friendly Version

Interactive Discussion

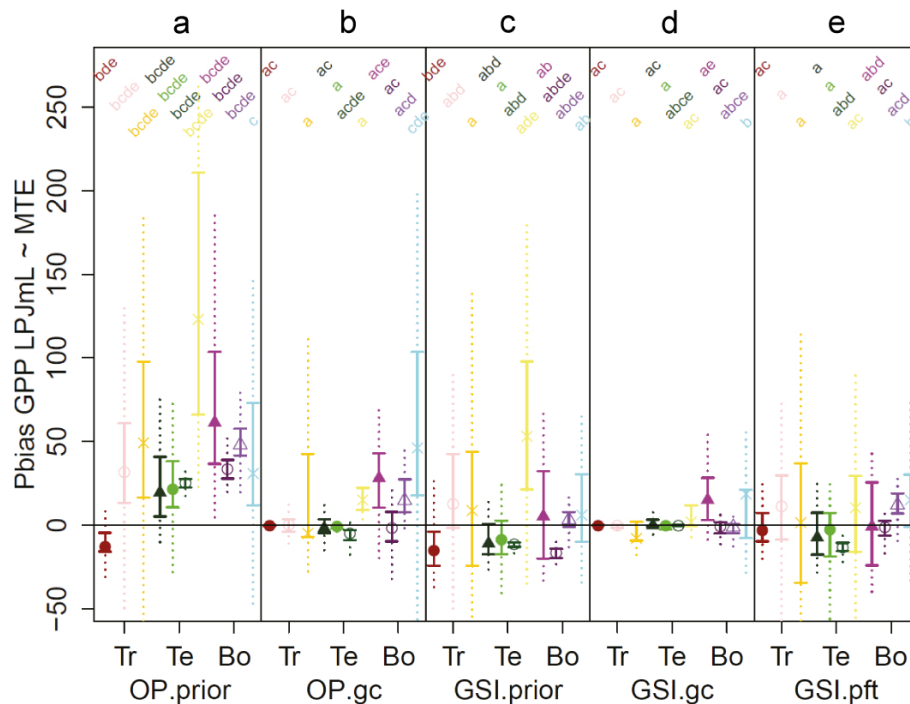


Figure D3. Distribution of the percent bias between LPJmL and MTE mean annual GPP (1982–2011) for several grid cells in prior model runs and optimization experiments grouped by plant functional types and biomes. See Fig. D2 for a further explanation of this figure.

Phenology controls
and model-data
integration

M. Forkel et al.

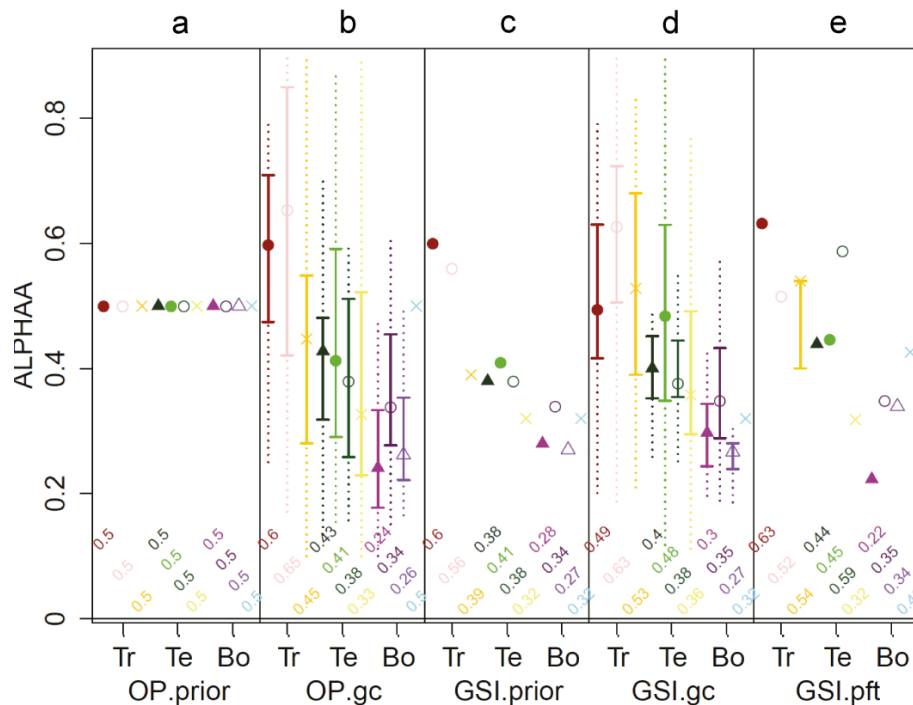


Figure D5. Prior and optimized values for the parameter α (fraction of radiation absorbed at leaf level relative to canopy level) grouped by plant functional types and biomes. The distribution of the parameter in the optimization experiments OP.gc and GSI.gc represents the spatial variability of the parameter from different grid cell-level optimization experiments. See Fig. D2 for a further explanation of this figure.

Title Page

Abstract

Introduction

Conclusions

References

Tables

Figures



Back

Close

Full Screen / Esc

Printer-friendly Version

Interactive Discussion



Phenology controls
and model-data
integration

M. Forkel et al.

Title Page

Abstract

Introduction

Conclusions

References

Tables

Figures



Back

Close

Full Screen / Esc

Printer-friendly Version

Interactive Discussion

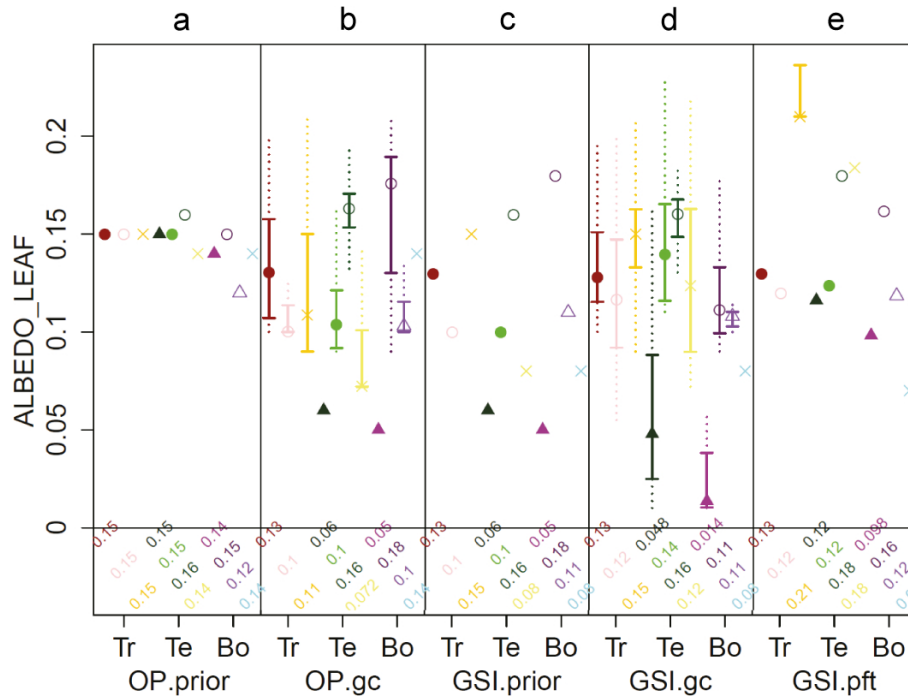


Figure D6. Prior and optimized values for the parameter β leaf (leaf albedo) grouped by plant functional types and biomes. The distribution of the parameter in the optimization experiments OP.gc and GSI.gc represents the spatial variability of the parameter from different grid cell-level optimization experiments. See Fig. D2 for a further explanation of this figure.

Phenology controls
and model-data
integration

M. Forkel et al.

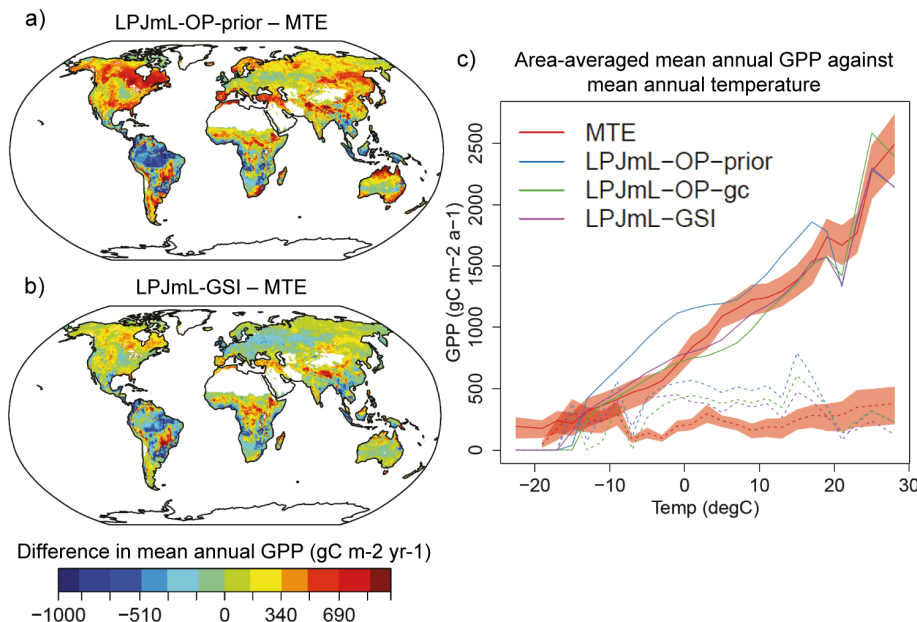


Figure E1. Comparison of patterns of mean annual total gross primary production from LPJmL and the data-oriented MTE estimate for the period 1982–2011. **(a)** Difference in mean annual total GPP between MTE and LPJmL-OP-prior. **(b)** Difference in mean annual total GPP between MTE and LPJmL-GSI. **(c)** Global spatial-averaged gradients of mean annual GPP against mean annual temperature. Dashed lines are dry areas with mean annual $P/PET < 15$ and solid lines are wet areas with mean annual $P/PET \geq 15$. The red area represents the uncertainty of the data-oriented GPP estimate expressed as the inter-quartile range of the MTE ensemble.

Phenology controls
and model-data
integration

M. Forkel et al.

Title Page

Abstract

Introduction

Conclusions

References

Tables

Figures



Back

Close

Full Screen / Esc

Printer-friendly Version

Interactive Discussion

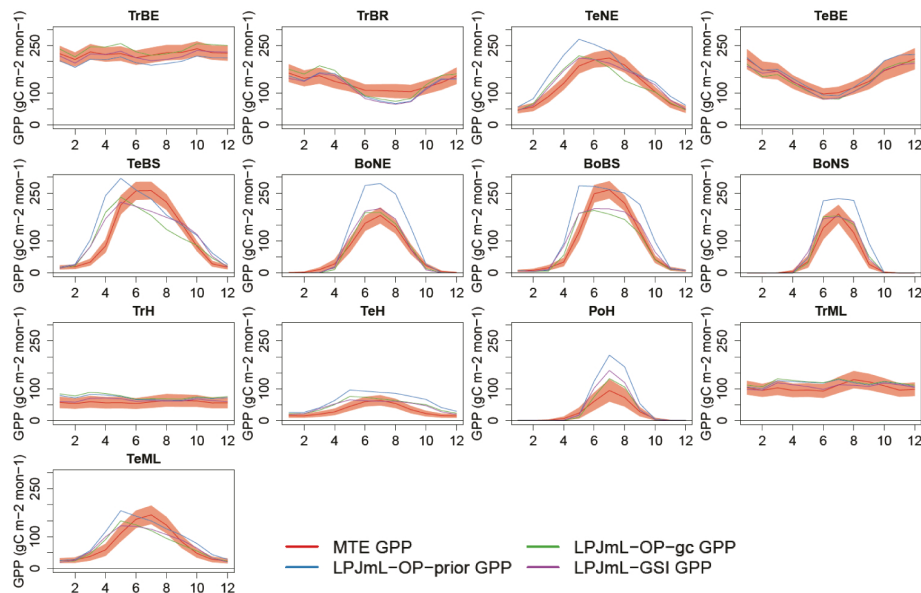


Figure E2. Comparison of the mean seasonal GPP cycle (averaged over 1982–2011) from MTE and LPJmL spatially averaged for regions with the same dominant PFT.

Phenology controls
and model-data
integration

M. Forkel et al.

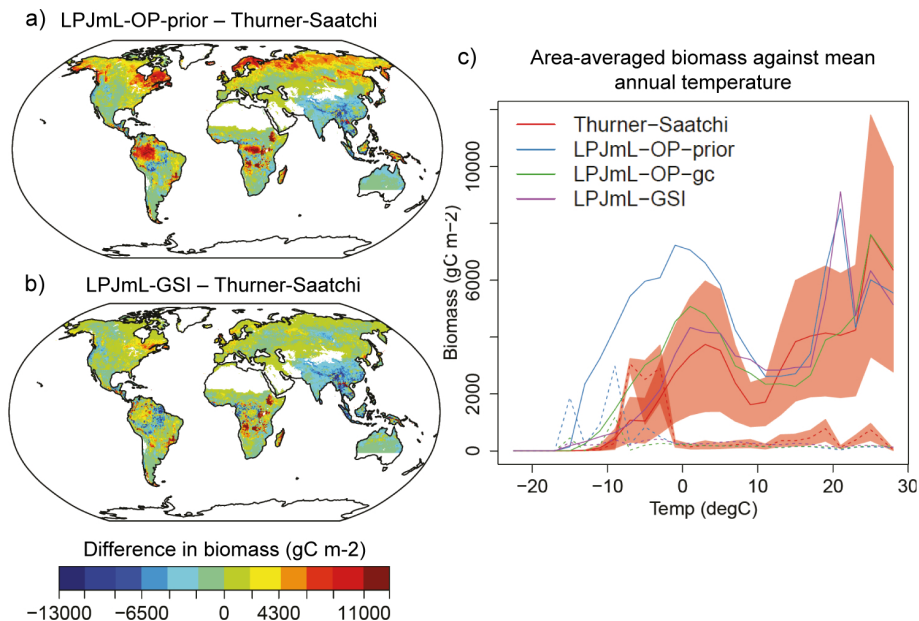


Figure E3. Comparison of biomass from data-oriented estimates (Thurner and Saatchi datasets) and from LPJmL (averaged 2009–2011). **(a)** Difference in biomass between LPJmL-OP-prior and datasets. **(b)** Difference in biomass between LPJmL-GSI and datasets. **(c)** Global spatial-averaged gradients of biomass against mean annual temperature. Dashed lines are dry areas with mean annual $P/PET < 15$ and solid lines are wet areas with mean annual $P/PET \geq 15$. The red area represents the uncertainty of the data-based biomass estimates expressed as the 0.05 to 0.95 quantile range of the data ensemble.

Phenology controls and model-data integration

M. Forkel et al.

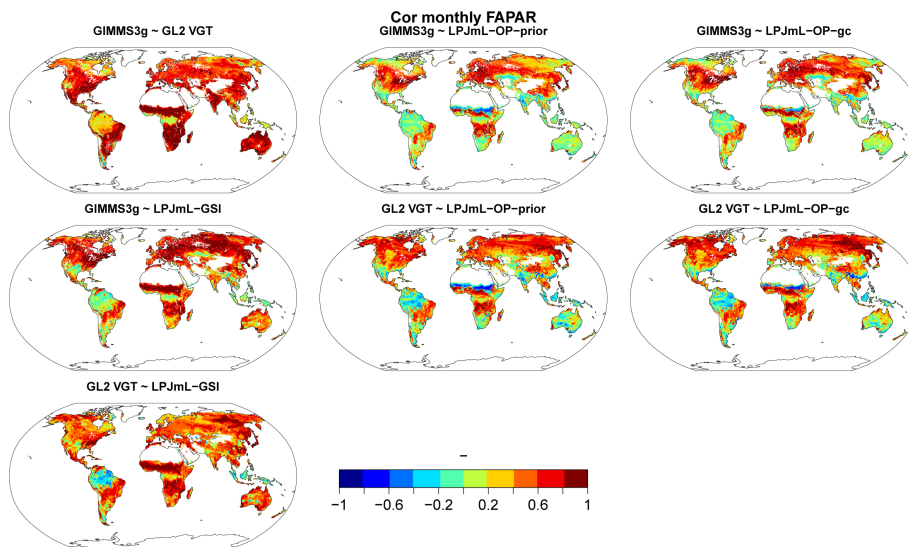


Figure E4. Correlation coefficients between monthly FAPAR time series from GIMMS3g, GL2 VGT datasets and LPJmL model simulations.

Title Page

Abstract

Introduction

Conclusions

References

Tables

Figures

◀

▶

◀

▶

Back

Close

Full Screen / Esc

Printer-friendly Version

Interactive Discussion



Phenology controls and model-data integration

M. Forkel et al.

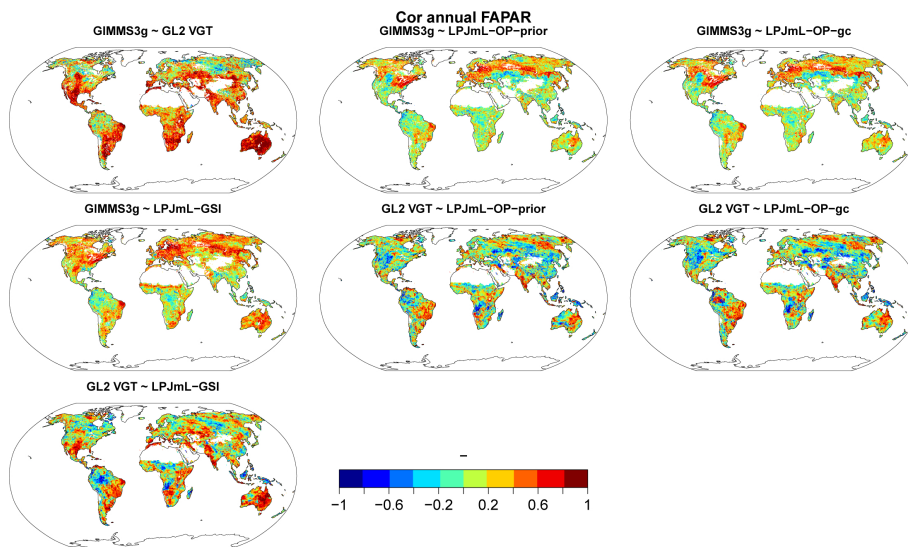


Figure E5. Correlation coefficients between annual FAPAR time series (annual mean averaged from monthly values with air temperatures $> 0^{\circ}\text{C}$) from GIMMS3g, GL2 VGT datasets and LPJmL model simulations.

Title Page

Abstract

Introduction

Conclusions

References

Tables

Figures



Back

Close

Full Screen / Esc

Printer-friendly Version

Interactive Discussion

